NTNU – Trondheim
Norwegian University of
Science and Technology

Preliminary Investigations on the Manufacture of Al-AZ31 Bimetallic Composites by the Screw Extrusion Process

Bodil Drange Pedersen

Materials Science and Engineering
Submission date: June 2013
Supervisor: Hans Jørgen Roven, IMTE
Co-supervisor: PhD-stud. Kristian G. Skorpen, IMT
Prof. II Oddvin Reiso, IMT
Prof. Em. Nils Ryum, IMT

Norwegian University of Science and Technology
Department of Materials Science and Engineering

Declaration

I, Bodil Drange Pedersen, hereby certify that this thesis is written by me, and is a presentation of my original work. I certify that this work contains no material, which has been accepted for any degree or diploma in any university or other institution in my name. To the best of my knowledge, I certify that wherever contributions of other are involved, due reference to the literature has been made.

Acknowledgments

First of all I would like to thank my supervisor, Professor Hans Jørgen Roven for his encouragement and support. His guidance has been very much appreciated.

I would also like to acknowledge my co-supervisor Professor II Odvin Reiso for his constructive advice. Special thanks are extended to PhD candidate Kristian Grøtta Skorpen, for his assistance and invaluable discussions. I would also like to thank Pål Christian Skaret and Yingda Yu at the Department of Material Science and Engineering for their technical assistance.

Furthermore, I would like to thank my fellow students at the 202-study hall for remarkably high spirits, and helpful counsels. Finally, I would like to extend my sincere gratitude to my parents, who have always given me their support and advice.

Abstract

The development of bimetals, or metallic composites, has in recent years been given increased attention. The motivation behind the development of bimetals is that, by combining two dissimilar metals it is possible to obtain an optimal combination of desired properties, while at the same time minimizing the restrictive properties of the metals involved. Aluminium and magnesium both have excellent material properties, but they also have the possibility of expanding their field of application by being combined as a bimetal. However, it is yet to be established a suitable manufacture method that can produce bulk metallic composites with fully integrated and void-free interfaces between the two materials. This thesis proposed screw extrusion as a possible solution for mass production of pure Al-AZ31 bimetallic composites. In the approach to evaluate this proposition, extrusion profiles with different pure Al-AZ31 compositions were produced, and characterized. It was not, in contrast to what was expected, achieved to produce a bimetallic composite system in any of the extrusion trials. The most profound observation was the total absence of AZ31 as a reinforcing constituent. The AZ31 constituents completely dissolved during the extrusion, instead, extrudates of bulk Al with Mg in solid solution were obtained. The relative small size of the AZ31 feed stock material plays most likely a key role for the absence of reinforcing AZ31 constituents and possible theories for the complete dissolution of the AZ31 turnings are: (1) high temperatures during the extrusion have led to local melting at the Al-AZ31 interfaces, or (2) high extrusion temperatures, together with the high strains involved in the process, have given rise to extensive diffusion of Mg and Zn into the Al. The extrusion profiles also contained a high degree of intermetallic phases, which were identified as Al_3Mg_2 and $Al_{12}Mg_{17}$. Furthermore, the microstructures of the profiles were greatly inhomogeneous, with large variations in grain structure, and in chemical composition. The inconsistent grain size was linked to the material flow of the screw extrusion process, while variation in chemical composition was believed to be a result of the mixing and compaction of the feed stock material. It was observed that oxide layers on the feed stock material might play a crucial role for mechanical properties, since extensive oxidation of the AZ31 turnings has a detrimental effect on the ductility. In fact, it can be argued that the condition of the feed stock material is just as important for the mechanical properties as the amount AZ31 added. Still, it must be mentioned that two of the extrudates displayed superior ductility, combined with relative high strength levels. So, even though the attempt in producing pure Al-AZ31 bimetallic composites was a failure, screw extrusion shows promising results for use in recycling of aluminium-magnesium alloys.

Sammendrag

En økende interesse for utvikling og fremstilling av såkalte bimetaller, også kjent som metalliske kompositter har manifestert seg i løpet av de siste ti-årene. Motivasjonen bak konseptet bimetaller, er at ved å forene to metaller, kan man oppnå et materiale som kombinerer de beste materialegenskapene til de individuelle metallene, samtidig som man minimerer de begrensende sidene ved hver komponent. Aluminium og magnesium er begge to materialer som er kjent for sine gode materialegenskaper. Samtidig har begge metallene muligheter for å utvide sitt bruksområde gjennom å bli forent som et bimetall. En av hovedutfordringene for utviklingen av bimetaller er å finne en fremstillingsmetode som klarer å produsere metalliske kompositter av tilfredsstillende kvalitet. Denne avhandlingen undersøkte skruekstrudering som en mulig fremstillingsmetode for masseproduksjon av rent aluminium-AZ31 bimetaller. I tilnærmingen ble det fremstilt skruekstrudater med forskjellige tilsatser av AZ31. I motsetning til hva som var forventet, oppnådde man ikke å fremstille en kompositt. Isteden ble det produsert et materiale med en sammensetning svært lik den man finner i vanlige binære Al-Mg legeringer. De tilsatte AZ31 komponentene var så å si totalt fraværende som forstrekningskomponenter, noe som tyder på at de har blitt fullstendig oppløst under ekstruderingen. Dette kan skyldes at AZ31-komponentene var av en finsiktet størrelse, noe som kan ha gjort dem lite bestandige i de relativt hardføre omgivelsene som oppstår under ekstruderingen. Mulig mekanismer for oppløsning av AZ31-komponentene er (1) høye temperaturer under ekstruderingen har ført til lokal smelting av Al-AZ31 grenseflatene, eller (2) høye temperaturer i kombinasjon med intense tøyninger, som igjen har ført til betydningsfull diffusjon av Mg og Zn inn i Al. Det ble også observert en høy andel intermetalliske faser i ekstrudatene. Disse ble identifisert som Al_3Mg_2 and $Al_{12}Mg_{17}$. Alle ekstruderingsprofilene hadde en fremtredende inhomogen mikrostruktur, med store variasjoner i både kornstørrelse og kjemisk sammensetning. Den inkonsistente kornstrukturen kan forklares ut i fra hvordan materialet flyter i ekstruderingskammerset. Variasjonen i kjemisk innhold derimot, antas å være et resultat av miksingen og kompakteringen av tilsatsmaterialet. Det observeres at oksidlaget på tilsatsmaterialet høyst sannsynlig spiller en avgjørende rolle for de mekaniske egenskapene, ettersom omfattende oksidering av AZ31-komponentene er direkte ødeleggende for duktiliteten. Det er klare indikasjoner på at tilstanden til inngangsmaterialet er like avgjørende for de mekaniske egenskapene til produktet, som mengden av tilsatt AZ31. Det må fremheves at to av ekstrudatene utviste en overlegen duktilitet. Dette i kombinasjon med et relativt høyt styrkenivå gjør at selv om det ikke ble oppnådd å fremstille metalliske kompositter gjennom skruekstrudering, viser prosessen lovende resultater for bruk i resirkulering av aluminium og magnesium.

Table of Contents

List of Abbreviations

ARB	Accumulative Roll-Bonding
AZ31	Mg-3wt% Al-1wt% Zn Alloy
CEC	Cyclic Extrusion Compression
ECAP	Equal Channel Angular Pressing
EDS	Energy Dispersive X-ray Spectrometry
DSA	Dynamic Strain Ageing
FCC	Face Centred Cubic
HAGB	High Angle Grain Boundary
HCP	Hexagonal Closed Packed
HPT	High Torsion Pressing
HV1	Vickers Hardness Value with 1 kg load
HV5gf	Vickers Hardness Value with 5 grams load
OM	Optical Microscope
PLC	Portevin Le-Chatelier
SEM	Scanning Electron Microscope
SPD	Severe Plastic Deformation
TE	Torsion Extrusion
UTS	Ultimate Tensile Strength
UFG	Ultra-fine grains
XRD	X-Ray Diffraction

1 Introduction

The development of bimetals, or metallic composites, has in recent years been given increased attention. A bimetal is a material consisting of two dissimilar metals joined together through solid state bonding mechanisms. The motivation behind the development of bimetals is that, by combining two dissimilar metals it is possible to obtain an optimal combination of desired properties while at the same time minimizing the restrictive properties of the metals involved.

Aluminium is a lightweight material; its density is 2.7 g/cm^3, a great contrast to iron with a density of 7.87 g/cm^3. Furthermore, due to the formation of the protective Al_2O_3 oxide layer on its surface, aluminium exhibits excellent corrosion resistance in a neutral environment, and aluminium are therefore of considerable engineering interest. However, the use of *pure* aluminium in engineering applications is limited by the inherent low strength. Generally, the strength of pure metals is strongly connected to the internal resistance to dislocation glide. This in turn depends on the crystal structure, where a high number of slip planes increase the possibility for dislocations to glide. Aluminium has a face-centred cubic (FCC) crystal structure, which has multiple slip planes, 12 possible slip systems. As a consequence, pure aluminium has as a high ductility, but low strength. However, aluminium can be alloyed to achieve more satisfactory mechanical properties.

Aluminium alloys can be divided into three groups: Wrought non-heat-treatable alloys, wrought heat treatable alloys, and casting alloys. The term heat-treatable refers to whether or not the alloy is able to precipitate particles during heat treatment. Wrought heat treatable alloys are precipitation hardened and can reach quite high strength levels. This group includes the aluminium-copper alloys: Al-Cu and Al-Cu-Mg, but also the aluminium-magnesium alloys: Al-Mg-Si and Al-Zn-Mg. It is the wrought heat-treatable alloys that are mainly employed in the automotive and aircraft industry. Wrought non-heat-treatable alloys are primarily hardened through cold working, and cannot achieve the same strength level as the precipitation hardened alloys. This group comprises of the commercially pure aluminum series, but also the manganese-, and silicon alloys. Casting alloys can be non-heat-treatable or heat treatable, and the main alloys here are the Al-Cu, and Al-Si + Cu or -Mg.

Magnesium is also a promising structural material for lightweight constructions. With a density of only 1.74 g/cm^3, it is about 35% lighter than aluminium, making it the lightest of all technological metals used today.(Solberg, 2010) Magnesium has a hexagonal closed packed (HCP) crystal structure, which is the crystal structure with the least number of available slip planes. This give magnesium a fairly high specific strength, but at the same time a poor ductility. Magnesium is therefore a stronger

material than Al, but exceedingly more brittle and has thus a limited formability. The use of magnesium in different engineering applications is furthermore restricted by the high reactivity of the metal. Magnesium has one of the highest galvanic potential of all metals and will as a consequence easily oxidise, making it susceptible for corrosion in most environments. In similarity to Al, magnesium is today mostly utilized in its alloyed form. The most common commercial magnesium alloying system is the precipitate hardened Mg-Al-Zn system, usually designated by AZXX. AZ31 is one such alloy and have the composition Mg-3wt% Al-1wt% Zn.

Aluminium and magnesium, along with their respective alloys, have both excellent material properties, but they also have the possibility of expanding their field of application by being combined as a metallic composite. By joining aluminium with a magnesium alloy, it may be possible to obtain a lightweight metallic composite that exhibits a high corrosion resistance and a relatively high specific strength combined with excellent ductility. Several studies in producing bimetallic systems have been carried out and reports confirm that metallic composites indeed show excellent mechanical, electronic, and magnetic properties.(Chang et al., 2012) However, the success of obtaining a bimetal with adequate properties depends upon the thermodynamics of the system and the mixing process.(Dehsorkhi et al., 2011) Achieving bonding without melting the materials is a challenge; not all materials can be bonded together, and if they can, the challenge is to develop a method that produces a one-body solid material with fully integrated and void-free interfaces between the two materials.(Kazanowski et al., 2004)

There are promising results for mass production of bulk metallic composites by the use of Severe Plastic Deformation (SPD) processes. SPD processes may be defined as: a metal forming processes in which an ultra-large plastic strain is introduced into a bulk metal in order to create ultra-fine grained metals(Azushima et al., 2008). Under this definition, the following processes are included: Equal Channel Angular Pressing (ECAP), High Pressure Torsion (HPT), Accumulative Roll-Bonding (ARB), Cyclic Extrusion Compression (CEC) and Torsion Extrusion (TE). These processes involve high pressure, with the possibility of a high processing temperature, in addition to large plastic strains; all parameters important for achieving good diffusion bonding between metals.(Gronostajski and Matuszak, 1999) SPD processes have been used successfully to consolidate scrap aluminium and aluminium alloys(Gronostajski and Matuszak, 1999, Cui, 2011), and the SPD processes involving methods of “repeated press and rolling”, and “repeated folding and rolling” of the material, such as the ARB process, is considered as a good candidate for multi-scale production of metallic multilayer composites.(Eizadjou et al., 2008) Examples of metallic multi-layer composite systems that have successfully been produced through the ARB process are: Al-Ti(Yang et al., 2010), Al-Cu(Eizadjou et al., 2008, Shabani et al., 2012, Sheng et al., 2011), Al-Zn(Dehsorkhi et al., 2011), and Al-Mg/Al-Mg alloys (Chang et al., 2012, Chen et al., 2007, MC Chen and Wu, 2007, Liu et al.,

2011, Liu et al., 2009, Paramsothy et al., 2008, Wu et al., 2010). Common for these systems is that they all contain aluminium as one of the bimetal components. It can thus be assumed that aluminium is a good candidate for bimetal systems, and that Al functions as a ductile matrix in a composite system.

Gronostajski et al., (Gronostajski and Matuszak, 1999) reviewed recycling of aluminium and aluminium alloy chips by plastic deformation. In their investigation they also examined the possibility of adding reinforcing phases to the aluminium. As possible reinforcing phases, aluminium oxide (from the surface of the chips), tungsten, carbon and ferro-chromium powders, and aluminium bronze comminuted chips were explored. Gronostajski et al. established that the following factors are significant contributors to solid state bonding in a system containing aluminium: the amount, form and size of the reinforcing phase, the degree of fragmentation of the aluminium chips, the pre-molding parameters, the shape of the extruding dies, the degree of extrusion reduction ratio, the lubrication method and the lubricants used, and the extrusion speed and temperature(Gronostajski and Matuszak, 1999).

Screw extrusion of aluminium is a new, continuous solid-state extrusion process developed at the Norwegian University of Science and Technology (NTNU) in collaboration with Norsk Hydro(Werenskiold et al., 2007).This thesis proposes screw extrusion as a possible solution for mass production of aluminium-magnesium bulk metallic composites. To the authors knowledge it has not been attempted to produce bimetals by screw extrusion before, and there are thus limited literature on the subject. It can be argued that screw extrusion is a potential manufacture method for metallic composites as the same solid-state deformation bonding mechanisms will occur during screw extrusion as in the comparable batch forming methods of ECAP and ARB. However, this cannot be proven without first being explored.

In this study screw extrusion will be utilized to produce aluminium-AZ31 magnesium alloy composites. Extrusion trials will be conducted for the following compositions: Al-5wt% AZ31, Al-7.5wt% AZ31, and Al-10wt% AZ31. Characterization of the extrudate profiles will be performed by microstructure examination in optical- and scanning electron microscopes, where the phase compositions will be examined by energy dispersive X-ray spectrometry (EDS). The mechanical properties of the extrusion profiles will be evaluated by room temperature tensile testing and through macro- and micro hardness testing.

2 Theoretical Background

2.1 Screw Extrusion

In traditional extrusion, the cross section of a solid block of metal is subjected to a high pressure and temperature, and then forced to flow plastically through a die opening.(Dieter and Bacon, 1988) Due to the high flexibility of the extrusion process, and the superior plasticity of aluminium at elevated temperatures, extrusion has for several years been a preferred metal forming method for aluminium alloys. A drawback with traditional extrusion is that it is a discontinuous batch process; after each extrusion has been performed, a new billet has to be loaded into the extrusion chamber. The extrusion process is furthermore dependent on pre-production of the billets, a step in which a considerably amount of energy and material is consumed. Also, left over material from machining processes, such as aluminium chips and -turnings are difficult to recycle by conventional melting processes.(Gronostajski and Matuszak, 1999) Traditional extrusion is therefore a high-energy consumption process with room for improvements.

Thus, in recent years, there has been an increasing interest for using extrusion as a method for recycling of scrap aluminium.(Gronostajski and Matuszak, 1999) Instead of having to melt and cast the scrap constituents into new ingots that have to be subjected to further deformation afterwards, consolidation can be achieved through solid-state processing. In a solid-state process, such as hot extrusion, the pressure, temperature and large deformations causes the scrap constituents to merge with strong weld-like bonds forming at the interfaces.(Widerøe and Welo, 2012) In fact, under proper condition, a fully dense material can be obtained with mechanical properties not inferior to extrudates manufactured from cast billets. Cui(Cui, 2011) investigated solid state recycling of aluminium scrap and found that conventional hot extrusion of aluminium turnings at 500°C produced a fully dense material, where both hardness and room temperature tensile strength values were 95-98% of the properties of the conventional reference material. However, also for conventional extrusion of scrap aluminium, the process is not continuous, as both pre-compression of scrap and the re-loading into the extrusion chamber must be carried out batch-wise, prior to the extrusion.

As already mentioned, screw extrusion of aluminium is a novel, continuous solid-state extrusion process. A schematic drawing of the single flight screw extruder is given in Figure 1. In screw extrusion, the material is in the form of small granulates or turnings, fed into the extrusion chamber through the feedhole. Inside the

chamber, a rotating screw is located. This screw generates the extrusion pressure, and the metal fragments are transported into the compacting chamber were they are compacted and subsequently extruded trough the orifice *in one single operation*. This enables continuous extrusion, which increases the overall energy efficiency of the extrusion process. Screw extrusion has successfully been applied to aluminium granules and chips to produce bulk aluminium with satisfactory mechanical properties.(Cui, 2011, Ringstad, 2009, Skorpen, 2011, Bilsbak, 2012)

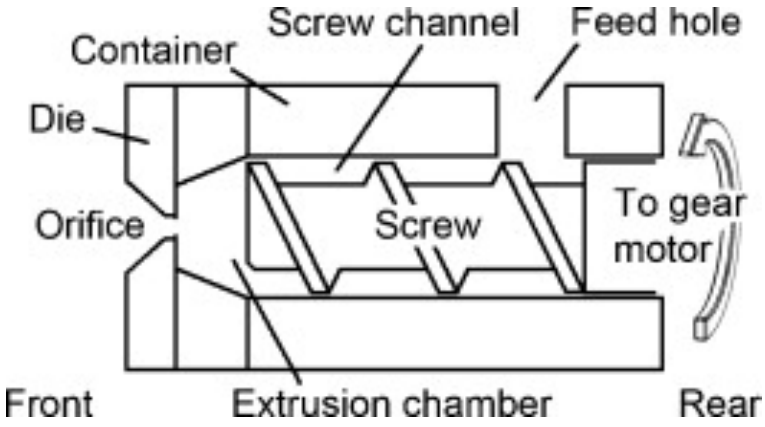

Figure 1: Schematic drawing of a single flight screw extruder(Werenskiold et al., 2007).

2.1.1 Material Flow

In screw extrusion, the material flow is far more complex than in traditional extrusion. In the traditional extrusion process, the most important process parameters are: working temperature, extrusion ratio, speed of deformation, and the frictional conditions in the die and at the container wall.(Dieter and Bacon, 1988) In screw extrusion there are complex flow characteristics inside the extrusion chamber in addition to extra frictional effects from interactions between material and screw. Widerøe and Welo(Widerøe and Welo, 2012) investigated the metal flow in screw extrusion of aluminium. They observed that in addition to pushing the material forward, the screw rotation subjects the material to a considerable amount of shear strain. They further observed that the material undergoes different degree of deformation, depending on the location inside the chamber.(Widerøe and Welo, 2012) It is therefore expected that inhomogeneity in the microstructure will arise due to the varying degree of deformation. Furthermore, Widerøe and Welo observed that the profiles are produced by the screw flights, continuously smearing new layers onto the pre-existing material. They managed to obtain an image of the material flow by adding a contrasting material into the extrusion chamber during extrusion of aluminium. The outcome is pictured in Figure 2. It can be observed that the extrusion profile comprises of numerous layers, and that close to the edges of the profile, the density of the layers

increases, and that each layer becomes thinner, compared to the layers towards the centre of the profile. The thickness of these layers was found to depend on both rotation, and feeding speed. An increase in rotation speed results in a decrease of layer thickness. The opposite was found to be true for the feeding speed: the more material fed into the extruder the thicker became the layers. The following macroscopic outline of the material flow in the screw extrusion process is directly cited from Widerøe and Welo's report(Widerøe and Welo, 2012):

1. *Aluminium granulates enters the screw extruder, falls to the bottom of the container and is then pushed forward, sliding on the screw and container surfaces.*
2. *Granulate surface starts to interact with pre-existing consolidated aluminium located at the active flight of the screw channel.*
3. *In a process synchronized with the screw rotation, granulates are partially consolidated and pushed down the screw channel. The main material flow path goes through the centre of the screw channel. Sticking friction prevails in this region and forward.*
4. *Fully consolidated material enters the region in front of the screw flight tip. The screw flights behaves like knives, continuously "smearing" aluminium layer by layer onto pre-existing material, pushing it forward into the extrusion chamber.*
5. *"Fresh" layers temporarily flow backward into the screw channel in the wake behind the screw flight tip, merging with the screw channel flow.*
6. *Each new layer displaces previous layers that are pushed forward through the extrusion chamber before finally being extruded, thus creating a profile.*

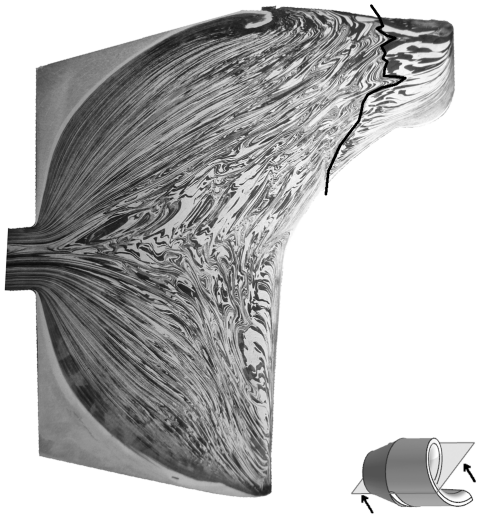

Figure 2: Etching of a cross-sectional plane obtained in screw extrusion of aluminium with a single flight screw, showing the material flow during the process. A contrasting material has been added for each revolution. The profile passing through the die is shown to the left(Widerøe and Welo, 2012).

2.1.2 Process Parameters

The role the different screw extrusion parameters play on the microstructure of extruded Al-Mg composites is outside the scope of this thesis. However, Kristian Grøtta Skorpen(Skorpen, 2011) investigated the impact of screw extrusion process parameters on the microstructure of an extruded AA6060 aluminium alloy. Through systematically varying the die temperature, material feed rate, and screw rotation speed, Skorpen concluded: A low die temperature and a low feed rate, together with a high screw rotation speed, are favoured as these will give the highest properties. With such parameter settings, the recrystallization of the deformed microstructure was kept at a minimum. Skorpen also observed that porosity was a problem in most extrudates, and the favoured parameters chosen would give maximum kneading of the material, i.e. decrease the amount of pores.

2.1.3 Feed Stock Surface Area

The surface condition of the feed stock material plays an important role, i.e. in the bonding process during extrusion, but also for the mechanical properties of the final product. Both aluminium and magnesium are prone to excessive oxidation, and will thus have oxide layers covering their surfaces where the amount of oxidation naturally increases with increasing surface area.(Hu et al., 2008) Furthermore, it has been shown that aluminium alloys containing Mg has a different oxidation mechanism from that of pure aluminium. Especially, results show that the oxidation rate of Al-Mg alloys changes at elevated temperatures, and becomes approximately linear above 400°C.(Kim et al., 1996) Investigations on the oxidation behaviour of Mg in a solid state revealed that at 437°C, an accelerated weight gain of the Mg test specimens was measured, and the weight gain was related to the formation of an non-protective MgO film.(Czerwinski, 2003) These are important observations, as the oxide layer of Al and Mg can both have a positive and a negative effect on the final extrusion product.

During severe plastic deformations, the oxide layers on granulate surfaces are effectively broken up.(Gronostajski and Matuszak, 1999, Cui, 2011) The oxide particles then become dispersed in the matrix material, and can give a similar effect on the mechanical properties as precipitation strengthening. Hu et al.,(Hu et al., 2008) investigated the effect of chip size on mechanical properties and microstructure of a magnesium alloy prepared by solid state recycling, and reported that oxide precipitates increased the strength. They explained the high strength by grain refinement and homogenous dispersion of oxide precipitates in the recycled magnesium specimens, but noted that the strengthening effect was on a compromise of ductility - excessive oxides were found to adversely affect the elongation to failure. Similar results are reported for aluminium. Here the internal

interfaces might contain small oxide particles and films, which can retard recrystallization and grain growth in the recycled material.(Cui, 2011)

As previously stated, during solid-state deformation bonding, weld-like bonds form between the interfaces of the material. The quality of the final product depends on the quality of welds. These welds are again dependent on the surface oxide layer.(Widerøe and Welo, 2012) The bonding occurs through diffusion of atoms and it is therefore crucial that the oxide layer is not too thick, but allow for diffusing species to pass. Excessive precipitation of oxide particles and large precipitates can also lead to poor bonding; for magnesium alloys it is found that the matrix adjacent to oxide precipitates is prone to form micro-voids, hence reduce the tensile strength.(Hu et al., 2008)

2.2 The Aluminium – Magnesium System

In the manufacture of metallic composites the temperature is normally below the melting temperature of the materials involved. In order to achieve a one-body material with fully integrated and void-free interfaces, there must be interdiffusion between the two metals. Interdiffusion here refers to the diffusion of unlike atoms in materials, where the diffusion proceeds until the elements become uniformly distributed.(Askeland and Phulé, 2006) In earlier sections, it has been mentioned that successful solid solution bonding between the interfaces of scrap Al-Al- and Mg-Mg constituents has been obtained during hot extrusion. A next step is to investigate if similar bonding can be obtained between aluminium and magnesium.

2.2.1 The Aluminium-Magnesium Binary Phase Diagram

To evaluate the bonding in the Al-AZ31 system, the solid phases of the Al-Mg phase diagram must be considered. Through the years, several phase diagrams for aluminium-magnesium have been proposed. In this study it will be referred to the phase diagram proposed by J.L. Murray(Murray, 1982), shown in Figure 3.

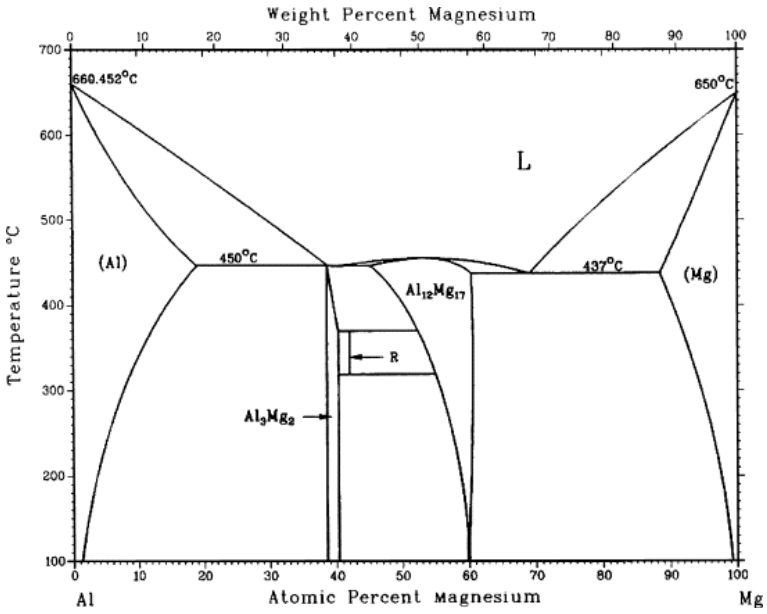

Figure 3: The Al-Mg Phase Diagram. (Murray, 1982)

The equilibrium Al-Mg system consists of five solid phases: Al(s), Mg(s), β, γ, and R (ε). The first phase is aluminium with magnesium in solid solution, with a FCC crystal structure and a melting point of 660.45°C. The solubility of magnesium increases with temperature and reaches maximum solubility of 18.9 at% at the eutectic temperature of 450°C. The reported solubility of Mg in Al at 420°C and 400°C is 15at% and 12.6 at%, respectively. The magnesium phase with aluminium in solid solution has a HCP crystal structure, a melting point of 649°C, and can maximum solve 11.8 at% Al at the eutectic temperature of 437°C. As for the aluminium phase decreases the solubility in magnesium with temperature.

The three remaining phases are intermediate phases; intermetallics with varying phase compositions. The β phase has the approximate stoichiometric composition Al_3Mg_2, and is from its congruent melting point of 451°C stable down to low temperatures. In the phase diagram β is given a fixed composition of 38.2 at% Mg at the eutectic temperature, but it is reported to have a composition range from 37.5 to 40.3 at% Mg(Murray, 1982) and the composition fits so the formula Al_8Mg_5 better. Both formulas for the β phase are used in the literature and in this thesis the Al_3Mg_2 formula will be used. The β phase has a complex cubic structure. Complex crystal structures have few available slip planes(Dieter and Bacon, 1988) and the β phase is therefore a hard and brittle phase.

The second intermediate phase is a line compound, usually denoted R (ε). It is given the composition 42 at% Mg, where a small variation of ±0.3 at% Mg is reported. The R (ε) phase is in the equilibrium system only present between 370 and 350°C. The last intermediate phase is the intermetallic γ phase $Al_{12}Mg_{17}$. This

phase has a wide composition range; at 450°C the Mg content varies from 45 to 60.5at%, but with decreasing temperature the composition range becomes narrower. $Al_{12}Mg_{17}$ has a complex α-Mn cubic structure. The solid phases of the Al-Mg system are summarized in Table 1.

Table 1: Crystal structure data of the equilibrium solid phases in the Al-Mg system.(Murray, 1982)

Phase	Approx. composition range (at% Mg)	Crystal structure
Al	0-18.9	FCC
Al_3Mg_2 (β)	37.5-40.3	Cubic
R (ε)	42	Rhombohedral
$Al_{12}Mg_{17}$ (γ)	45-60.5	Cubic
Mg	88.2-100	HCP

2.2.2 Diffusion in the Al-Mg System

Diffusion is a complicated matter, and becomes significantly harder to assess in a severe plastic deformation process such as the process of screw extrusion. As this thesis is only a preliminary investigation of the Al-AZ31 metallic composite system, it will only be given a short and generalized introduction to the matter of diffusion in the Al-Mg system.

A general way to describe migration of atoms in solid state is by Ficks' 2nd law of diffusion, equation 1:

$$\frac{\partial C}{\partial t} = D \times \nabla^2 C \qquad (1)$$

Here D is the diffusion coefficient and C the concentration of atoms. The diffusion coefficient depends on the direction of diffusion, the solute concentration and the temperature. However, a common approach is to assume an isotropic material with D independent of concentration. The diffusion coefficient may then be expressed in terms of the following Arrhenius relationship, equation 2:

$$D = D_0 \exp\left[\frac{Q}{RT}\right] \qquad (2)$$

Here D_0 is the pre-exponential coefficient, Q is the activation energy for diffusion, R is the universal gas constant and T is the absolute temperature.

2 THEORETICAL BACKGROUND

In the Al-AZ31 system, there will be chemical concentration gradient across the Al-AZ31 interfaces. There will thus be a driving force for diffusion of the Al and Mg atoms into the AZ31 and Al matrix, respectively. This is known as interdiffusion. In an isolated system, the diffusion will continue until the original concentration gradient has disappeared. For a given system, an interdiffusion coefficient $\widetilde{D}_{int}$ can be defined. This coefficient gives the rate at which the original concentration gradient disappears, and is often a weighted average of the individual (intrinsic) diffusion coefficients. The intrinsic diffusion rates are usually unequal, and as a consequence, there will often be a net flux of atoms across the plane of the diffusion zone.

In interdiffusion, the atoms can distribute themselves in two possible ways, depending on the system. If the system favours phase separation, the intermixing will stop when the initially pure materials reach their solubility limit. In this case, the impurity atoms will be randomly distributed on both sides of the interface, but with different compositions. The second scenario is for a system that favours ordering. For this system, the atoms will combine in a stoichiometric arrangement and interdiffusion will continue until the whole sample has achieved that arrangement.

There is limited literature on the subject of interdiffusion in Al-Mg systems. Brennan et al,(Brennan et al., 2012) investigated interdiffusion of Mg and Al in the Mg-Al system by using solid-to-solid diffusion couples. They found that that the interdiffusion of Al in Mg (ss) requires markedly higher activation energy than the Mg interdiffusion in Al (ss). Furthermore, the calculated *impurity* diffusion coefficient of Mg in Al was an order of magnitude higher than the corresponding coefficient for Al in Mg.(Brennan et al., 2012) As a consequence, the rate of diffusion of Mg into the Al matrix will be much faster than the rate of diffusion of Al into the Mg matrix. Lastly, the high degree of deformation, and corresponding grain refining, the material is subjected to during the screw extrusion process will affect the rate of diffusion. Fujita et al,(Fujita et al., 2002) investigated interdiffusion of Mg in Al-Mg alloys with ultrafine grain sizes. The ECAP process was used to refine the grain size of an Al-3wt% Mg alloy. By the use of diffusion couples, the interdiffusion coefficients for Al and Mg were determined. Fujita et al. found that the interdiffusion coefficients are larger in the ultrafine-grained material. The calculated pre-exponential factor D_0 and activation energy Q for interdiffusion of Mg and Al at C_{Mg} =0%, in a coarse grained-, and ultrafine-grained material are(Fujita et al., 2002): 7.5×10^{-5} m^2s^{-1} and 128 $kJmol^{-1}$, and 9.9×10^{-7} m^2s^{-1} and 100 $kJmol^{-1}$.

Another method to evaluate interdiffusion in the Al-Mg system is by visual examination of the diffusion joint. In the following section, a short summary of findings from previous studies on diffusion bonding of Al -Mg (AZ31) systems, are

presented. The results are primarily collected from experiments involving the SPD processes: ARB, and ECAP. It can be argued that these findings may be relevant for the present study, as the ARB and ECAP processes involve similar pressure, temperature, and deformation conditions, as the screw extrusion process. Particularly, any results on temperature dependency of interdiffusion in the Al and Mg atoms are noteworthy.

The accumulated roll bonding process has particularly been successfully applied to produce aluminium-magnesium multi-layered composites.(Chang et al., 2012, Chen et al., 2007, MC Chen and Wu, 2007, Liu et al., 2011, Wu et al., 2010) Liu et al.,(Liu et al., 2011)investigated ARB processing of Al-AZ31 composites at 280°C. The authors reported that void and crack free Al-AZ31 interfaces were achieved for all ARB passes. In addition, examination of the interface revealed that interdiffusion of Al and Mg atoms had taken place, and the authors concluded that homogenous bonding between Al and Mg is possible. Chen et al.,(Chen et al., 2007, MC Chen and Wu, 2007) reported similar results: Al-AZ31 composites processed at 300°C showed superior bonding interfaces, and the authors facilitated the bonding success to the high rolling temperature, and to the heat produced by the large plastic deformation strain during the rolling. However, it was revealed that thick intermetallic compounds had formed at the Al-Mg interface. The compounds were identified as Al_2Mg_3 and $Al_{12}Mg_{17}$.(Chen et al., 2007) The latter intermetallic was also found at the Al-AZ31 interface of composites manufactured by ARB processing at ambient temperature.(Chang et al., 2012) The formation of the $Al_{12}Mg_{17}$ layer was attributed to the high strain during the rolling: high rolling strains can accelerate the diffusion between different layers of multi-layered composites and enhance the formation of intermetallic compounds.

Wu et al.,(Wu et al., 2010) investigated the mechanical properties of Al-AZ31 composites prepared by ARB processing at 400°C. They found large numbers of massive intermetallic compounds at the Al-Mg interface, where obvious cracks were observed. The intermetallic compounds were identified as Al_2Mg_3 and $Al_{12}Mg_{17}$ and it was observed a clear pattern in where the intermetallics were located: the Al_2Mg_3 was found beside the Al layer, while $Al_{12}Mg_{17}$ was located beside the Mg layer. Wu et al. furthermore reported that there was a strong correlation between the fracture surface of the tensile specimens, and the intermetallic phases. Evident cracking of the coarse Al-Mg intermetallic compound and rupture of the Al layer led to a dramatic decrease of yield strength.

Liu X.B. et al.,(Liu et al., 2009) investigated the fabrication of Al-AZ31 composites by equal channel angular extrusion. The ECAP process was performed at 250°C and 300°C, and for both temperatures satisfying interface bonding between AZ31 and Al were achieved. No obvious defects, such as microcracks, cavities, or discontinuities were detected in the samples. Furthermore, it was observed a clear

increase in extent of atomic diffusion at the Al- AZ31 interface with increasing temperature. For the ECAP performed at 300°C a thin diffusion transition zone of approximately 3μm thickness was observed and in this zone a gradual composition change of Mg and Al across the interface was measured. The sample fabricated at 250°C, did not contain any obvious reaction phases near the AZ31-Al interface. Based on these findings, Liu X.B. et al. concluded that solid solution between Al and AZ31 can be achieved through atomic inter-diffusion, but high ECAP temperatures are required (T≥ 300°C). The same study remarks that all elements in the material were involved in the diffusion, including zinc.

In accordance with the above observations, Li Yajiang et al.(Li et al., 2007) established that the chemical reaction process of Mg and Al atoms in a diffusion joint consist of three stages: (1) a diffusion transition region on the Mg side, (2) a diffusion region on the Al side, and a mixed-diffusion region (3):

$$3Mg + 2Al \rightarrow Mg_3Al_2 \qquad (1)$$
$$2Mg + 3Al \rightarrow Mg_2Al_3 \qquad (2)$$
$$Mg + Al \rightarrow MgAl \qquad (3)$$

In equation (1) above, the Mg_3Al_2 is an alternative expression the $Mg_{12}Al_{17}$ phase. The above equations are furthermore only the primary reactions mechanisms for the Mg-Al compounds. The actual chemical reaction process will depend on the concentration distribution of Mg and Al atoms near the interface, the interdiffusion rate of the atoms, and the holding time of the diffusion.(Li et al., 2007) In Figure 4, the concentration distribution near the interface of a pure Al and pure Mg coupling is given.(Peng et al., 2006) In the same figure, a model illustrating the phases formed in the diffusion zone is displayed. This model is in agreement with the three reaction processes proposed by Li Yajiang et al.

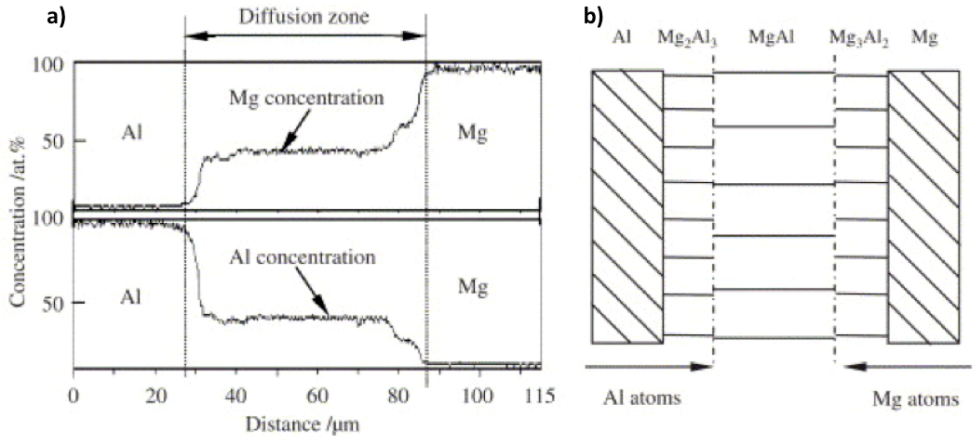

Figure 4: a) concentration variations of Al and Mg across the diffusion zone of a Al-Mg joint, b) corresponding model showing the direction of diffusion for the Al and Mg atoms, and the possible phases in the diffusion joint. (Peng et al., 2006)

2.3 Strengthening of Aluminium and Magnesium

It is generally known that for most metals the mechanical properties, like strength and hardness, can be improved by subjecting the metals to proper treatments. The strengthening is achieved by restricting the movement of dislocations and is done by either introducing barriers into the material in form of lattice strain or precipitates, or by increasing the density of dislocations in the material.(Dieter and Bacon, 1988) In fact, both aluminium-, and magnesium alloys can, after appropriate treatments, obtain strength levels comparable to traditional construction steel.(Solberg, 2010) The strengthening can be accomplished in three ways: by solid solution strengthening, precipitation strengthening, and by mechanical working the metal. The three strengthening methods can also be combined to provide even higher strength levels in the alloys; solid solution strengthened alloys can be mechanically worked, and precipitation strengthened alloys can be worked prior to the aging treatment.

2.3.1 Solid Solution and Precipitation Strengthening

In solid solution strengthening the alloying elements are mixed with the matrix material at the atomic level. The solute-atoms can either be interstitial or substitutional solved in the lattice, but in either case the solute-atoms will create a lattice strain in the matrix that will interact with the dislocation glide, resulting in what is known as solute hardening. The higher amount of atoms in solid solution, the larger amount of strain created, and the greater the strengthening effect.

However, most alloying systems have a solubility limit. When the solubility limit is reached, the excess solute-atoms will precipitate either as particles or as intermetallic compounds.(Askeland and Phulé, 2006, Dieter and Bacon, 1988) The solute atoms are regarded as immobile at low temperatures, but with increasing temperature their mobility increases considerably and the solute atoms may diffuse to the dislocations present in the material. This effect is known as dynamic strain ageing and is further discussed in later section.

For the Al-Mg system both elements will be interstitially solved in each other, and both Al and Mg have a relatively high solute solubility. As already presented, the maximum solubility of Mg in Al is 18.9 at%, while the maximum solubility of Al in Mg is 11.8 at%. However, it is rarely produced Al-Mg alloys with more than 10wt% Mg in solid solution. Further increase in Mg content will adversely affect the mechanical properties, as it will give an increased amount of intermetallic compounds in the material.

Precipitation strengthening is the method that can give the largest increase in strength. In precipitation strengthening it is added more alloying elements than the matrix material can solve. The matrix is supersaturated, and precipitates are formed as fine particles inside the metal. The particles are in a size range of <0.001 mm. In precipitation strengthening, the precipitates works as obstacles for dislocation glide. This can either be caused by the particle itself hindering the dislocation movement, or by a misfit strain effect the particle causes in the lattice due to incoherency with the matrix. Not all alloys can be precipitation strengthened, and the specific aluminium alloys that can be strengthened in this way are: Al-Cu, Al-Mg-Si, Al-Zn-Mg, and Al-Zn-Mg-Cu. (Askeland and Phulé, 2006, Solberg, 2010)

2.3.2 Mechanical Strengthening

The third method for strengthening aluminium and magnesium is by plastic deformation. During the deformation dislocations are generated, and the overall dislocation density of the material is increased. The deformation is performed through metal forming processes such as rolling and extrusion, and is the most commonly used method for strengthening aluminium. It is distinguished between cold and hot working, where the latter is performed at temperatures above 200°C. The high temperature provides a more suitable flow stress, the degree of softness and ductility of the material. Example of a cold working method is the rolling process, while extrusion is a hot working method.

Because of its superior plasticity at all temperatures, aluminium, and its alloys, can be subjected to most metal forming methods. However, extrusion is the one most

commonly utilized for aluminium. Magnesium and magnesium alloys are more a challenge to manufacture because of their HCP crystal structure.(Chandrasekaran and John, 2004) During deformation at ambient temperatures, Mg alloys have a limited workability and tend to break up and fail.(Chandrasekaran and John, 2004) However, with increasing temperature the ductility of Mg and Mg alloys readily improves. Chandrasekaran et al.,(Chandrasekaran and John, 2004) investigated the effect of materials and temperature on the forward extrusion of magnesium alloys and found that at a temperature of 300°C, the AZ31 magnesium alloy could easily be formed, and normal processing temperature of wrought magnesium alloys ranges from 250 to 450°C. Hot extrusion can therefore be a suitable forming method for magnesium alloys.

2.3.3 Dynamic Strain Ageing and the Portevin-Le Chatelier Effect

A strengthening mechanism that is strongly related to solid solution strengthening is the process of Dynamic Strain Ageing (DSA). DSA occurs during plastic deformation of the material and involves pinning of moving dislocation by solute-atoms.(Dieter and Bacon, 1988) DSA manifests itself as serrated yielding in stress-strain curves, or by a series of bands in rolled products. The phenomenon of serrated yielding is referred to as the Portevin-Le Chatelier (PLC) effect and occurs within a certain regime of temperatures and strain, and for certain strain and loading rates. DSA and PLC are often used interchangeably, but dynamic strain aging is believed to be the underlying mechanism that causes the PLC effect. In the serrated stress-strain curved, each step or serration corresponds to the nucleation and/or propagation of a deformation band along the tensile specimen.(Chen et al., 2009, Abbadi et al., 2002) The phenomenon of serrated yielding is of commercial significance, in particular where products are to be produced using cold forming operations.(Robinson, 1994) The occurrence of PLC goes along with a loss of ductility in the material, in addition to cause poor surface quality of the finished products.(Abbadi et al., 2002) In Figure 5, a stress-strain curve showing typical serrated flow behaviour is displayed.

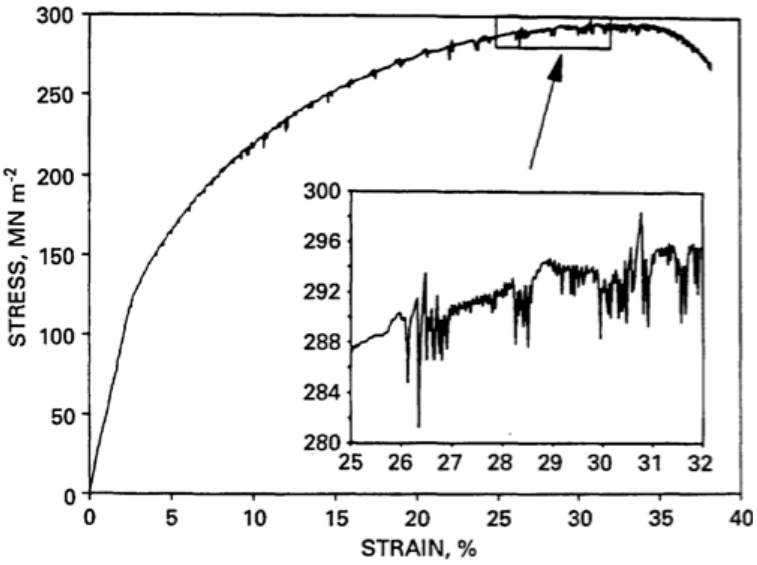

Figure 5: Room temperature tensile deformation of a commercial Al-Mg alloy showing typical serrated flow behavior. (Robinson, 1994)

The mechanism of DSA is not fully understood, but two main models are proposed: the dislocation-solute atom interaction model, and the dislocation-precipitate interaction model. In the first model, DSA is though to occur when the bulk diffusion of solute atoms has acquired a speed (through vacancies created during the deformation) high enough to drag the moving dislocations.(Wen and Morris, 2003, Wen and Morris, 2004) In the other model, it is assumed that solute-atoms diffuse to dislocations that are temporarily arrested at obstacles such as grain boundaries, or precipitates. The solute-atoms create an atmosphere around the dislocations, which become effectively pinned. To continue their movement (and the deformation process), the dislocations have to break away form the solute-atmosphere.(Dieter and Bacon, 1988, Chen et al., 2009, Wen and Morris, 2003) This process of dislocation pinning and dislocation break away is repeated as the dislocations move through the material, causing the characteristic serrated stress-strain curve: To break away, an extra amount of load has to be applied and a peak in the stress-strain curve is attained. Subsequently, when the dislocations manage to tear away from the solute-atmosphere, and are free to continue their movement, a drop in load is observed. Recent studies show that researchers tend to favour the latter model. However, which of the factors: grain boundaries or precipitates, predominantly responsible for arresting the dislocation movement are still unclear. Results indicate that the grain boundaries are the main source of obstacles as when the grain size increases the grain boundaries decrease, and consequently the magnitude of serration goes down.(Wen and Morris, 2003)

The PLC effect is observed in a broad range of both steel and aluminium alloys, where both interstitial and substitutional solutes are considered to participate in creating the solute-atmosphere around the dislocations. It is now generally

accepted that for aluminium alloys, magnesium atoms in interstitial solid solution are the main contributor to DSA, and that Mg causes the PLC effect at both ambient and elevated temperatures.(Robinson, 1994) Wen and Morris(Wen and Morris, 2003) investigated the effect of Mg concentration on the serrated yielding of 5000 series aluminium alloys, and confirmed that with increasing Mg content, the magnitude of the serrations increased. The theory behind this is that a larger amount of Mg atoms is involved in pinning the dislocations, and therefore an even higher stress is needed for the dislocations to break away. Wen and Morris also observed that at low temperatures, where the Mg atoms had started to precipitate out of solid solution, not only did the magnitude of the serration decrease, but also the whole serration phenomenon was delayed. Wen and Morris therefore proposed that in addition to there being fewer Mg atoms available for pinning the dislocation, the secondary precipitates are not strong enough obstacles – the dislocations are not arrested long enough by the precipitates for the Mg atoms to diffuse to the site.(Wen and Morris, 2003) Serrations in Al-Mg have been observed to occur with an upper critical strain; the strain at which the deformation again becomes homogenous, and the serrated tensile curve becomes smooth.(Robinson, 1994) This was examined during room temperature tensile testing, and confirmed.

The surface finish of the specimens is found to influence the serrated yielding. Abbadi et al.,(Abbadi et al., 2002) investigated the effect of surface finish on serrated yielding and found that polishing the tensile specimens prior to testing had a considerable effect on the onset behaviour of the PLC effect. In the polished case, the alloy exhibited homogenous plastic flow with a perfectly smooth tensile curve, whereas in the unpolished case serrations were induced by the inferior surface quality of the specimen. They concluded that geometrical defects on the specimen surface constitute stress raisers and thus represent fluctuations, which may induce the nucleation of deformation bands.(Abbadi et al., 2002)

Lüders band, also known as the yield point phenomena, is often observed together with serrated yielding in stress-strain curves.(Dieter and Bacon, 1988) It is an accepted phenomenon, occurring in a high range of materials and is reported observed in low carbon steel, and some aluminium alloys. When Lüders band appear during tensile deformation, a flow curve with no gradual transition from elastic to plastic behaviour is obtained. Instead, after the load has steadily increased during the elastic strain region, it suddenly drops and fluctuates about some approximately constant value of load, before it rises with further strain. This creates the characteristic yield point associated with Lüders band. As with serrated yielding, the yield point is usually associated with small amounts of interstitial or substitutional impurities.(Dieter and Bacon, 1988)

2.3.4 Recrystallization, Recovery and Grain Growth

Hot working will produce a material with a lower strength than a material subjected to the same degree of cold work. This is due to three phenomena occurring at elevated temperatures: recrystallization, recovery and grain growth.
During deformation, the internal energy in the material increases. This stored energy is associated with the energy of the dislocations introduced to the material, and boundary energy of the deformed subgrains. Recrystallization, recovery and grain growth all have the common driving force of lowering the total energy and each phenomenon involves a mechanism that in some way works to cancel out the accumulated strain of the deformed material.(Doherty et al., 1997, Humphreys, 1997, Humphreys and Hatherly, 2004) Consequently, the three phenomena are often hard to distinguish from each other.

Recovery and recrystallization are two similar phenomena, as both are thermally activated processes in which the deformed structure is gradually replaced by a new set of un-deformed grains. The two processes are also competitive, but it is believed that recovery take place prior to the recrystallization process.(Humphreys and Hatherly, 2004) For both phenomena, it is distinguished between the static and the dynamic form of the process. The first refer to the transformation taking placing during the successive heat treatment of a deformed material, while the latter refer to same transformation process taking place *during* the deformation of the material, at elevated temperatures of $T>0.5T_m$. As the screw extrusion process involves large deformations at temperatures above the given threshold value for the onset of dynamic recovery- and recrystallization, the further presentation will focus on the dynamic portion of these phenomena.

Recovery primarily involves changes in the *dislocation* structure. In dynamic recovery, the dislocations become rearranged through a series of micro-mechanisms known as dislocation climb, cross-slip and glide.(Humphreys and Hatherly, 2004) In dynamic recrystallization, the deformed grains are replaced by a new set of un-deformed grains. This new set of grains will nucleate and grow while strain is being applied, and will continue this process until the original deformation microstructure has been entirely consumed.(Doherty et al., 1997) Because new grains are nucleated, dynamic recrystallization give rise to grain refinement, with the new recrystallized grain structure consisting of approximate equiaxed, defect-free, and predominantly bounded by high angle boundaries.(Guo-Zheng, 2013) The new grains can often be in the submicron size range.(Doherty et al., 1997) However, if held long enough at elevated temperatures, the new grain structure will become coarser as grain growth will occur. The microstructural changes occurring dynamic recovery and –recrystallization is summarized schematically in Figure 6.

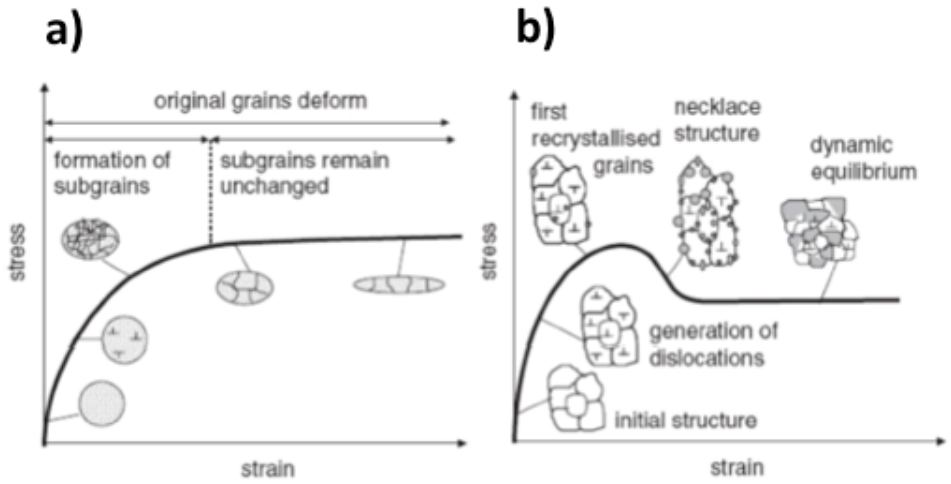

Figure 6: Schematic illustration of the microstructural changes during a) dynamic recovery, and b) dynamic recrystallization. (Guo-Zheng, 2013)

In both dynamic recovery- and recrystallization, a new microstructure with lower dislocation density will be established. This usually increases the ductility of the material, but with a simultaneous reduction in the strength and hardness. As a consequence, dynamic recrystallization and –recovery usually increase the plastic flow of the material, which will improve the workability during the metal forming process. For aluminium and magnesium, dynamic recrystallization and -recovery during hot forming operations, is frequently observed.(Chandrasekaran and John, 2004)

The specific occurrence of continuous recrystallization at high strains and at elevated temperatures is often referred to as geometrical dynamic recrystallization.(Humphreys and Hatherly, 2004, Doherty et al., 1997) This is a relatively new concept of dynamic recrystallization, and has been confirmed to occur in Al-Mg alloys at conditions where classic dynamic recrystallization was originally believed to occur.(Doherty et al., 1997) The most profound microstructural observation, believed to be a product of this process, is that the subgrain structure of heavily deformed material tend to remain relatively equiaxed and of consistent size through the ultra-large deformation.(Doherty et al., 1997) The absence of grain growth may be due to a higher density of high angle boundaries present in the subgrain structure. A suggested mechanism for geometrical dynamic recrystallization is presented in the following section, with a corresponding schematic illustration given in Figure 7.

During dynamic recovery, the high angle grain boundaries (HAGB) develop serrations. The wavelengths of these serrations are of the same magnitude as the subgrain size. When the material becomes deformed by a reduction of the cross-sectional area, the original grain structure becomes flattened out. It is established that at elevated temperatures, the subgrain size is almost independent of strain. As

a consequence, the boundaries are pushed together, increasing the fraction of HAGB surrounding the subgrains. Eventually, the grain boundary serrations will be of the same size as the grain thickness. The boundaries will as a result impinge, and a structure consisting of small, equiaxed grains of subgrain size, is formed. (Humphreys and Hatherly, 2004)

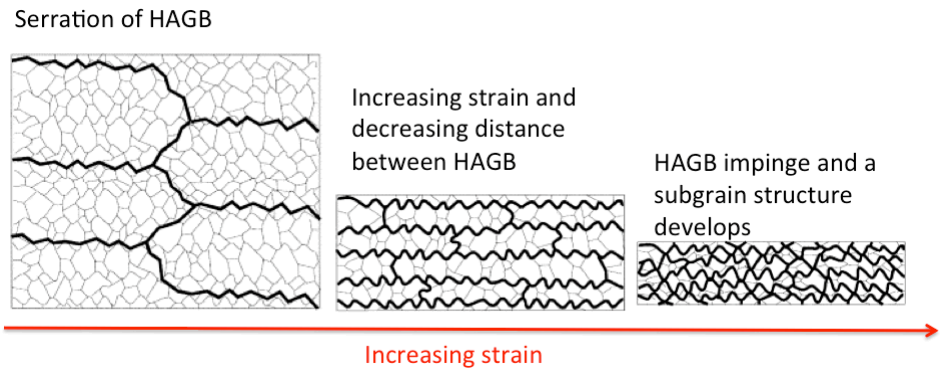

Figure 7: Microstructural changes during geometrical dynamic recrystallization. Figure adapted from(Humphreys and Hatherly, 2004).

2.4 Mechanical properties for SPD Processed Al-Mg Alloys and Composites

Lastly, it is given a short presentation of the mechanical properties of some Al-Mg systems prepared by different SPD forming methods. The ECAP process involves similar degrees of strain as in screw extrusion, and is usually executed at elevated temperatures. For an Al 1560 (Al-6Mg-0.6Mn) alloy subjected to ECAP, the following mechanical properties were reported(Markushev and Murashkin, 2004):$\sigma_{0.2}$ = 355 MPa, UTS=435 MPa, and ε_f = 20%. The high UTS is linked to the ultra-fine grains (UFG) structure obtained in the ECAP process. ECAP processed Al-AZ31 metallic composites yielded a material with lower UTS (<300 MPa), but with a fairly comparable ductility(Liu et al., 2009). Audun Bilsbak investigated screw extrusion of an AA6060 aluminium alloy. In his experiments, he obtained profiles with a strength inferior to the ECAP processed material, $\sigma_{0.2}$ = 75 MPa, UTS=164 MPa, but with an elongation at failure of 27%.(Bilsbak, 2012) It must be mentioned that the AA6060 alloy contain low amounts of Mg, and may therefore not be a good reference for the material examined in the present study. For Al-AZ31 metallic composites manufactured by the ARB process, the mechanical values depends greatly on the number of ARB passes. Therefore, the mechanical properties are often reported as approximate values. For an Al-AZ31 metallic composite, ARB processed at 400°C, mechanical testing yielded: $\sigma_{0.2}$ = 225 MPa, UTS=275 MPa, and ε_f <15%.(Wu et al., 2010) Please notice the low ductility for the ARB processed composite. This is not unusual, as the ARB composites often contain a high number of cracks that are deleterious for the ductility.

3 Experimental Procedure

This chapter outlines the experimental work performed in this study. The experimental route is summarized in Figure 8.

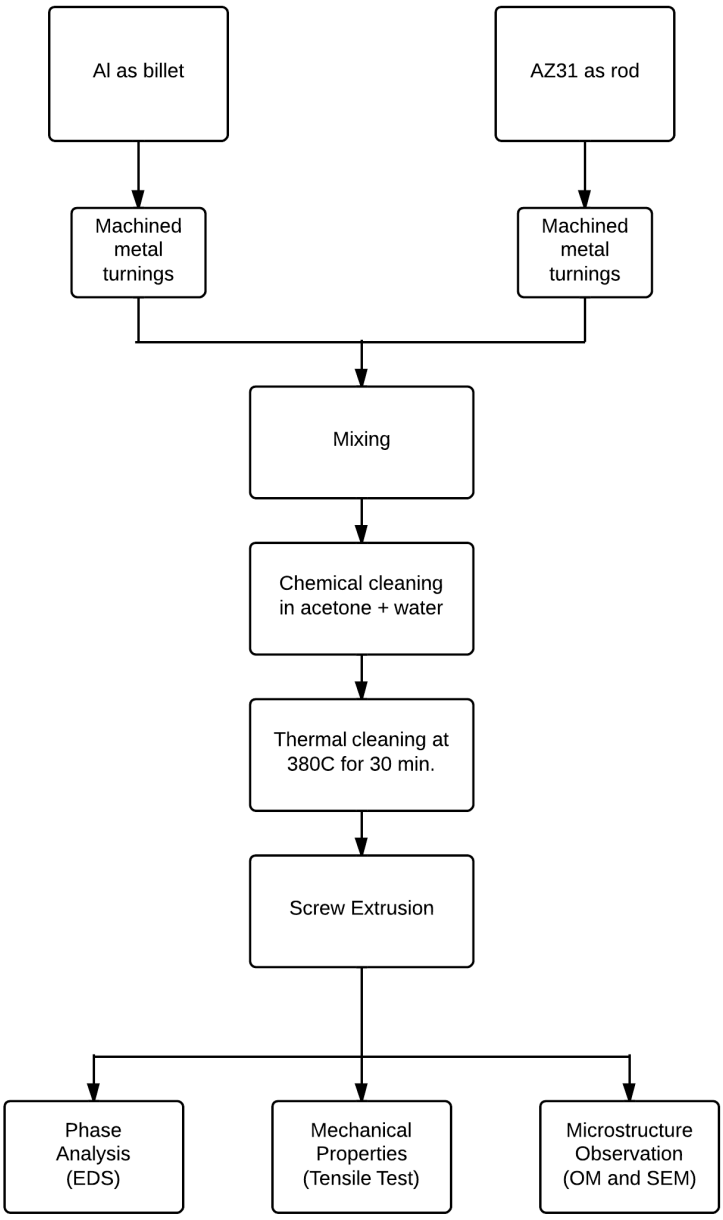

Figure 8: The flow chart illustrates the experimental route of this study, from preparation of feed stock material, to the screw extrusion trials, and finally, the examination, testing and characterization of the extrusion profiles.

3 EXPERIMENTAL PROCEDURE

3.1 Experimental Material and Feedstock Preparation

The materials used in this study were commercial pure aluminium and an AZ31 magnesium alloy. The chemical compositions of the materials are presented in Table 2. The aluminium was provided by Hydro and delivered as cast bars with dimensions 55x75x1500mm. The AZ31 alloy were marked HJR China Import and delivered as cast bars with dimensions 12x12x100mm.

Table 2: Chemical composition of feed stock materials: Al and AZ31.

Material	Element Concentration [wt%]							
	Mg	Al	Zn	Mn	Si	Fe	Cu	Ni
Al	0.0012	99.81	0.0023	0.0008	0.0758	0.0809	0.0007	0.0037
AZ31	95.46	3.091	1.023	0.421	-	0.001	0.001	-

Feedstock material for extrusion was prepared by machining the Al and AZ31 into turnings. Personnel at the Machine Tool Laboratory at NTNU performed all machining. The Al and Mg turnings were mixed to give following compositions: Al-5wt% AZ31, Al-7.5wt% AZ31, and Al-10wt% AZ31. The mixture was afterwards cut to further reduce the feedstock material size, and to achieve a homogenous distribution of AZ31 in the mixture. Pictures showing individual Al- and Mg turning sizes after final cutting are given in Figure 9.

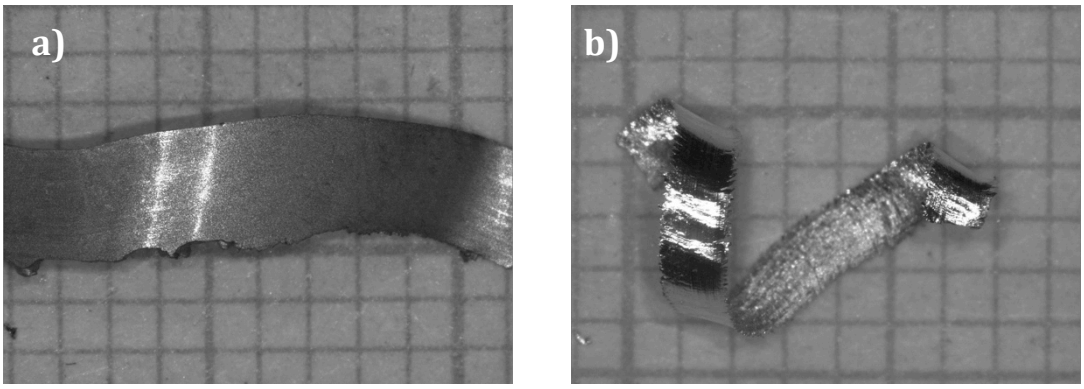

Figure 9: The feed stock material geometry after final cutting: a) aluminium and, b) magnesium. Pictures acquired with a millimeter grid paper background.

During the machining of turnings, lubricants are introduced to the feedstock material and a degreasing of the turning mixture is therefore required. Cui(Cui, 2011) investigated degreasing of scrap aluminium and found that oil residue in aluminium turnings is effectively removed by a two-step chemical and thermal treatment. Based on his results, the following treatment was performed: turnings were first cleaned in acetone and water and dried at 200˚C for 6 hours. Afterwards, the turnings were thermally treated at 380˚C for 30 minutes in a muffle furnace and finally air-cooled to room temperature.

3.2 Screw Extrusion

Extrusion was performed with a single flight research screw extruder with a 15 mm die opening. During the extrusion process, the following parameters were varied: external heating, feeding rate, rotation speed, and air-cooling. The primary focus during the extrusion trials was to keep the temperature in the die and the compact chamber around 400˚C. To ensure this, the remaining driving parameters were adjusted accordingly. It was also attempted to maintain a high rotation speed without adversely increasing the die temperature. Temperatures of the whole screw extrusion system were carefully monitored by thermoelements positioned in die, compact chamber, and linear rear, and in the screw attachment. A schematic showing the thermocouple positions are given in Figure 10.

Thermoelement no.	Position
1	Die
2	Compacting chamber
3	Liner rear
4	Screw attachment

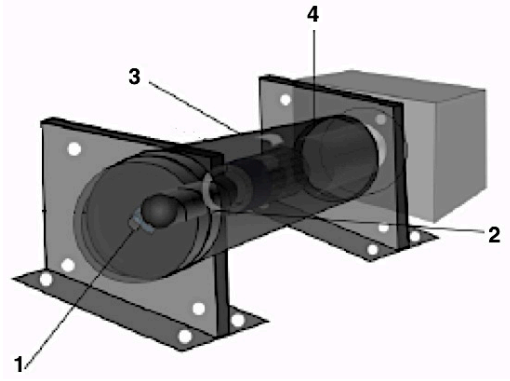

Figure 10: A schematic showing the position of the thermoelements in the screw extruder. Figure adapted from (Skorpen, 2011).

A total of four extrusion trials were conducted and extrudates with the following composition were produced: Al-5wt% AZ31, Al-7.5wt% AZ31, and two extrudates with 10wt% AZ31 content. The 10wt% AZ31 profiles are labelled Al-10wt% AZ31-1 and Al-10wt% AZ31-2: referring to first and second extrusion trial, respectively.

3.3 Sample Examination

3.3.1 Sample Preparation

Samples were collected from the cross-sectional and the longitudinal direction of the extrusion profiles, as illustrated in Figure 11, and prepared for examination in OM and SEM. The cross-sectional samples were cut, cold mounted, and prepared by conventional metallographic grinding and polishing techniques. A Discotom was utilized in the cutting and cold mounting was done in Struers Epofix epoxy. The longitudinal samples were not cold mounted, but cut and prepared by the same grinding and polishing technique. For reference, two samples were collected and prepared from the as-delivered aluminium and AZ31 bars, respectively.

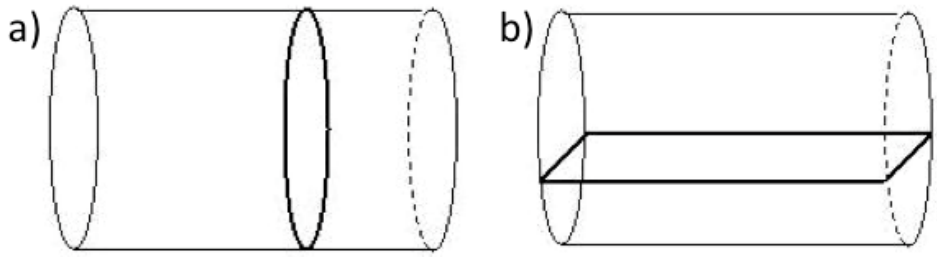

Figure 11: Schematics showing the positions within in the extrusion profile the examination samples were collected from: a) cross-sectional samples, and b) longitudinal samples.

The stepwise sample preparation was:

1. Grinding with Struers paper (SiC) from 80 to 4000-mesh size.
2. Polishing with Stuers cloth (DAC) with 3-µm diamond particle size.
3. Polishing with Struers cloth (NAP) with OP-S suspension.

3.3.2 Optical Microscopy

A Leica Reichert MeF4M Optical Microscope with polarized light was used to study the grain- and macrostructure of the extruded profiles. The samples for examination in OM were therefore anodized in 5vol% HBF_4 aqueous solution at 20 volts for 90 seconds prior to microscopy. The optical micrographs were acquired with a ProgRes C10 camera.

3.3.3 Scanning Electron Microscopy

A Zeiss Supra 55 VP Field Emission Scanning Electron Microscope (LV FE-SEM) equipped with a Bruker QUANTAX Energy Dispersive X-ray Spectrometry system (EDS) was utilized for quantitative microstructure characterization and chemical analysis.

To examine phase composition differences, Z-contrast imaging in SEM were utilized. It is generally accepted that fraction backscattered electrons, expressed by the BSE emission coefficient (η), strongly depends on the atomic number (Z) of the phase. With increasing Z, fraction BSE increases, and high Z phases will therefore appear bright in a BSE image. A specimen consisting of only a single phase will have a constant Z, and hence also a constant η, and will therefore be imaged without any contrast. In a polyphase specimen, on the other hand, Z and η will vary from phase to phase, and the phases will consequently be imaged with different intensities and contrasts.(Lloyd, 1987, Hjelen, 1989) This is schematically illustrated in Figure 12.

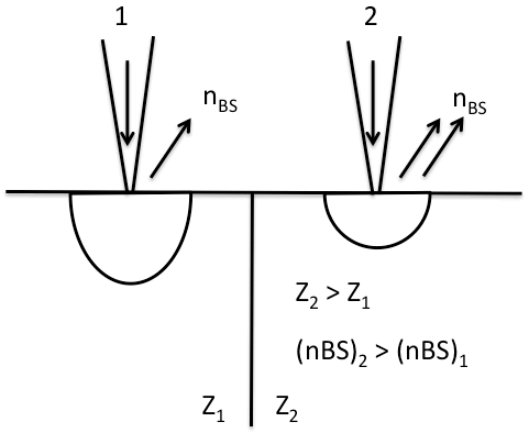

Figure 12: A schematic illustration showing how fraction emitted electrons from two phases varies with the atomic number of the phases. Here, n_{BS} is the number of backscattered electrons. Figure adapted from (Hjelen, 1989)

The backscattered signal can further be used to give information about the relative differences in mean atomic number $\bar{Z}$ of the phases consisting of multiple elements.(Hjelen, 1989) The mean atomic number for a multiple element phase is calculated by equation 3:

$$\bar{Z} = \frac{\sum(NAZ)}{\sum(NA)} \qquad (3)$$

Here N is the number of atoms of each element with atomic weight A, and atomic number Z. As an alternative, the weighted mean BSE coefficient $\bar{\eta}$ can be used, equation 4:

$$\bar{\eta} = \sum_{i=1}^{n} C_i \eta_i \qquad (4)$$

Here C_i is the concentration by weight of each element in the composition, η is the elemental BSE coefficient, and n is the number of elements present.

3.3.4 XRD Spectroscopy

Oxide powder collected from the chemical-, and thermally treated batch feed stock material, was examined by X-ray Diffraction (XRD) Spectroscopy. In the XRD analysis, an AXS D8-Focus X-ray Diffractometer was utilized. The spectrum was obtained with a 0.02 step size.

3.4 Mechanical Testing

3.4.1 Tensile Testing

The mechanical properties of the extruded profiles were examined by a standard tensile test. As test equipment, a MTS 810, 100kN servo-hydraulic universal test frame with a 5mm extensometer were utilized. The testing was conducted at room temperature and with a constant displacement rate of 2 mm/min. A total of 16 tensile test specimens were machined from the four extrusion profiles, and minimum three test specimens were prepared from each profile. A schematic showing the tensile specimen dimensions is given in Figure 13. In Table 3, the tensile test specimen abbreviations and corresponding extrusions profiles are given. The fracture surfaces of the tensile test specimens were examined in a SEM for fracture type characterization.

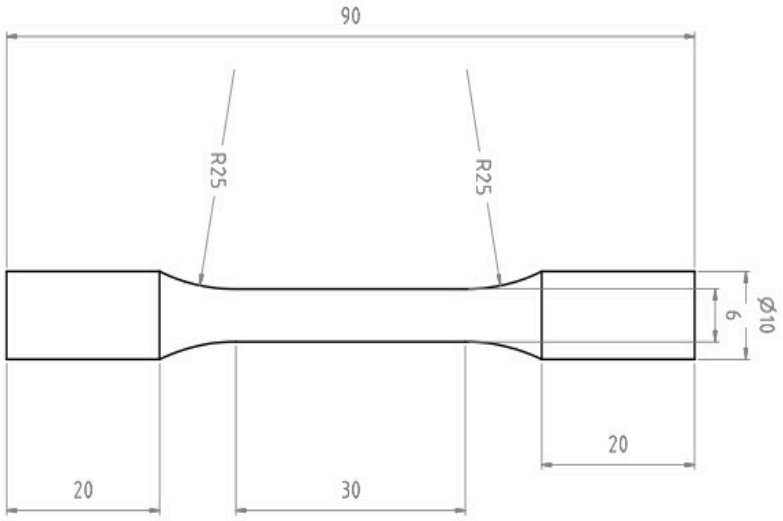

Figure 13: Schematic showing the geometry of the tensile test specimens, Specimen dimensions are given in millimeters.

Table 3: Overview of tensile test parallels and tensile test specimen abbreviation.

Extrusion Profile	Tensile Test Specimen Abbreviation
Al-5wt% AZ31	5-1, 5-2, 5-3
Al-7.5wt% AZ31	7-1, 7-2, 7-3, 7-4
Al-10wt% AZ31-1	10.1-1, 10.1-2, 10.1-3, 10.1-4, 10.1-5
Al-10wt% AZ31-2	10.2-1, 10.2-2, 10.2-3, 10.2-4

3.4.2 Macro and Micro Hardness Measurements

The macro hardness measurements were performed on a Matsuzawa DVK-1S Vickers Hardness Tester. The measurements were performed with an applied load of 1 kg, with a loading time of 15 seconds, and with a loading speed of 100 µm/sec. The micro hardness measurements were performed on a Leica WMHTMOT Vickers Hardness Tester. The measurements were performed with an applied load of 5gf, with a loading time of 12 seconds, and with a loading speed on 50 µm/sec.

The macro hardness measurements were conducted on the longitudinal samples, and a total of 12 indentations across the cross-section of the sample were performed. A schematic illustrating the position of the hardness measurements is shown in Figure 14. The micro hardness measurements were conducted on a longitudinal sample taken from the Al-10wt% AZ31-2 extrusion profile.

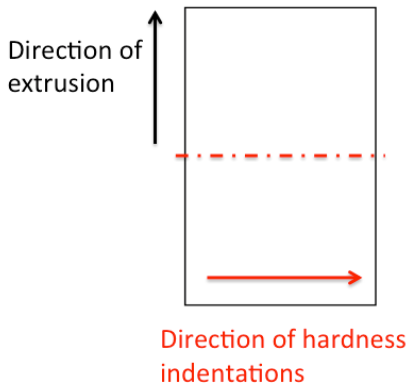

Figure 14: A schematic showing the position of macro hardness measurements conducted on a longitudinal sample.

4 Results and Discussion

Due to the limited literature available on the screw extrusion process, specifically the use of this method to manufacture metallic composites, the author has decided to combine the experimental results with discussion.

The main objective of this work is to characterize the microstructure and mechanical properties of screw extruded aluminium - AZ31 magnesium alloy bimetallic composites. The experimental results will therefore focus on the microstructure and the properties of the final extrusion profiles, and not on the extrusion execution. However, the extrusion processing parameters: temperature and rotation speed, from the four different extrusion trials will be presented, as these are relevant for the final microstructure.

4.1 Feed Stock Material

As presented earlier, it is found that oxide layers on the surface of Al and Mg turnings strongly influence the microstructure, and thus the mechanical properties, of extrudates. Therefore, the *condition* of the feed stock material is important for the mechanical properties of the final extrusion product.

The feed stock material was machined by personnel at the NTNU machine tool laboratory and delivered in three batches. The Al-5wt% AZ31 profile was produced with material from the first batch, Al-10wt% AZ31-1 with material from the second batch, while Al-7.5wt% AZ31 and Al-10wt% AZ31-2 were produced with material from the third batch. It was reported by the personnel that a different machine lubricant had been utilized during machining of the second batch.

It was a challenge to achieve properly degreasing of the material from the second batch compared to the two other batches; after full acetone- and thermal treatment, oil residue could still visually be detected in the feed stock material. In addition, an error occurred during thermally cleansing of the Al-10wt% AZ31 batch; the temperature in the muffle furnace had wrongly been adjusted from 380 to 415°C during the treatment. Taking into account that these furnaces have in addition a measurement deviation, it is probable that the temperature during the thermal treatment of this batch has been even higher than 415°C. When the feed stock material was collected from the muffle furnace, the material was completely covered by a grey powder. The powder was collected and examined by XRD and identified as magnesium oxide, MgO. XRD results are included in Appendix C: XRD

results. It is known that the rate of oxidation of magnesium rapidly increases at temperatures about 400°C.(Kim et al., 1996, Czerwinski, 2003) The high temperature during the thermal treatment of the first batch may thus explain the difference in oxidation of feed stock material of the two 10wt% AZ31 batches.

In Figure 15, the difference in condition of the feed stock material used in the two Al-10wt% AZ31 extrusion trials, is illustrated: in Figure 15a, the abnormal oxidized Al- and Mg turnings used as feed stock material in Al-10wt% AZ31-1 trial is show. In the second extrusion trial of 10wt% AZ31, the material in Figure 15b was used. In extrusion of the 5-, and -7.5 wt% AZ31 profiles feed stock material resembling the material pictured in Figure 15b was utilized. It was attempted to remove the excess oxide powder from Al-10wt% AZ31-1 batch. However, this was unsuccessful: During the feeding of feed stock material into the extruder, it was observed large agglomerates of oxide powder amongst the feed stock material, which accompanied the feed stock material into the extrusion chamber.

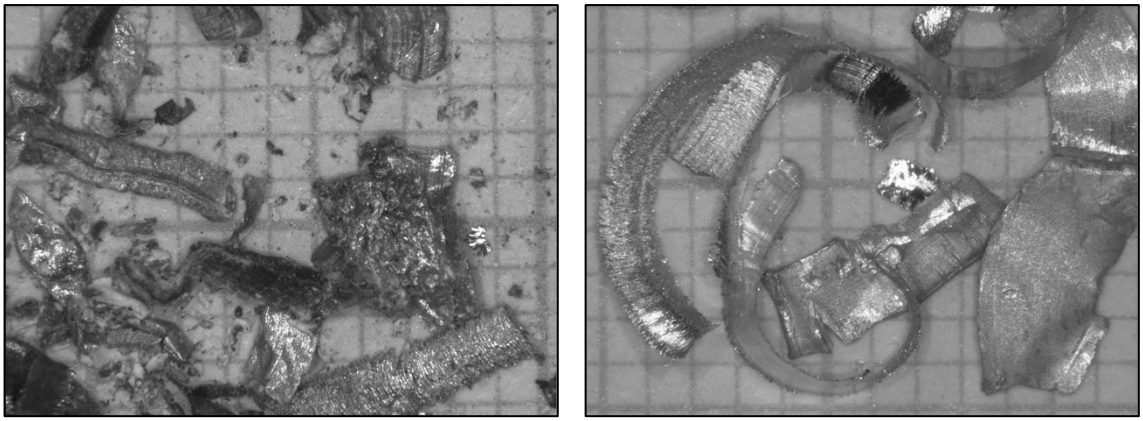

Figure 15: Difference in feed stock material condition after full chemical and thermal treatment. a) Material used in the first Al-10wt% AZ31 extrusion trial. Notice the oxidized surfaces of the material. b) Material used in the second Al-10wt% AZ31 trial.

4.2 Screw Extrusion

If success is defined as whether or not it was managed to produce a full-body extrusion profile through the screw extrusion process, four extrusion trials were conducted successfully. It has been produced extrusion profiles with the following compositions: Al-5wt% AZ31, Al-7.5wt% AZ31, Al-10wt% AZ31-1, and Al-10wt% AZ31-2. In this section the screw extrusion processing parameters; i.e. extrusion temperature and rotation speed, for the four individual extrusion trials are presented. Furthermore, the surface structure and the microstructure of the extrusion profiles are presented and discussed.

4.2.1 Extrusion Processing Parameters

In Figure 16, the temperature measured in various positions in the extruder, during the complete extrusion trial of Al-10wt% AZ31-1, is plotted. Similar plots for the three remaining extrusion trials are included in : Screw Extrusion Process Parameters. The temperature was measured in four positions: i.e. in the die, compacting chamber, liner rear, and screw attachment positions. The two latter positions are important for controlling the temperature in the machinery, and do not effect the material being extruded. The die- and compact chamber temperatures, on the other hand, strongly influence the extrudates microstructure. Recrystallization, recovery, grain growth, and diffusion, are all strongly strain and temperature dependent phenomena. Furthermore, from the Al-Mg phase diagram it is given that the eutectic temperature for the aluminium rich area is 451°C. Temperatures of this magnitude may thus cause local melting of the material, which may lead to chemical mixing of the Al and AZ31 alloy, chemical segregation and local concentration differences.

Unfortunately, the extrusion trials were conducted with limited control of the process parameters. As earlier stated, primary focus during the extrusion process was to keep the die and compact chamber temperatures around 400°C. In Figure 17a-d, the variation in die and compact chamber temperatures during the four extrusion trials, are plotted. From the temperature plots it is clear that it was not achieved to maintain temperatures within the temperature restriction, in neither of the extrusion trials. It can be seen that large variations in temperature occurred in all four trials, and that the temperature in the die was far above 400°C and that in all trials a die temperature of 420°C was recorded. However, due to flow variations inside the extrusion chamber; most likely there will be regions in the extrusion profile that have experienced locally, both higher and lower temperatures. Furthermore, there may also be local areas that have experienced higher friction, which also affects the temperature.

From the graphs in Figure 17, it is obvious that it was not achieved to keep a constant temperature in the die and compact chamber. Furthermore, it is observed that only during extrusion of the Al-5wt% AZ31 profile, the temperature was maintained below 420°C. That friction influences the temperature in the screw extruder can be observed in Figure 18. In this figure the die temperature and rotation speed during the extrusion of the Al-7.5wt% AZ31 profile, are plotted. Please notice that as the rotation speed increases, a subsequent increase in die temperature is achieved. The same pattern was observed in the other extrusion trials as well. Due to the effect of the rotation speed on temperature, it was hard to maintain a high rotation speed during the whole trials.

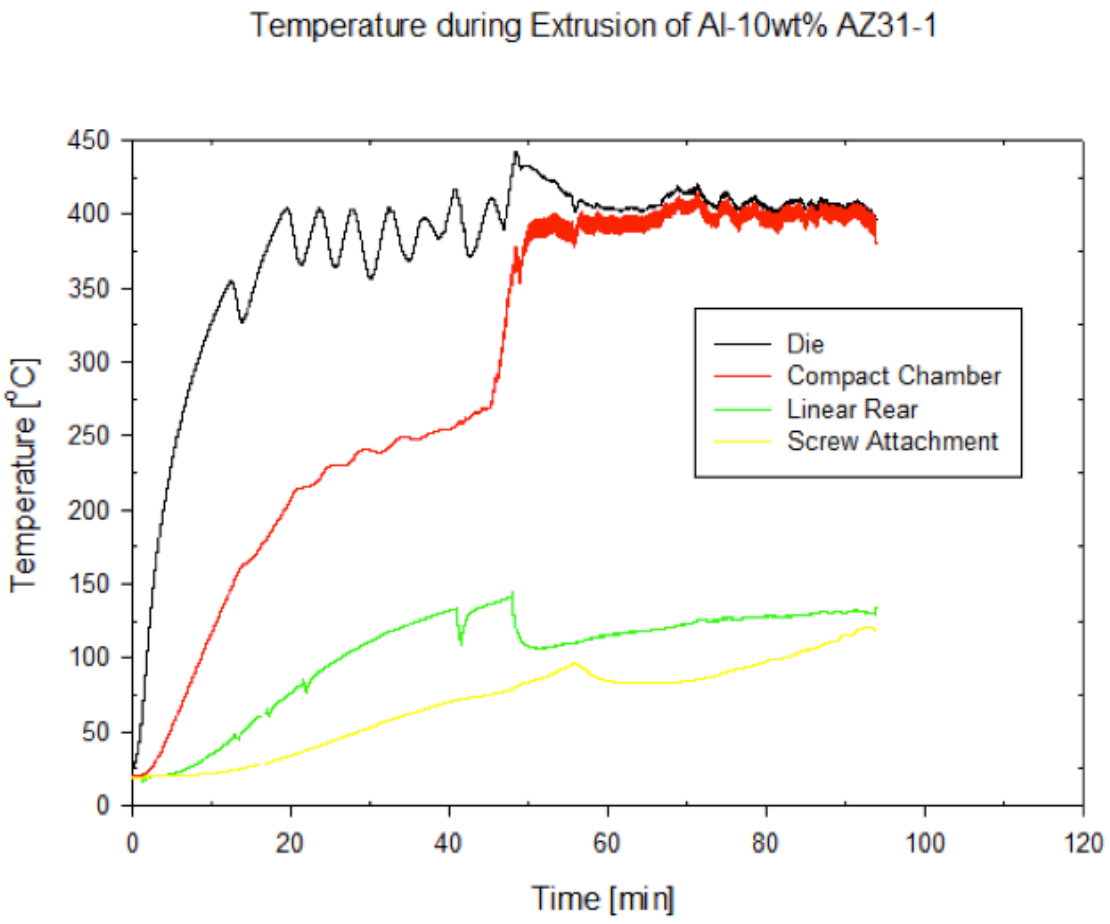

Figure 16: The temperature measured in the screw extruder during the extrusion of the Al-10wt% AZ31-1 profile.

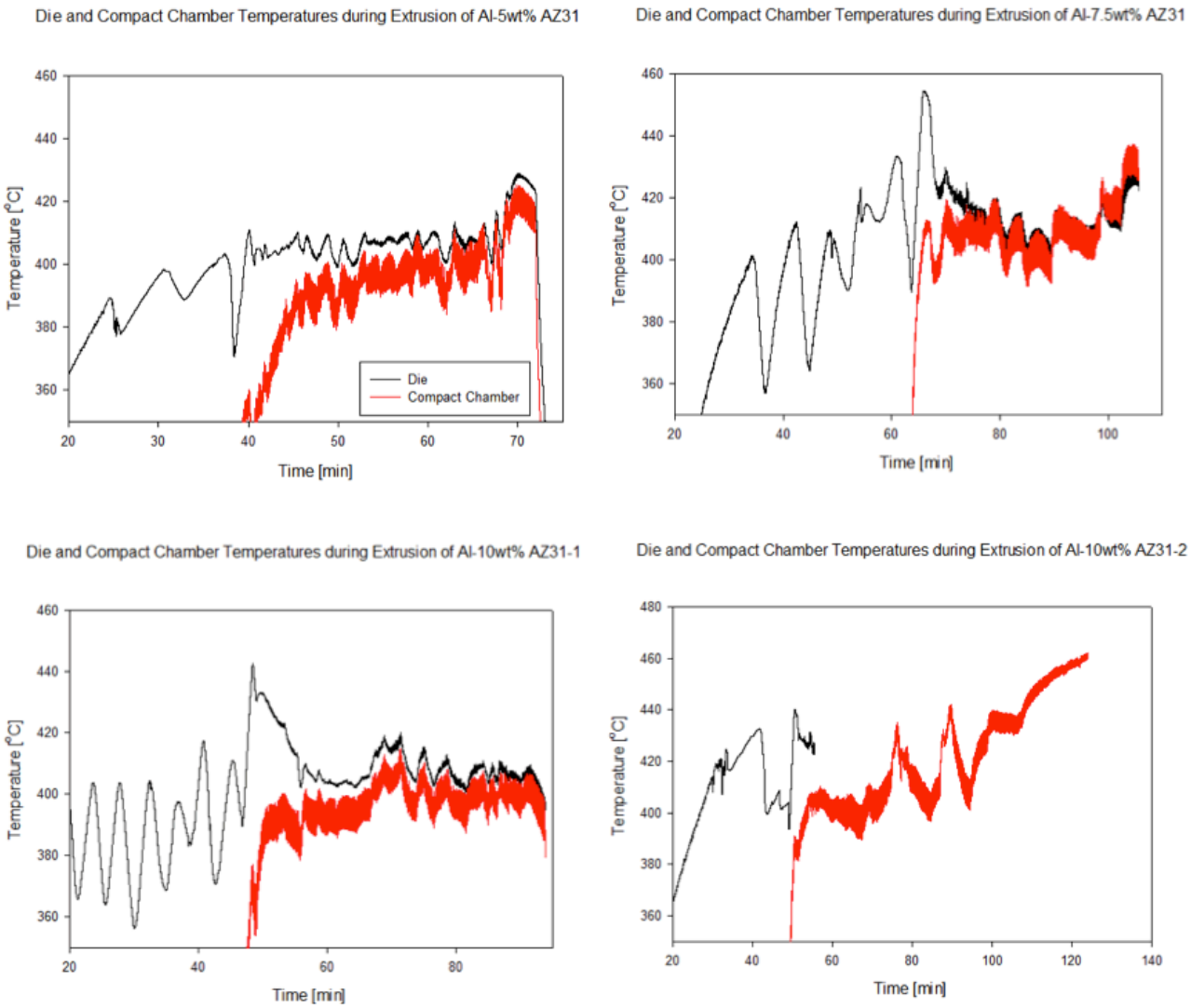

Figure 17: Variation in die and compact chamber temperatures during extrusion of a) Al-5wt% AZ31, b) Al-7.5wt% AZ31, c) Al-10wt% AZ31-1, and d) Al-10wt% AZ31-2. Please notice the difference in temperature scale in d)-

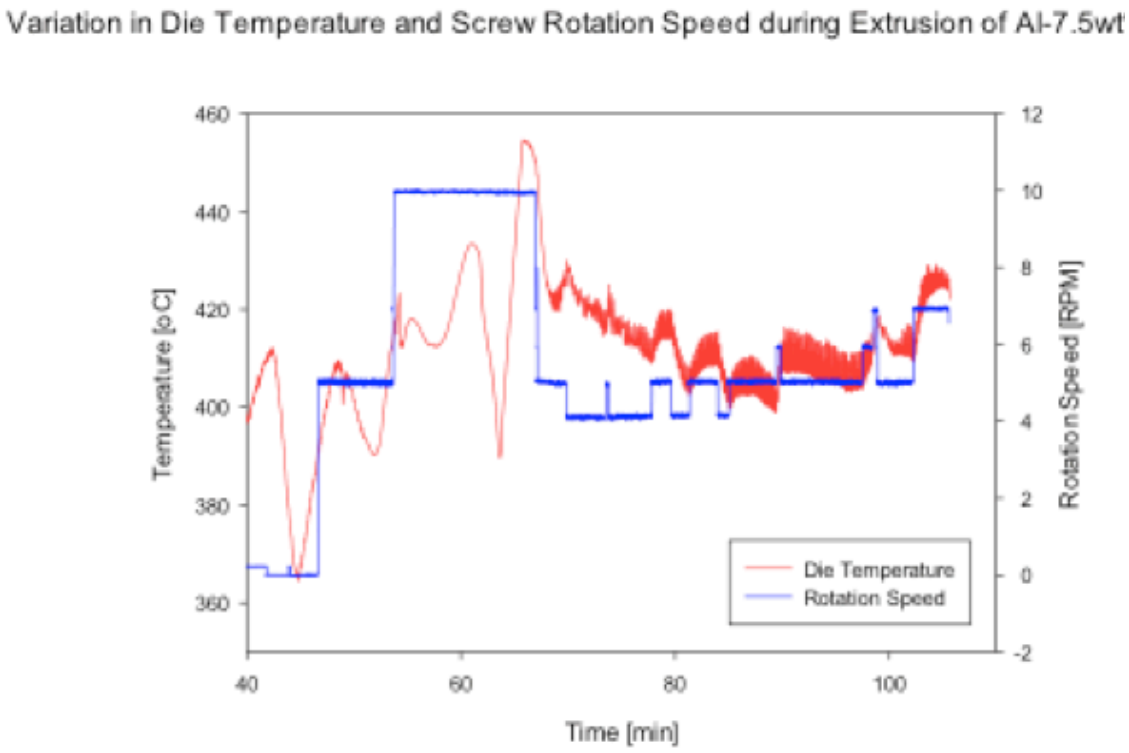

Figure 18: Variations in die temperature and rotation speed during the extrusion of the Al-7.5wt% AZ31 profiles. Please notice that a high peak in die temperature was obtained when a high rotation speed was utilized, but also the corresponding fall in temperature when the rotation speed was lowered.

4.2.2 Extrusion Profile Surface Appearance

Macrographs showing the surfaces of the Al-5wt% AZ31, Al-7.5wt% AZ31, Al-10wt% AZ31-1, and Al-10wt% AZ31-2 extrusion profiles are given in Figure 19. The four profiles differ from each other in both surface finish and in profile geometry. Profile geometry here refers to the cross-sectional area of the profile, and it is observed that in some of the extrusion profiles, the cross-section radius is less than 15 mm. The surfaces vary from being smooth with a metallic glossy finish, to having a rough and matte grey finish. There are also variations in surface appearance along each individual profile.

During the screw extrusion process it could be observed that the profile surface finish depended greatly on die temperature and rotation speed. When these two parameters were changed, it could be observed a response in the surface layer of the extrusion profiles. At high die temperatures (T>420°C) the profile surface suffered a “burnt” look – the surface became matte grey, started to flake and cracks in the surface layer appeared. Variation in rotation speed manifested itself as ring

marks in the profile surface layer. Rotation speed is here referred to as being low, medium or high where a low rotation speed produced a profile with a high density of ring markings and a high rotation speed yielded a smoother profile.

The Al-5wt% AZ31 profile is illustrated in Figure 19a. The profile has a metallic surface finish and the high density of rings markings can be observed. The profile has an overall homogenous surface finish with little variance in surface appearance along the profile, but cracks are observed. Even though the profile has ring markings, the geometry is less affected and has an overall constant cross-sectional radius.

The Al-7.5wt% AZ31 profile is presented by three macrographs, Figure 19b-d. The macrographs represent three different sections of the profile. The sections differ from each other by the screw extrusion speed they were subjected to during extrusion. Specimen 7-1 (Figure 19b) was produced at low rotation speed; specimen 7-2 (Figure 19c) represents the section of the profile produced at medium rotation speed, while specimen 7-3 (Figure 19d) was produced at high rotation speed. Of these three, sample 7-3 has the overall best finish, not only for the three Al-7.5wt% AZ31 samples, but also for all four profiles.

Two attempts in producing an Al-10wt% AZ31 composite were performed. The first Al-10wt% AZ31 extrusion profile is shown in Figure 19e. This profile has the most distinctive appearance and is untypical from the rest of the extrusion profiles. The profile has a matte and rough surface finish and a jagged geometry. The second 10wt% AZ31 profile resembles the 5wt% AZ31 profile, only with less ring markings.

In Figure 20a-b, the cross-sections of Al-7.5wt% AZ31 (sample 7-3) and Al-10wt% AZ31-1 profiles are compared. Please notice that sample the 7.5wt% sample has a smooth and continuous cross-section surface geometry, while the 10wt% sample has a jagged, in-continuous appearance. As a consequence, the 10wt% AZ31 profile has an effective smaller profile radius than the Al-7.5wt% AZ31 profile. It is possible that the variations in profile geometry will effect the tensile testing of the specimens; tensile test specimens are machined from the profiles and will be machined to the same dimensions.

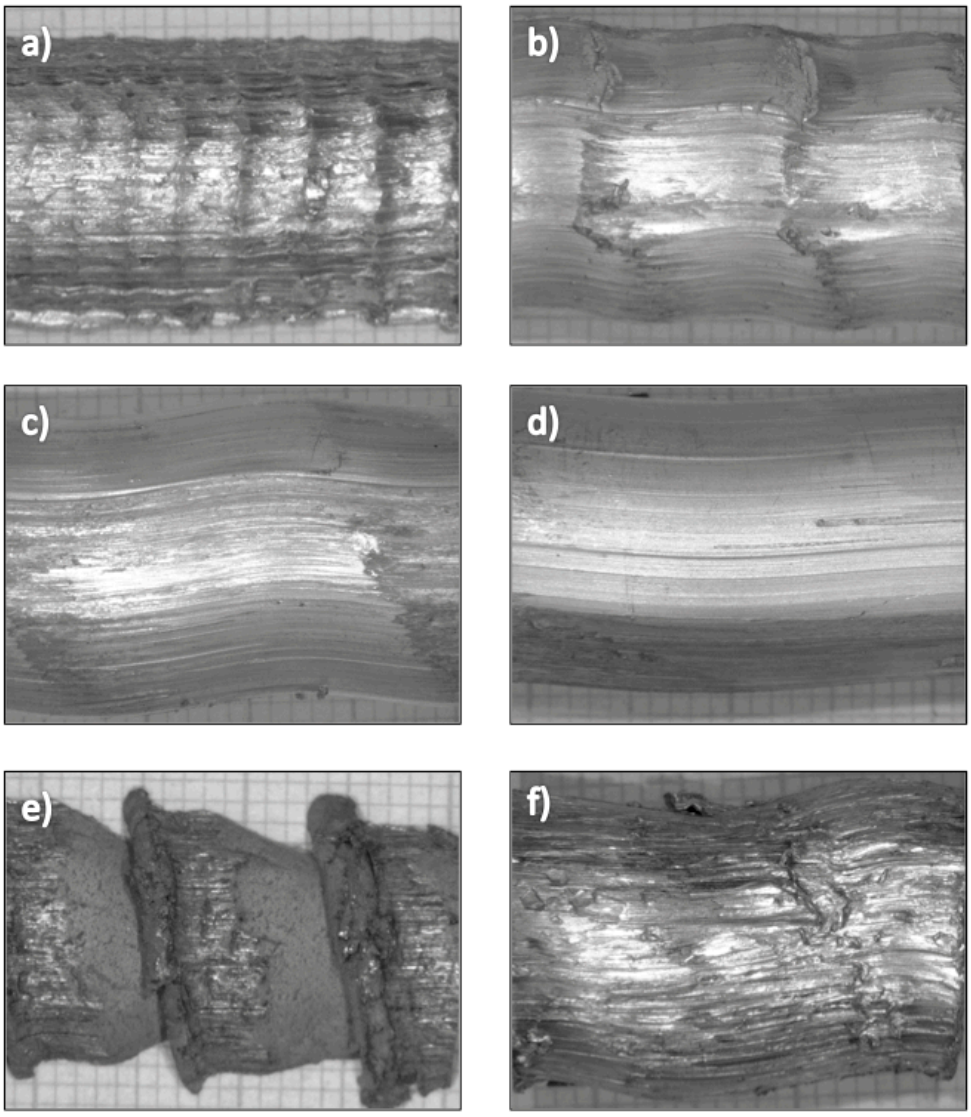

Figure 19: Macrographs showing the surface of the extrusion profiles: a) Al-5wt% AZ31, b) Al-7.5wt% AZ31, lowest rotation speed (7-1), c) Al-7.5wt% AZ31, medium rotation speed (7-2), d) Al-7.5wt% AZ31, highest rotation speed (7-3), e) Al-10wt% AZ31-1, and f) Al-10wt% AZ31-2

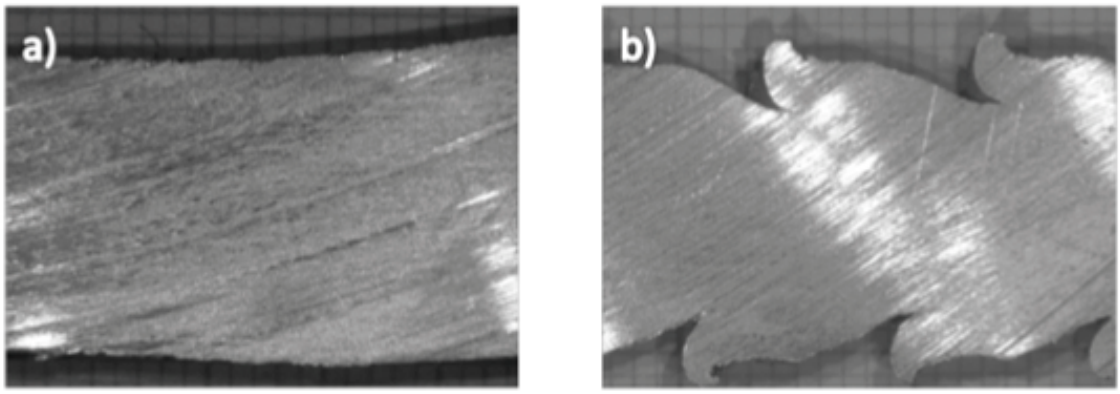

Figure 20:In the pictures, the difference in geometry of the cross-sectional area, between the a) Al-7.5wt% AZ31 profile (sample 7-3), and b) the Al-10wt% AZ31-2 profile.

4.3 Extrusion Profile Microstructure

The grain structure is one of the main dictating elements for the mechanical properties of a metal. Extruded products normally have a complex grain structure owing to the plastic deformations they are subjected to, in addition to the different phenomena, i.e. recovery, recrystallization, and grain growth, taking place both during, and after, the extrusion process. In a composite system, the mechanical properties of the final product will furthermore greatly depend on how the strengthening phases are present in the matrix. For the present study, it is central to understand how the AZ31 magnesium alloy interacts with the aluminium matrix. To investigate this, the microstructure of the extrusion profiles was examined in an OM under polarized light, and in a SEM, where a backscatter detector was utilized. The SEM examination was combined with EDS phase analysis.

4.3.1 Optical Microscopy

All samples illustrated in this section were anodized in a 5vol% HBF_4 electrolyte and acquired in polarized light by an OM. In Figure 21, optical micrographs showing the pre-machining-into-turnings microstructure of the reference Al and AZ31 material are shown. It is obvious that the constituents Al and AZ31 reacted differently on the anodization treatment: In Figure 21a, the as-cast microstructure of aluminium, consisting of large grains, is clearly displayed. The AZ31 microstructure is attempted displayed in Figure 21b. It is evident that AZ31 becomes severely corroded in a HBF_4 electrolyte. The AZ31 surface appears dark in the polarized light, and it is not possible to distinguish the individual grains.

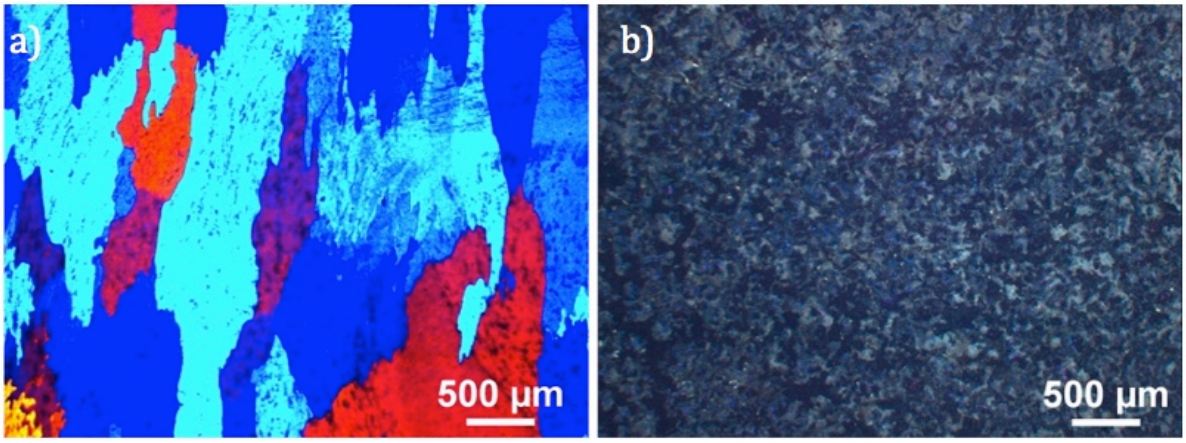

Figure 21: Optical micrographs showing the initial microstructure of the feed stock material prior to machining: a) aluminum, and b) AZ31.

During preparation of the extruded samples, it was observed that with higher contents of AZ31 in the sample, it became harder to obtain a properly anodized sample surface. During anodization of the 10wt% AZ31 cross-sectional samples, the HBF_4 solution became unstable, and started to simmer when the samples were immersed in the electrolyte. It was observed that this effect became even more pronounced during anodization of the longitudinal samples, where anodization of both 5- and 7.5wt% AZ31 samples produced instability in the HBF_4 solution. The behaviour resembled what was observed during the anodization of the AZ31 reference sample.

Figure 22 gives an overview of the structure in the cross-section area of the four extrusion profiles: a) Al-5wt% AZ31, b-d) Al-7.5wt% AZ31, e) Al-10wt% AZ31-1, and f) Al-10wt% AZ31-2. The images have been obtained by assembling five micrographs acquired at 2.5X magnification, into one picture. A general observation is that it has been managed to produce four full-bodied, relatively fine-grained extrudates by the screw extrusion process. However, except for the Al-7.5wt% AZ31 profile, the microstructure of the profiles are far from homogenous. There are observed regions with a very-fine-grained microstructure, and regions with a more pronounced grain size. These regions are especially visible in the 5-, and 10-2wt% AZ31 profiles. Furthermore, a spiral pattern descending inwards to the centre of the specimens can be observed. The spiral pattern is a characteristic feature of the screw extrusion process, and has been observed in all of the extrusion profiles produces in earlier work, and the pattern usually comprises of grains of uneven size.(Ringstad, 2009, Skorpen, 2011, Bilsbak, 2012, Widerøe and Welo, 2012) In the extrusion profiles produced in this study, grey regions are

observed to accompany the spiral pattern. These grey regions will be discussed further in later sections.

The inhomogeneity in the microstructures are consistent with the theory for the material flow of the screw extrusion process, described by Widerøe and Welo: The extrusion profiles are composed of various layers of material subjected to different degrees of strain, temperature, and also time in the compacting chamber. This will affect the microstructure, as each of these layers will be subjected to a different amount of recrystallization, recovery and grain growth (i.e. thermo-mechanical history).(Widerøe and Welo, 2012)

The areas subjected to the largest amount of deformation have, as a consequence, experienced a higher strain and a higher temperature. The threshold temperature for onset of dynamic recrystallization in a given material is at a temperature $T>0.5T_m$. For Al and AZ31, dynamic recrystallization will roughly occur at temperatures above 330°C, and 315°C, respectively.(Murray, 1982) Since the temperatures measured in the die, and compacting chamber, Figure 17, were far above 400°C during the whole extrusion process, it is very likely that dynamic recrystallization has occurred in all profiles. Dynamic recrystallization will result in a fine-grained microstructure, as long as the holding time at an elevated temperature is short, but at long holding times, extensive grain growth may occur. After the extrusion of the material through the die, the material becomes rapidly cooled, and grain growth in the extrusion profile will as a consequence be limited. It is therefore likely that the observed fine-grained areas are areas consisting of recrystallized grains. The areas consisting of larger grains appear as distinct bands, located near the edge of the samples, and at a position midway from the centre. These bands are particularly observed in the 5-, and 10-2wt% AZ31 samples.

In Figure 23, the microstructure in the longitudinal direction of the 5wt% AZ31 sample is shown. In this figure two regions of different grain size are highlighted. It can be observed that the large grains are elongated in the direction of extrusion. It can therefore be argued that these areas are remains of the deformation structure, and have not undergone extensive recovery or recrystallization. In Figure 22b-d, the microstructure for the Al-7.5wt% AZ31 extrusion profile, at different rotation speeds, is displayed, and it can be seen that with increasing rotation speed, the less clear the spiral pattern become. In Figure 22d, which displays the microstructure in the sample subjected to the highest rotation speed, the spiral pattern is almost undetectable. Remembering that increasing rotation speed induced higher temperatures in the die, and in the compacting chamber, the absence of spiral pattern may indeed be explained by a higher extrusion temperature (i.e. most likely initiating local melting where Al and AZ31 are neighbouring).

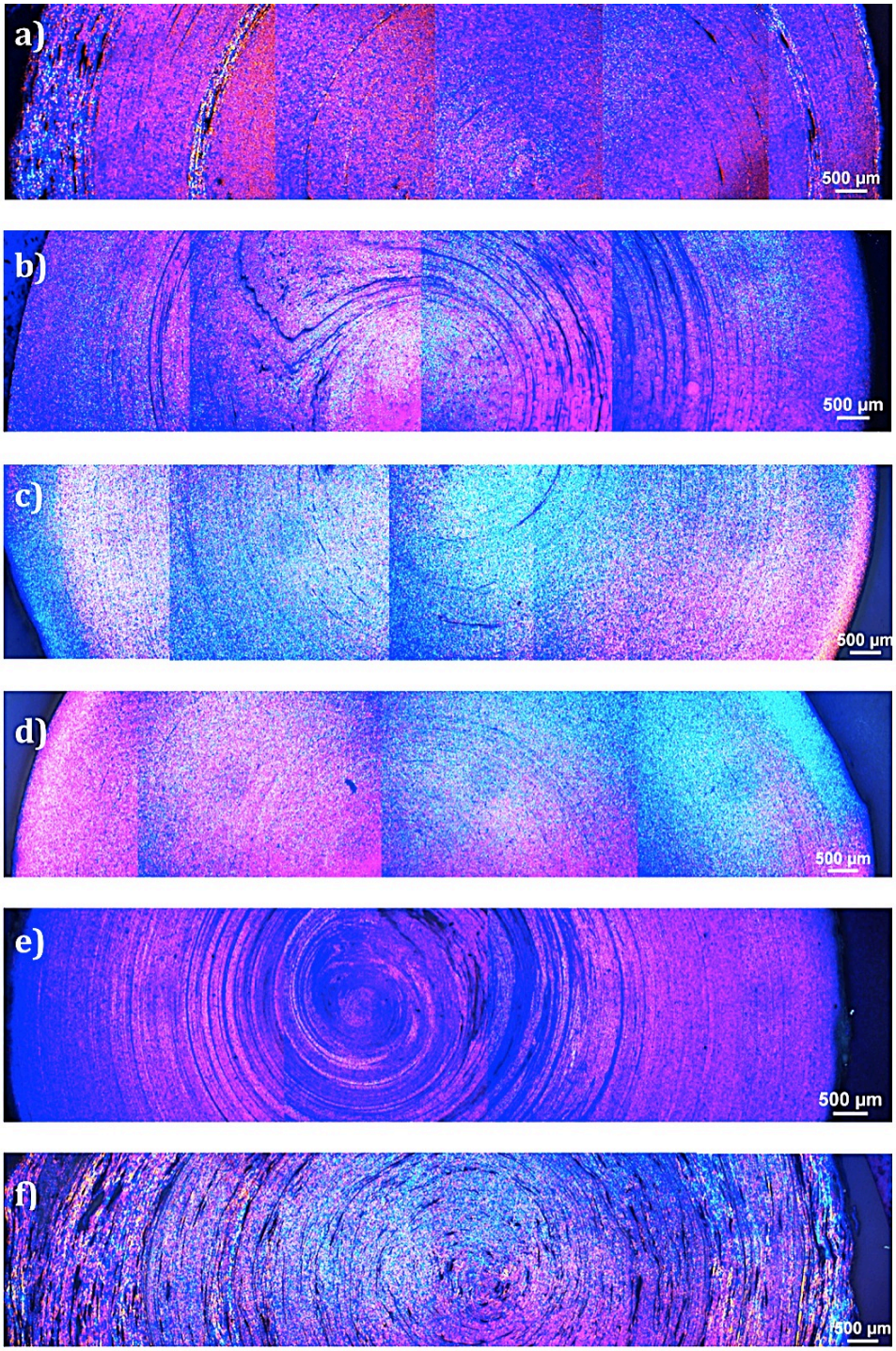

Figure 22: Optical macrographs showing the cross section microstructure of the extrusion profiles: a) Al-5wt% AZ31, b) Al-7.5wt% AZ31 (7-1), c) Al-7.5wt% AZ31 (7-2), d) Al-7.5wt% AZ31 (7-3), e) Al-10wt% AZ31-1, and f) Al-10wt% AZ31-2.

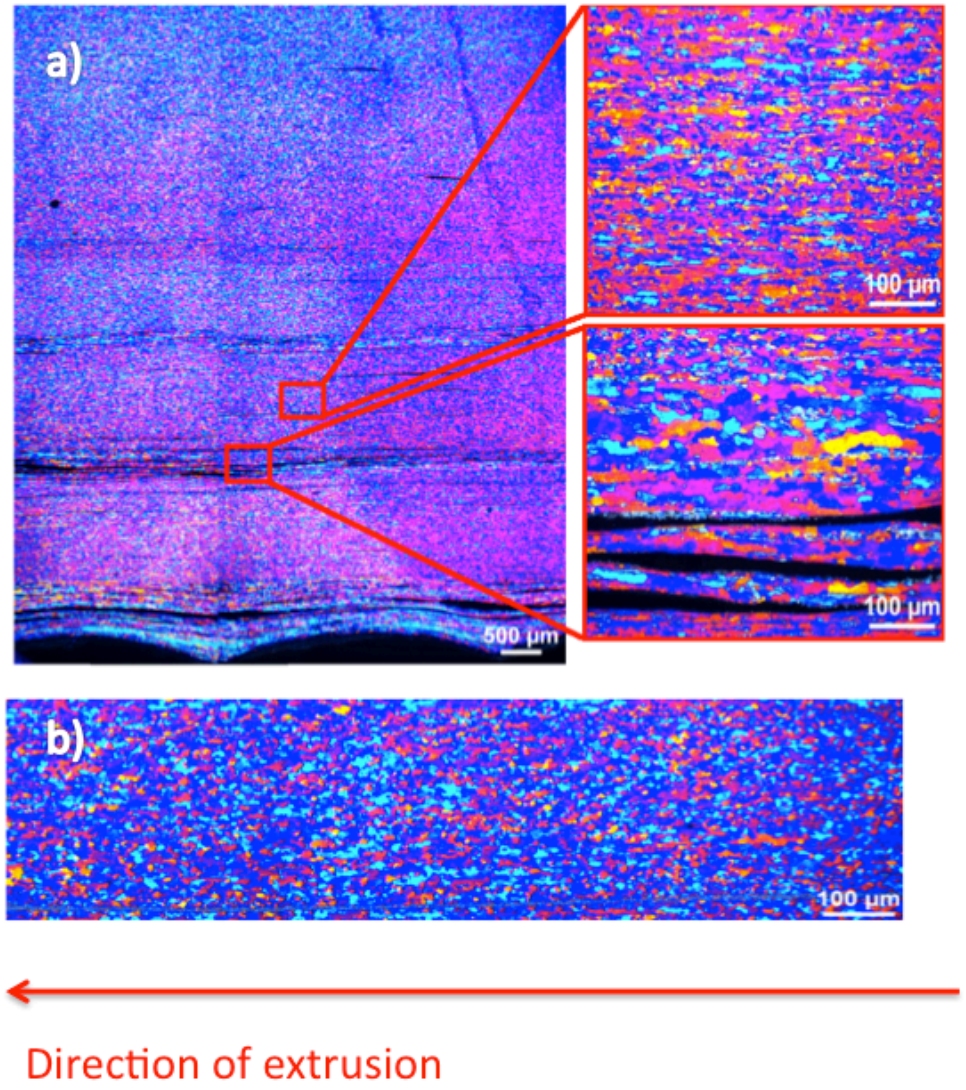

Figure 23: a) Optical micrographs of Al-5wt% AZ31 in the longitudinal direction, showing the difference in grain size at two positions. b) Grain size in the center of the same longitudinal sample. The grain structure is fairly homogenous, and

Examination in the OM could not detect any individual AZ31 regions in neither of the samples. However, there are observed distinct black, and grey areas. The black regions are located near the surface, and midway to the centre of the extrudates. The grey areas are distributed through the cross-section, and as already mentioned, can be observed to accompany the spiral pattern descending inwards to the centre of the specimen. The grey areas are observed, in varying amounts, in all of the four extrusion profiles. The areas bear a resemblance to the surface appearance of the anodized AZ31 reference sample, Figure 21b. With the general high reactivity of Mg in mind, and the behaviour displayed by the samples with high AZ31 content during anodization, it is likely that the grey areas are regions

containing a higher concentration of magnesium than the bulk microstructure. An example of black and grey areas observed near the edge, and in the centre of the Al-10wt%AZ31-2 profile, are shown in Figure 24. The black areas appear like shallow pits or pores. Adjoining these black areas, are the bands of large, elongated grains, as recently discussed. A possible explanation can therefore be that these areas have experienced a lower temperature than the surrounding regions, and that this has led to unsuccessful bonding, hence the pits, and a delayed onset of dynamic recrystallization, which explains the remaining deformation grain structure.

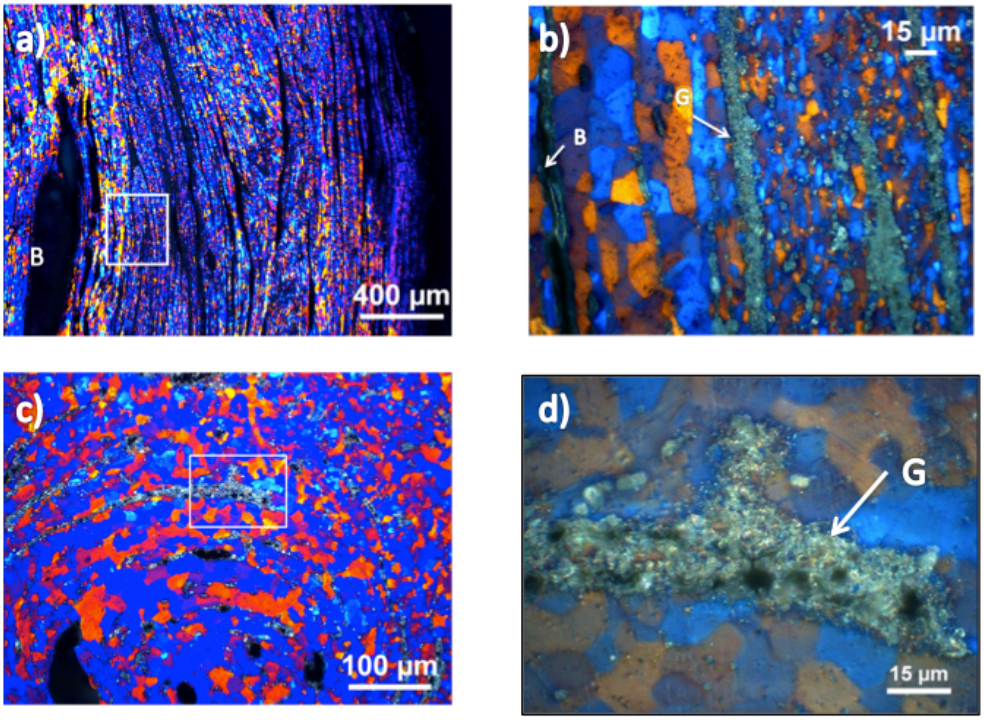

Figure 24: Optical micrograph of the cross-section of the Al-10wt% AZ31-2 extrusion profile. In a) a large black region (B) in the microstructure, is shown. In b) the section highlighted in a) is magnified, and both black (B), and grey (G) areas are indicated with arrows. Please notice the large grains surrounding the black regions.

In Figure 25, the grain structure in the centre of the cross-section of the four profiles is displayed: a-b) Al-5wt% AZ31, c-d) Al-7.5wt% AZ31, e-f) AL-10wt% AZ31-1, and g-h) Al.-10wt% AZ31-2. It is obvious that screw extrusion of Al-AZ31 components produces profiles with a very fine-grained microstructure. But, as already discussed, the grain size varies from profile to profile. The most noticeable observation is the extreme small grain size in the Al-10wt% AZ31-1 sample - especially in comparison to the other 10wt% AZ31 profile. It is also noticed that there is an excessive amount of grey constituents present in the microstructure of the 10-1 sample. There are such constituents present in the other extrusion

profiles as well, but neither in the same amount, or of the same size, as observed in the 10-1 sample. It is well known that oxide dispersion particles prevent growth of matrix grains during deformation.(Gronostajski and Matuszak, 1999, Hu et al., 2008, Cui, 2011) Recalling the extensive oxidation the feed stock material of the 10-1 profile underwent; it is possible that the precipitates observed are indeed oxide particles – and that these have effectively restricted the grain growth in the 10-1 profile. There are two possible scenarios for how the oxide particles can have been introduced into the matrix: 1) the oxide particles originates from oxide films, initially present on the surface of the Al- and AZ31 turnings, that have been broken up during the extrusion, due to the severe deformation, or 2) the particles have been introduced as excess bulk oxide powder. The latter is most likely the case for the 10-1 sample as large agglomerates of oxide powder were observed amongst the Al- and AZ31 turnings during feeding of the feed stock material into the extruder. In either case, dispersion of oxide precipitates in the matrix give rise to grain refinement and a corresponding increase in strength. However, as discussed by Hu et al., excessive amount of oxides can adversely affect mechanical properties, where especially the ductility decreases dramatically.(Hu et al., 2008) Furthermore, as always with precipitate strengthening, small and homogenously dispersed particles are always preferred –it is therefore expected that the first scenario for oxide precipitate dispersion will be most effective in favouring the mechanical properties of the extrudates.

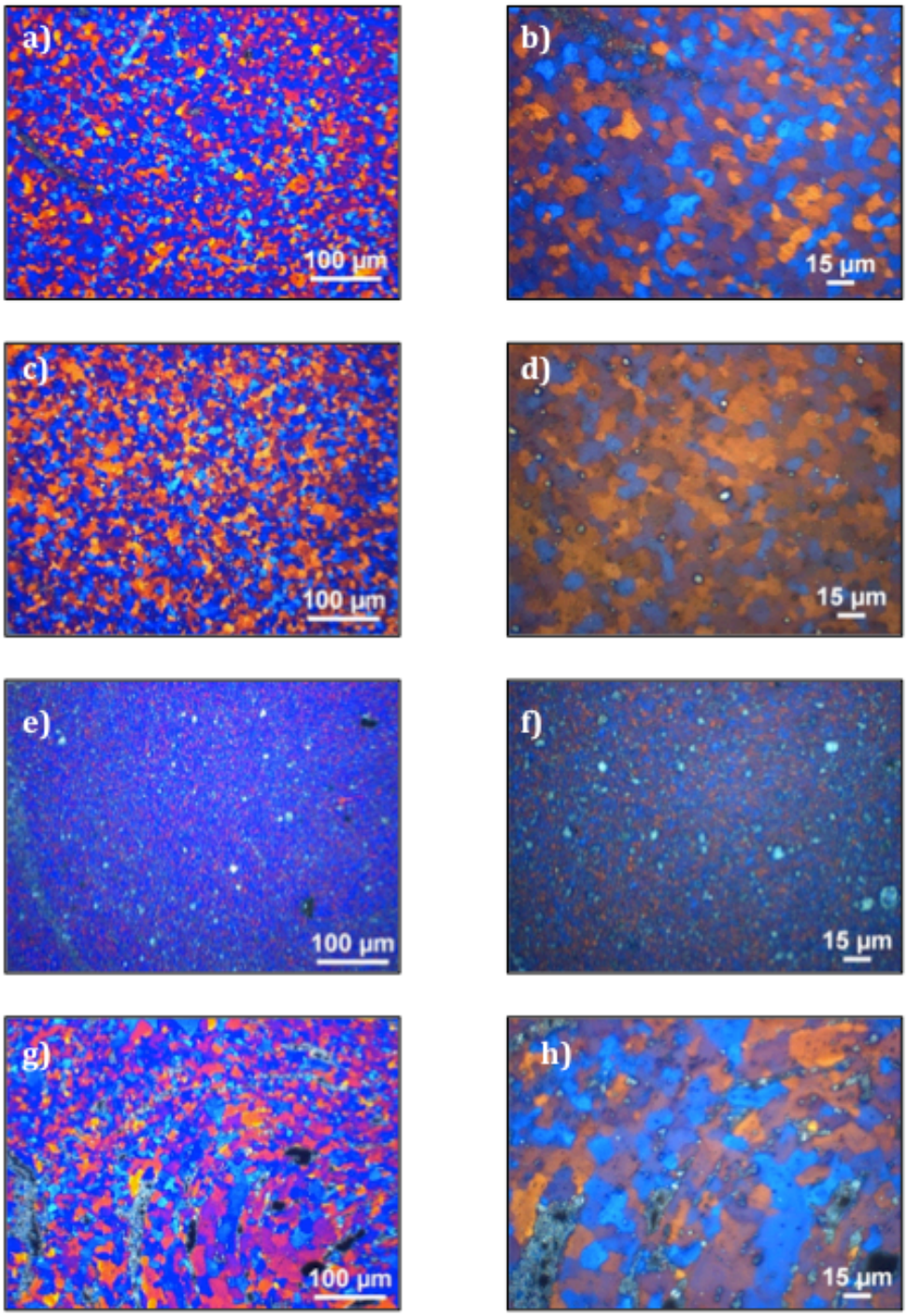

Figure 25: Optical micrographs showing the microstructure in the centre of the extrusion profiles: a-b) Al-5wt% AZ31, c-d) Al-7.5wt% AZ31, e-f) Al-10wt% AZ31-1, and g-h) Al-10wt% AZ31-2.

4.3.2 Scanning Electron Microscopy

In this section a selection of SEM micrographs of the four extrusion profiles are presented and compared. Characteristic features in the extrusion microstructure are also presented. The SEM examination was combined with EDS point analyses to determine the chemical composition of the different features. The SEM micrographs were acquired with a backscatter detector, with a 120-µm aperture, at 10 mm working distance, and with a 20kV electron gun acceleration voltage.

In Figure 26, SEM micrographs showing the microstructure of the four extrusion profiles are given: a) Al-5wt% AZ31, b) Al-7.5wt% AZ31, c) Al-10wt% AZ31-1, and d) Al-10wt% AZ31-2. These images give a similar presentation of the microstructure as the images acquired in the OM in polarized light: the profiles have an inhomogeneous microstructure, built up of numerous layers of different thicknesses. Whereas the polarized light imaged these layers as layers of alternating grain size, the grain structure cannot be observed in the SEM micrographs. In stead, the layers are imaged in varying shades of grey, and varying amounts of particles are observed in the layers. As in the optical micrographs, distinct grey and black areas, or *phases,* are observed. The phases are observed to assemble in distinct bands. As detected in the optical microscope, these bands are located towards the outer edge of the sample, and at a position midway to the centre, and are primarily observed in the 5-, and the 10-2wt% AZ31 profiles. The grey phases are most likely secondary phases, and must not be confused with what is referred to as grey layers. In Figure 27, it is indicated what is referred to as a layer, and what is called a grey phase. In the latter figure one can distinguish between two different phases, denoted the type 1, and the type 2 grey phase. These phases will be more thoroughly discussed below.

Again, the Al-7.5wt% AZ31 profile stands out as the extrudate with the most consistent, homogenous microstructure. First of all, no *bands* with high density of secondary phases and pores are observed in this profile. There are, however, observed a few, dispersed grey phases, but not of same magnitude as in the 5-, and 10-2wt% AZ31 samples. The Al-10wt% AZ31-1 profile also stands out; no secondary phases can be detected, and the intensity of the alternating grey layers are more profound in the 10-1 sample than in the rest. In addition, the Al-10wt% AZ31-1 profile contains large amounts of massive dark particles.

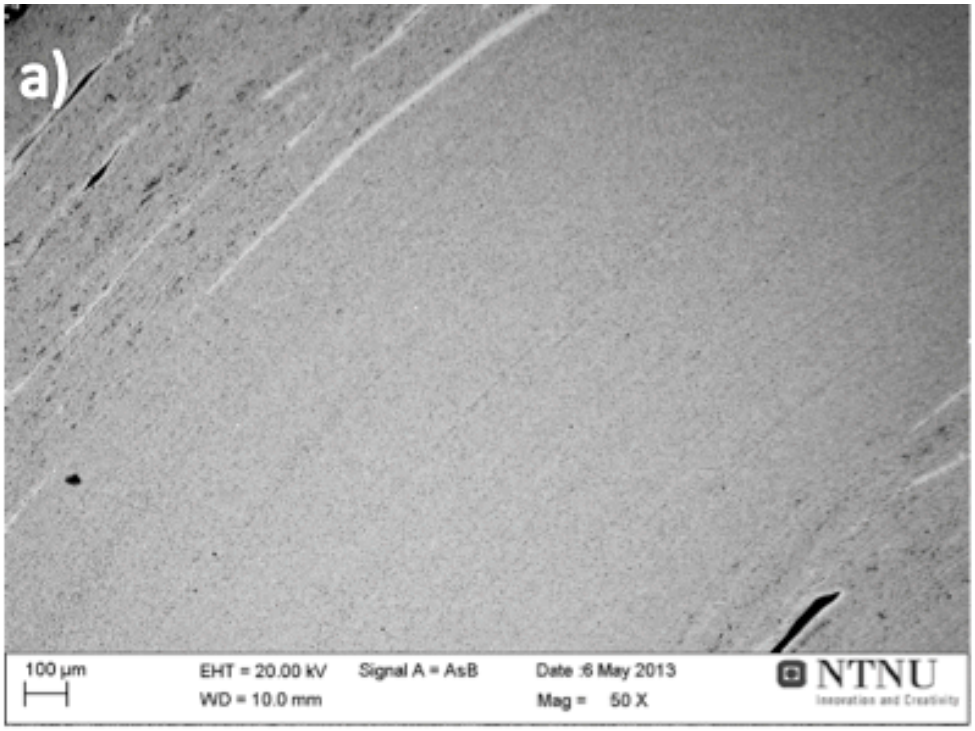
a)
100 µm
EHT = 20.00 kV
WD = 10.0 mm
Signal A = AsB
Date :6 May 2013
Mag = 50 X
NTNU
Innovation and Creativity

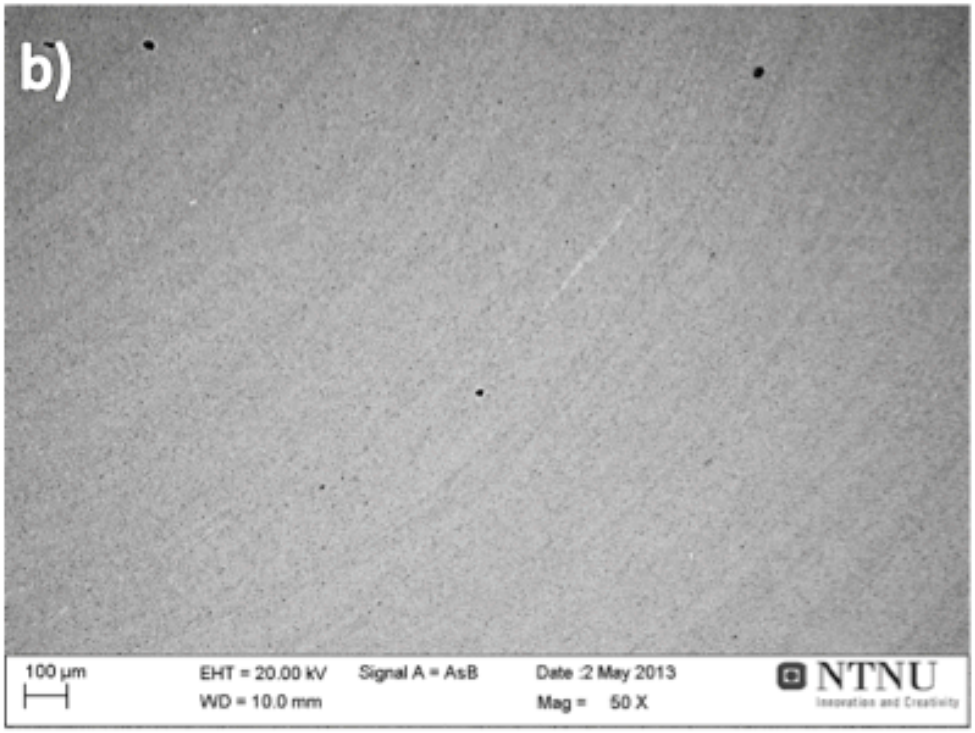
b)
100 µm
EHT = 20.00 kV
WD = 10.0 mm
Signal A = AsB
Date :2 May 2013
Mag = 50 X
NTNU
Innovation and Creativity

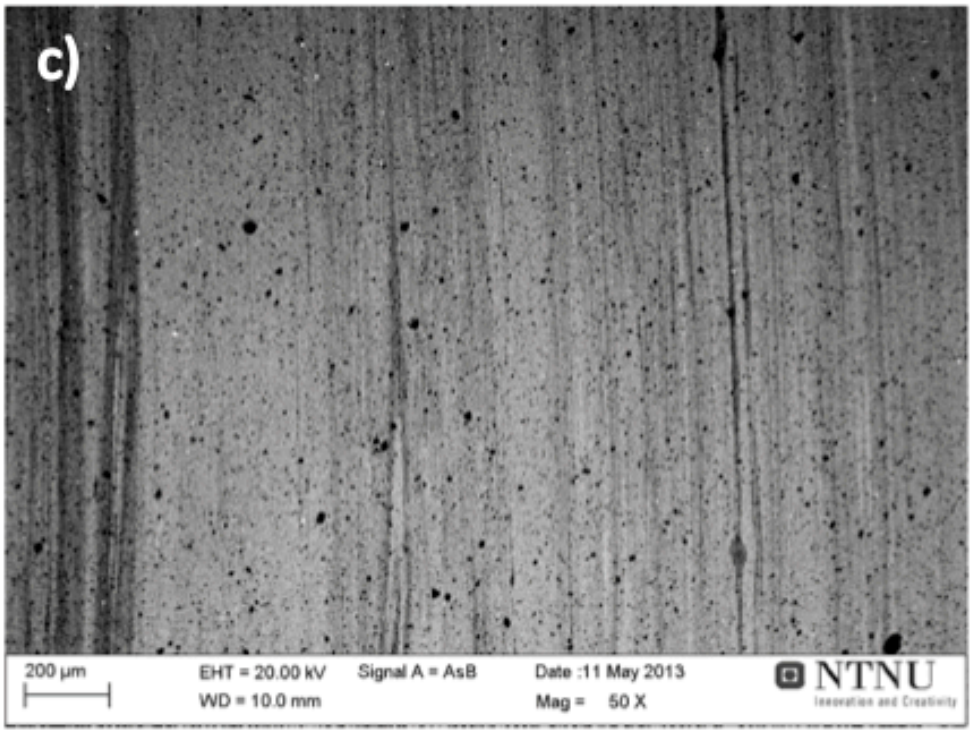

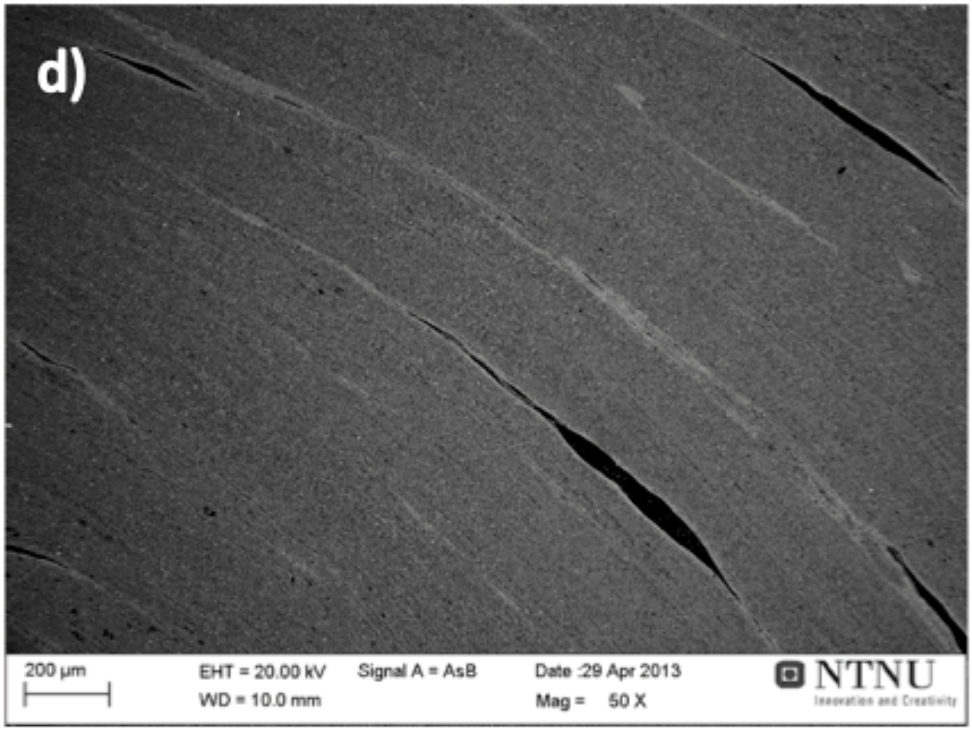

Figure 26: SEM micrographs acquired at 50X magnification, and at 10 mm WD, with a backscatter detector, showing the microstructure of a) Al-5wt% AZ31, b) Al-7.5wt% AZ31, c) Al-10wt% AZ31-1, and d) Al-10wt% AZ31-2 extrusion profiles.

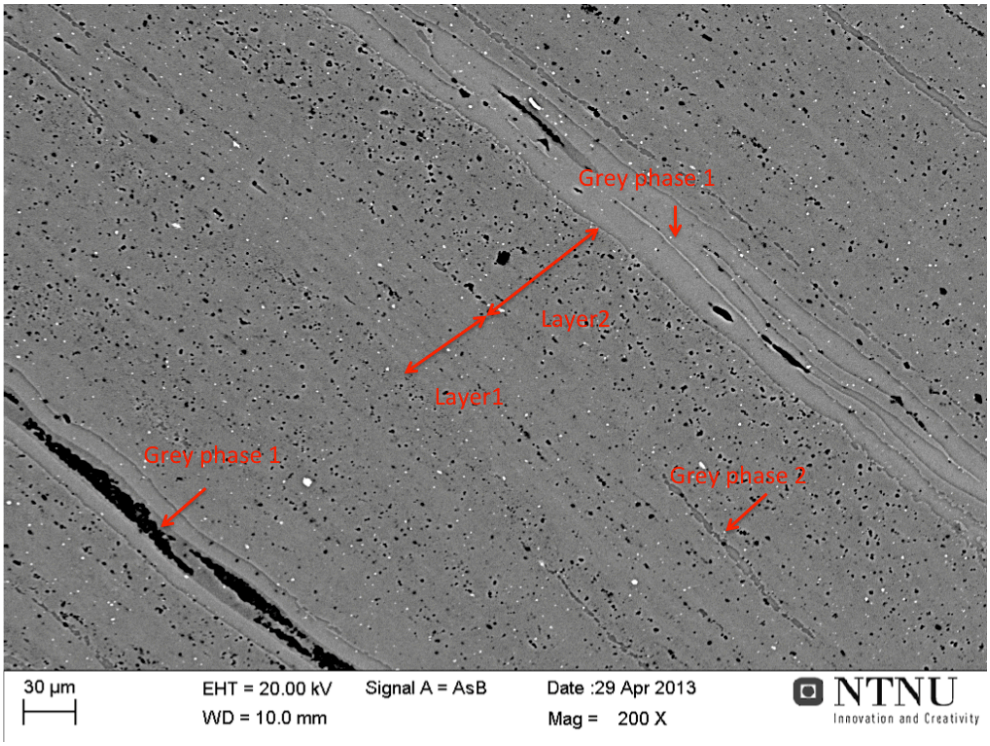

Figure 27: SEM micrograph acquired at 200X magnification and at 10 mm WD, showing the microstructure of an Al-10wt% AZ31-2 sample. Different features are marked out, as referred to in the text: layers, type 1 grey phase, and type 2 grey phase.

4.3.2.1 Examination of the Layered Structure

As presented above, in BSE imaging, different phases or areas will be imaged with various degrees of contrasts and intensities, depending on the atomic number of the phase. High Z phases will give a higher emission of BSE, and hence be imaged brighter than the lower Z phases. BSE imaging can therefore be utilized to examine the distribution of the Al and AZ31 constituents in the profile microstructure. Aluminium and magnesium are neighbouring elements, with atomic number 13 and 12, respectively. The contrast between these two elements will therefore be small, but not undetectable. As Al has a higher atomic number than Mg, Al will be imaged brighter than Mg. The three possible intermetallic phases will have a mean atomic number somewhere between the atomic numbers of Al and Mg. Also, as both Al and Mg easily oxidises, there is a possibility that different oxide products are present in the microstructure. The atomic number of oxygen is 8, and if present, the oxides will be imaged much darker than Al and Mg. The most common oxide for aluminium is the aluminium (III) oxide: Al_2O_3, while magnesium usually combines with oxygen to form MgO. The mean atomic numbers for these two oxides are (by equation 3) 10.68, and 11.02, respectively, i.e. appearing darker than Al and Mg. The amount of Mg atoms in solid solution in the Al matrix will also

affect the contrast intensity; e.g. areas enriched in Mg will be displayed as darker, ref. equation 4.

From the BSE imaging theory, a probable explanation for the layers in different shades of grey may thus be an effect arising from concentration differences of Al and Mg in the profile. To further evaluate the layered structure in the microstructure, it was conducted an EDS element mapping. In Figure 28a, a section of the microstructure in the longitudinal direction of the Al-10wt% AZ31-2 profile is displayed. In Figure 28b-d, the same section is imaged by the relative concentration of oxygen, magnesium, and aluminium, respectively. In this image, areas with a high concentration of the given element will be imaged with high colour brightness intensity. It is obvious from these figures that there are indeed significant differences in the Al- and Mg concentration, and that the concentration vary from layer to layer. There are especially large variations in the Mg concentration, as can be observed in Figure 28c.

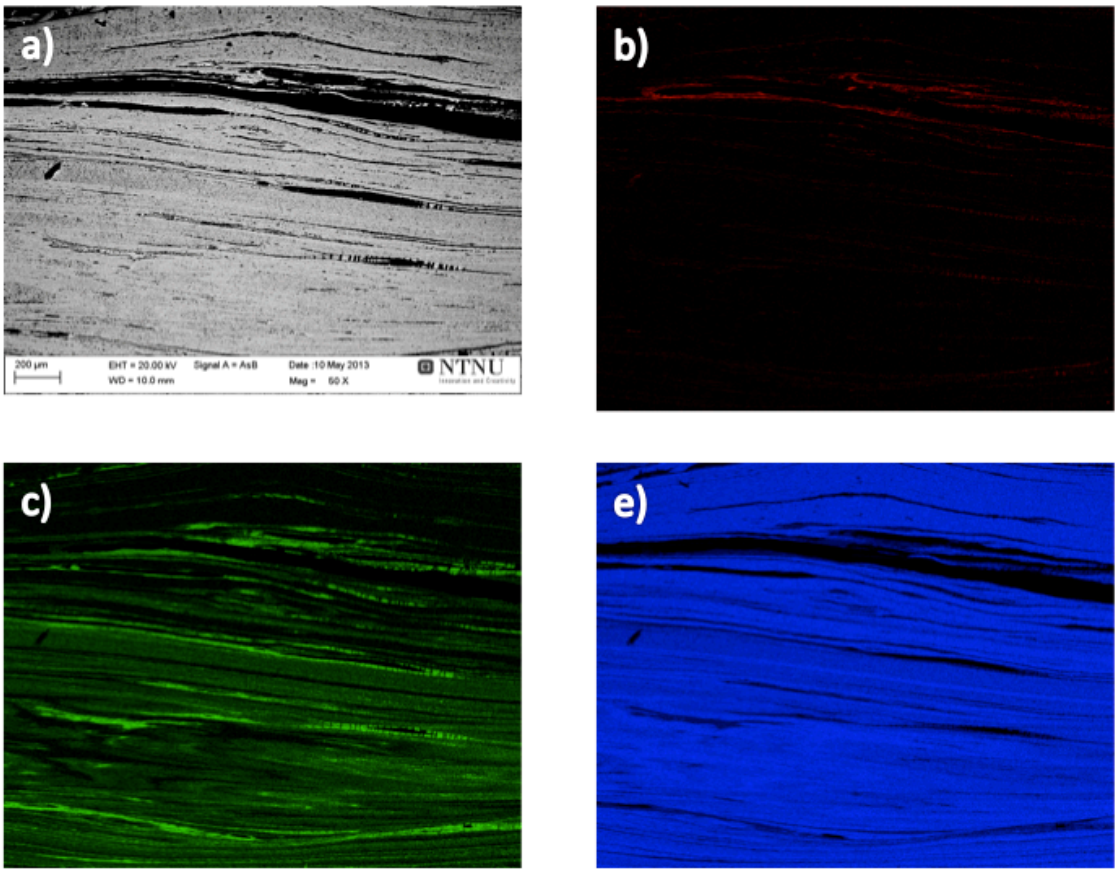

Figure 28: EDS element mapping of an Al-10wt% AZ31-2 longitudinal sample. a) Reference picture, b) oxygen content, c) magnesium content, and d) aluminium content. Notice the grey phases light up in the magnesium image, i.e. high in Mg content.

Another way to evaluate concentration variations through the sample surface is by the use of EDS line scans. Just as with EDS element mapping, the EDS line scan only gives the relative element concentrations, but it is still an effective way to get an overview over the composition of a material. In Figure 29, a line scan performed in the matrix of an Al-10wt% AZ31-1 sample, is shown. The figure displays the line scan, together with the respective graphs for oxygen, magnesium, and aluminium concentration. It can be observed that there are fluctuations in the concentration of Al, Mg and O along the line. Furthermore, it is noticed that the variation in oxygen concentration is in direct correlation to the variation in concentration of magnesium. There are also observed six distinct peaks in magnesium and oxygen concentration. For each of these peaks there is a simultaneously significant drop in the aluminium concentration. By detailed inspection of the line scan area it can be observed that each of the six peaks corresponds to a black particle of significant size. From the line scan results a likely identification of these particles is MgO.

The screw extrusion material flow theory presented by Widerøe and Welo(Widerøe and Welo, 2012) has already been discussed in respect to the variation in grain size structure. The theory can further be used to evaluate the semi-systematically variation in chemical composition observed in the samples. By semi-systematically it is here referred to the variation in Mg content between layers in the structure. A hypothesis is that if the screw flights functions as a knife, and continuously smears new layers onto the pre-existing material, the composition of each of these layers will be given by the specific composition of the feed stock material being fed into the extruder. It is not unthinkable that the Al- and AZ31 turnings initially were not 100% homogenously mixed. In stead, small variations in feed stock composition existed when the material was fed into the extruder. As a consequence, layers with small variations in Al-AZ31 composition has been produced. Within each of these layers, diffusion of Mg and Zn into the Al matrix has occurred. For some layers, a very high concentration of AZ31 turnings may have been present, and regions with high Mg concentrations have been produced. Even the occurrence of Al-Mg intermetallics might be explained from higher content of AZ31 turnings in the given feed stock mix. For the Al-10wt% AZ31-1 profile, it was visually observed large agglomerates of MgO powder following the feed stock material into the compacting chamber.

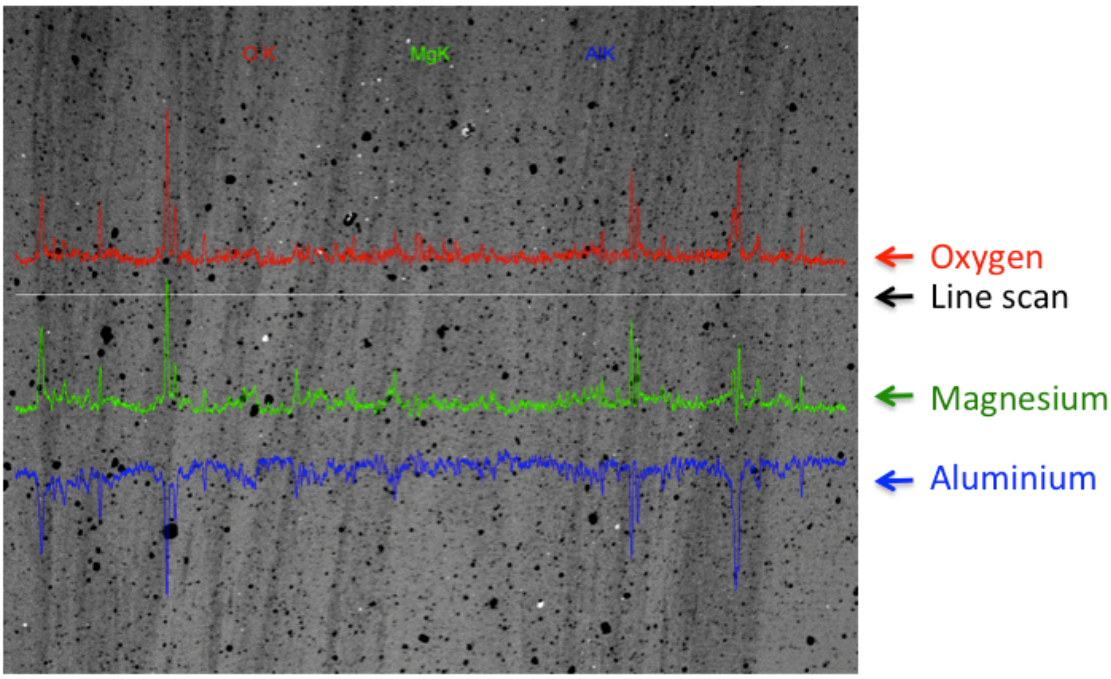

Figure 29: Line scan in the matrix of the Al-10wt% AZ31-1 sample, displaying the variation in concentration of oxygen, magnesium, and aluminium: red, green, and blue graphs, respectively.

4.3.2.2 Examination of Particles

In all of the four extrusion profiles particles are observed. In Figure 30, particles in the Al-10wt% AZ31-1, and the Al-7.5wt% AZ31 profiles are displayed. Notice the difference in particle size and distribution between the two samples. The Al-10wt% AZ31-1 sample contains massive, dark particles that are distributed randomly in the matrix. In Figure 30a, one particle is measured to be 30 μm in diameter. The Al-7.5wt% AZ31 sample also contains dark particles, but they are fine-sized and are located within distinct layers. Also, found very small sized, bright particles are observed in all of the samples. EDS point analysis was utilized to evaluate the composition of the particles. The analysis was performed at low voltage, 5kV, to obtain more accurate results. The EDS analysis identified the large, dark particles in the Al-10wt% AZ31-1 matrix as MgO; just as suspected in the line scan results. In the spectrum obtained for some of the largest particles in the Al-10wt% AZ31-1 profile, significant traces of carbon and oxygen were also detected. A possible explanation for this may be due to unsuccessful removal of oil grease after the machining process of the feed stock material.

Furthermore, the bright particles were identified as Fe. The small dark particles distributed in the layers were found to contain Al, Mg, and O - and may be residues from broken-up oxide films. In Figure 30b it is indicated with arrows two areas that seems to have a higher density of particles. EDS analysis of this area shows that these features have a relatively higher concentration of Mg than the rest, around 12at%. Here, it is interesting to note that the reported solubility of Mg in Al phase at 400°C is 12.6 at%.(Murray, 1982) In the present case, the surrounding areas have a concentration about 7 at% Mg.

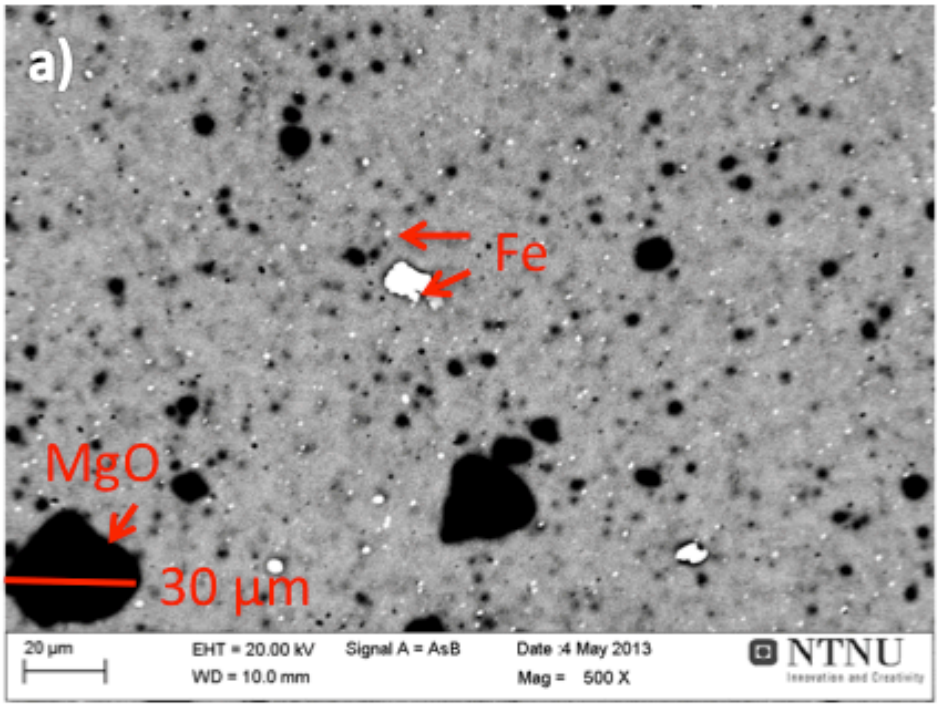

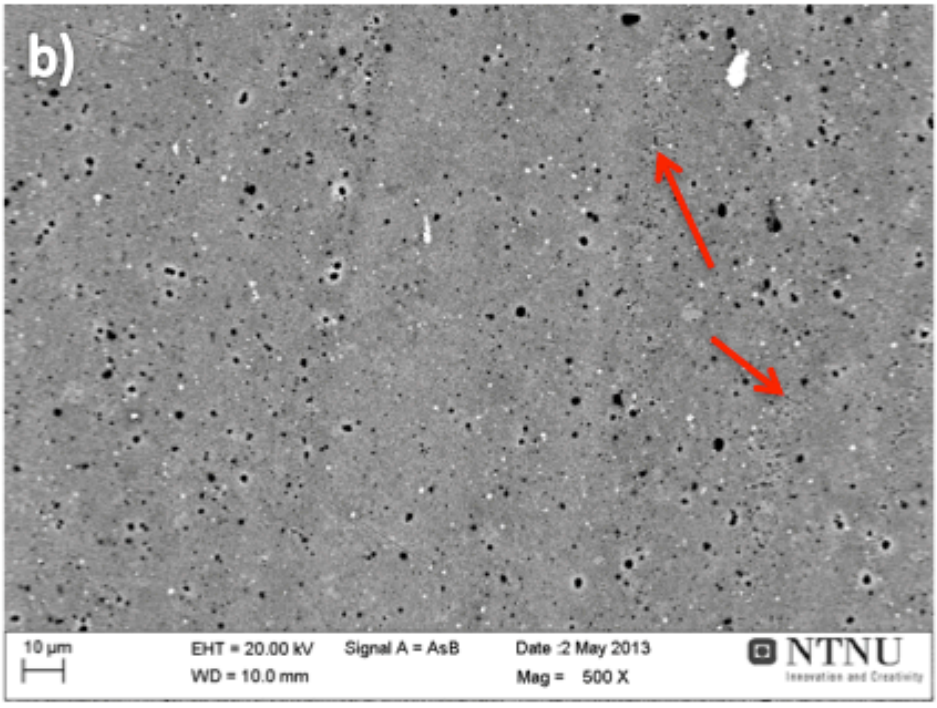

Figure 30: SEM micrographs acquired at 500X magnification and at 10 mm WD, showing particles in the matrix. a) MgO-, and Fe particles in the Al-10wt% AZ31-1, sample. b) Dispersed small oxide particles in the Al-7.5wt% AZ31 sample. In the latter figure, please see the red arrows indicating areas with a high density of particles.

4.3.2.3 Examination of Secondary Phases

As already mentioned, there are observed grey elongated areas resembling secondary phases, e.g. in the 5-, 7.5, and 10-2wt% AZ31 profiles. The position of these phases, together with the morphology, indicates that these phases are the same as those observed as grey, corroded areas in the optical microscope. EDS element mapping of one of the regions referred to as "grey phase 1" in Figure 27, was performed to analyse the concentration of magnesium and aluminium of that area. The results are shown in Figure 31 where a) displays the Mg concentration, and b) the concentration of Al. From these figures it is confirmed what was suspected after optical microscopy; namely the corroded regions have indeed a higher content of magnesium.

As indicated in Figure 27, it is distinguished between two types of phases, categorised based on their appearance: Figure 32 displays the phase referred to as a type 1 grey phase, while a typical type 2 grey phase is shown in Figure 35. In the following section, the feature and composition of these two phases will be further presented and discussed.

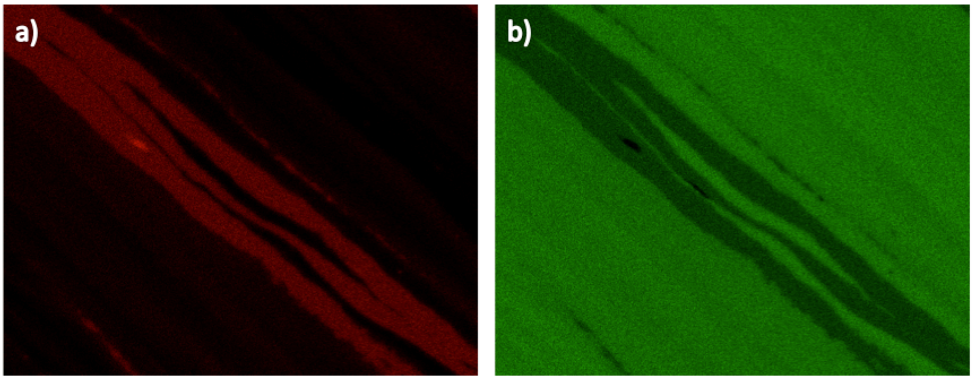

Figure 31: EDS element mapping of the type 1 grey phase referred to in Figure 27. a) Variation in magnesium concentration .The red, bright bands indicate that the phase contains a much higher amount of Mg compared with the surrounding matrix. b) Corresponding concentration of aluminium. The clear green colour of the matrix indicates that it mostly contains Al.

The type 1 grey phase shown in Figure 32 was found in the Al-5wt% AZ31 profile, and resembles the Al-Mg diffusion-joined interfaces observed in various experiments on solid-state bonding of aluminium and magnesium (alloys).(Chang et al., 2012, Chen et al., 2007, MC Chen and Wu, 2007, Liu et al., 2011, Liu et al., 2009, Paramsothy et al., 2008, Peng et al., 2006, Wang et al., 2008, Wu et al., 2010) The phase is symmetrically built up of several zones with well-defined borders. The symmetry is well illustrated through the graph obtained by an EDS line scan across the phase, Figure 34. The line scan measures the relative concentrations of aluminium and magnesium along the line, and in the corresponding graph it can be seen that the Al and Mg content changes gradually across the zone boundaries, but within each zone, the composition is quite constant. Furthermore, it should be noticed that the graphs of Al and Mg are more or less inverse of each other.

EDS multipoint analyses were performed at eight different positions within, and outside, the phase, to determine the chemical composition of the different zones. The position of the point analysis, and corresponding results are given in Figure 33, and Table 4, respectively. The EDS results show that the centre of the phase, point 1, is rich in magnesium, and with a high concentration of zinc and aluminium. The fact the magnesium concentration is outside the limit of possible intermetallic compositions, together with the high concentration of Zn, 1.57wt%, indicate that this is the remains of an AZ31 turning. The Al concentration is within the solubility limit of Mg(ss), and indicates that diffusion of Al atoms from the surrounding Al turnings/matrix, have occurred. The black spots are most likely oxide residues.

Point 2 and 3 are identified as two of the intermetallic phases of the Al-Mg system: namely $Al_{12}Mg_{17,}$ and $Al_3Mg_{2.}$ These phases are located in a similar manner as in the model proposed by Peng et al(Peng et al., 2006);The magnesium rich γ-phase is located closest to what is believed to be the remains of an AZ31 area, while the Al-rich, β-phase, is located close to the border to the Al-matrix. The composition of the Al-matrix was measured in position 4-8. Position 4 is at the Al_3Mg_2-Al border, and a relatively high concentration of Mg is measured, 10at%. This is however, within the solid solubility limit of the Al phase. The positions 5-7 have fairly similar compositions: Al with around 2-3 at% Mg in solid solution. Remembering that the feed stock material consisted of pure Al turnings, it is clear that a significant degree of Mg diffusion has taken place. Point 8, on the other hand, was measured in an area with a characteristic appearance. The area has a very high Mg concentration, 23 at% Mg, which is outside the solid solubility limit in Al. The oxygen content is also low, indicating that it is not remains of an MgO oxide film. This area is what is referred to as a type 2 grey phase.

The type 2 phase illustrated in Figure 35 was found in the Al-7.5wt% AZ31 profile. In contrast to the type 1 phase recently discussed, this phase does not have straight borders, and does not consist of multiple zones. In stead, a solidification-like structure consisting of dendrite-like formations, with a center region imaged in a darker shade of grey, can be observed. The chemical composition of the phase was examined by four EDS multipoint analyses. The position of analysis, and corresponding results are given in Figure 36 and Table 5, respectively. Point 2 and 3 are located in the matrix just outside the phase, at opposite sides. These two points give similar composition results, i.e. Al with ca. 7wt% Mg in solid solution, with a negligible amount of oxygen and zinc. These are reasonable results for a material with an intended composition of Al-7.5wt% AZ31. However, the EDS results from point 4 shows a structure with dendrite-like appearance, which has a magnesium concentration at the upper limit of aluminium solubility. The centre region, point 1, has the chemical composition close to that of the intermetallic Al_3Mg_2 phase, but with a Mg value just below the concentration range for the β phase. The EDS results imply that the type 2 grey phases have been formed by partially melted regions during the extrusion process. According to solidification theory, as the aluminium solidifies, the solubility decreases. As a result, the region ahead of the solidification front, here the area measured by point 1, will be enriched in magnesium. The last region solidifying will as a result have a high concentration of magnesium, and often have the composition closest to the eutectic point. For an Al-7.5wt% Mg system, the closest eutectic point is that of the phase Al_3Mg_2.

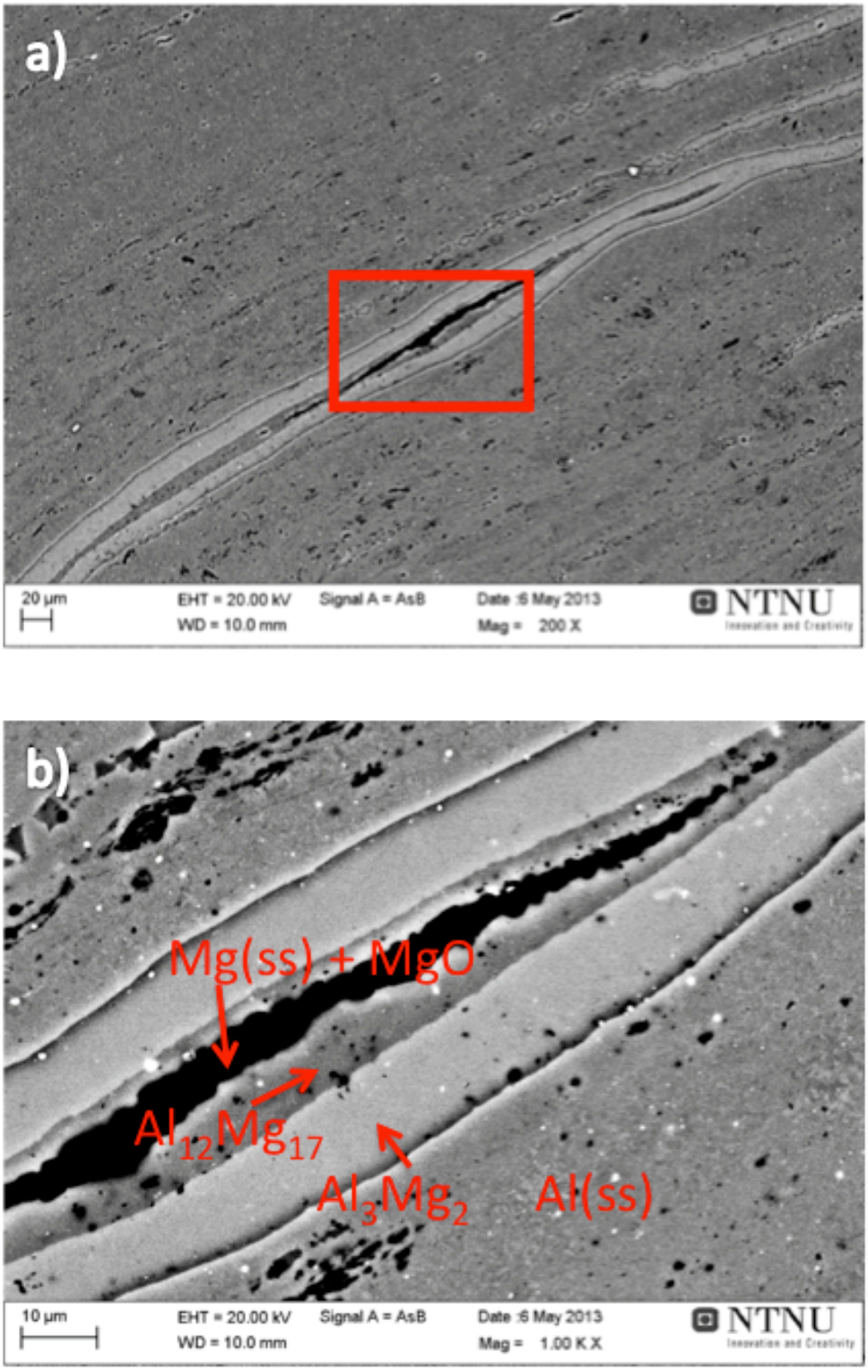

Figure 32: SEM micrographs acquired at 200 and 1k magnification, respectively and at 10 mm WD. a) A type 1 phase observed in the Al-5wt% AZ31 sample. b) The same phase magnified. Based on the EDS results, Table 4 most probable constituents of the phases are indicated.

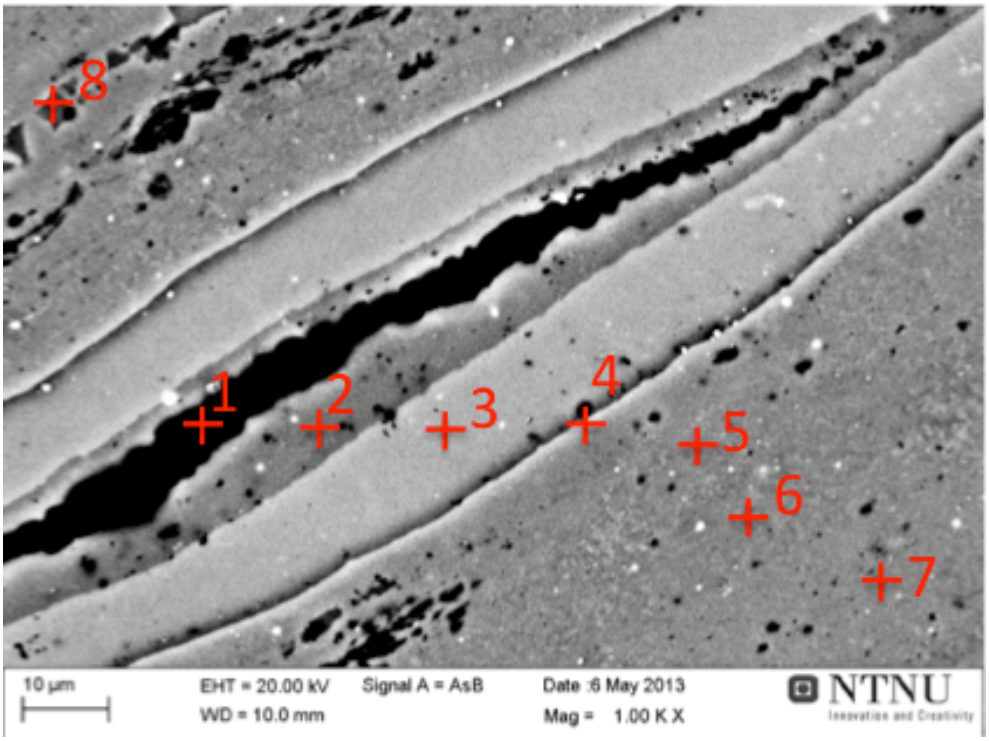

Figure 33: Position of the EDS multipoint analyses performed on the type 1 phase.

Table 4: Results from the EDS point analysis of the type 1 phase, located in the Al-5wt% AZ31 sample (Figure 33).

Element concentration [at%]	Point of analysis (Ref Figure 33)							
	1	2	3	4	5	6	7	8
O	13.8*	1.17	1.14	0.53	0.58	0.74	2.25	1.69
Mg	69.7	55.3	37.6	10.0	1.94	3.19	2.31	23.0**
Al	15.9	43.2	61.0	89.3	97.2	95.9	95.3	75.0
Fe	0.05	0.04	0.07	0.06	0.13	0.11	0.13	0.05
Zn	0.50*	0.32	0.19	0.08	0.09	0.09	0.05	0.22
Possible phase (Ref Table 1)	Mg(ss)*	$Al_{12}Mg_{17}$	Al_3Mg_2	Al(ss)	Al(ss)	Al(ss)	Al(ss)	Al(ss)**

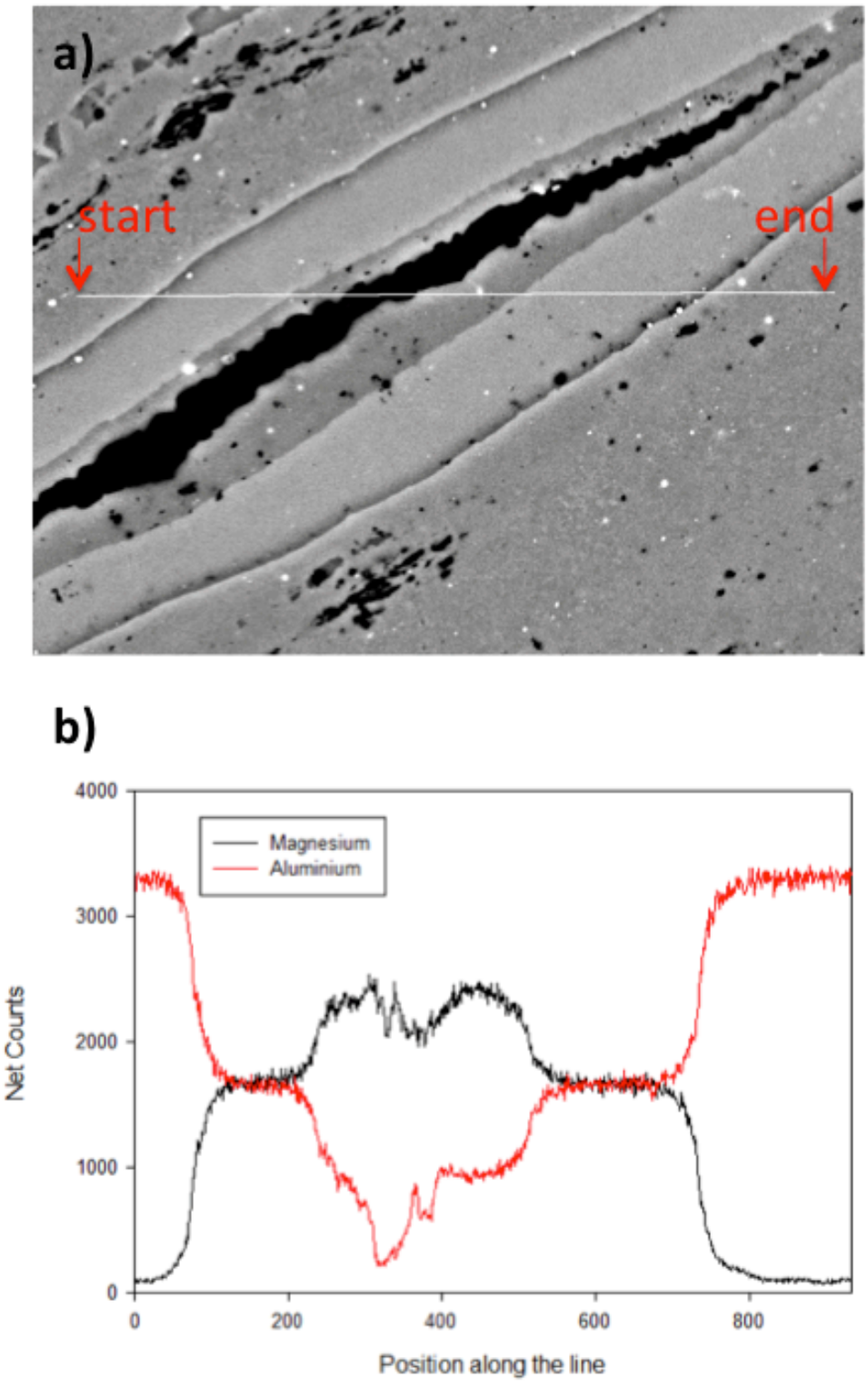

Figure 34: a) Position of the EDS line scan performed across the type 1 phase in the Al-5wt% AZ31 sample. b) Corresponding graphs showing the relative concentrations of Al and Mg along the line.

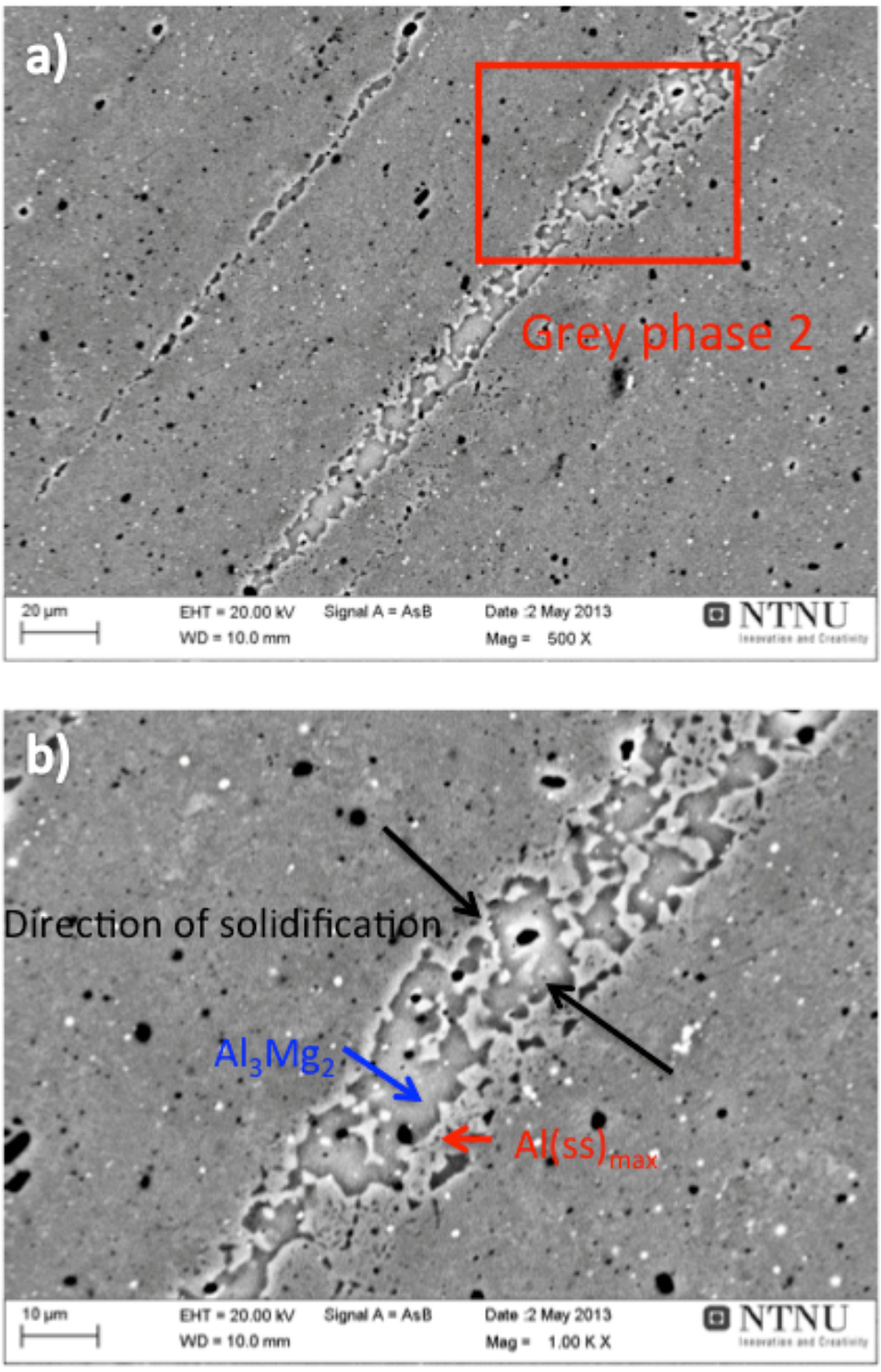

Figure 35: SEM micrographs acquired at 500 and 1kX magnification, respectively, and at 10 mm WD. a) A type 2 grey phase located in the Al-7.5wt% AZ31 sample. b) The same phase magnified. Based on the EDS analysis of this phase, given in Table 5, the probable constituents of the phase are indicated. As it is believed that the phase is the result of local melting, it is also indicated the most likely direction of solidification.

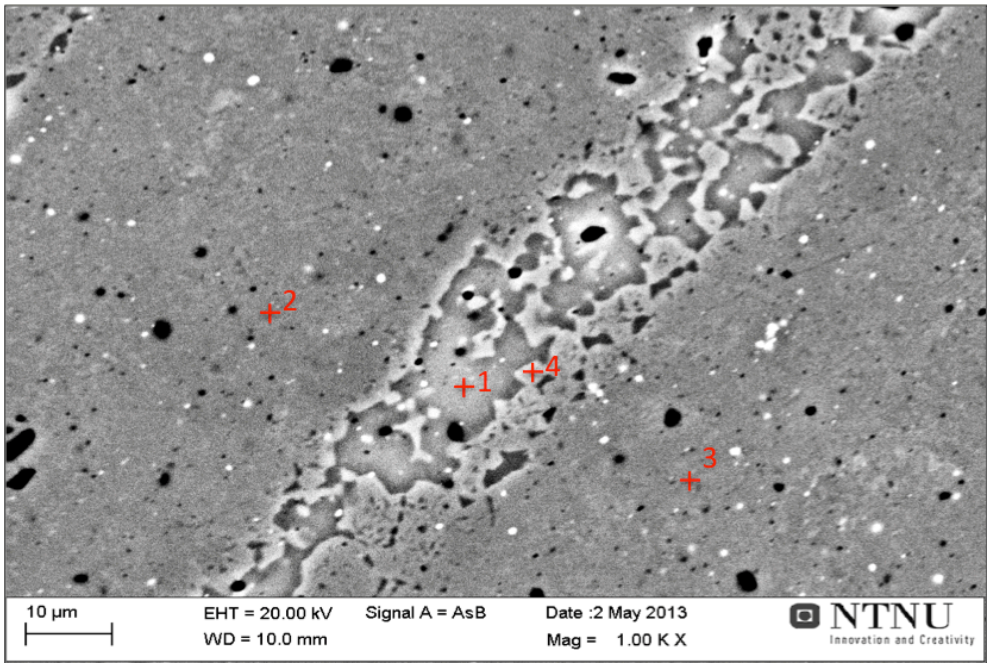

Figure 36: Position of the EDS multipoint analysis performed of the type 2 phase located in the Al-7.5wt% AZ31 sample, see Table 5.

Table 5: Results from the EDS point analysis of the type 2 phase located in the Al-7.5wt% AZ31 sample

Element concentration [at%]	**Point of analysis (Ref Figure 36)**			
	1	2	3	4
O	0.31	0.43	0.39	0.29
Mg	35.3	7.30	8.27	16.2
Al	64.1	92.2	91.3	83.4
Zn	0.29	0.08	0.06	0.09
Possible phase (Ref. Table 1)	Al_3Mg_2	Al(ss)	Al(ss)	Al(ss)

Lastly, a large crack in what has just been identified as an Al_3Mg_2 phase, located in the longitudinal section of the Al-10wt% AZ31-2 profile, is shown in Figure 37. Several similar cracked phases were observed in this profile. Intermetallic phases are known to be hard and brittle, and cracking of these phases is therefore very likely. The high density of these phases in the 5-, and 10-2 profiles may thus indicate that these profiles will have low fracture strength. This will be further evaluated in the next section, which presents the results from the mechanical testing of the extrusion profiles.

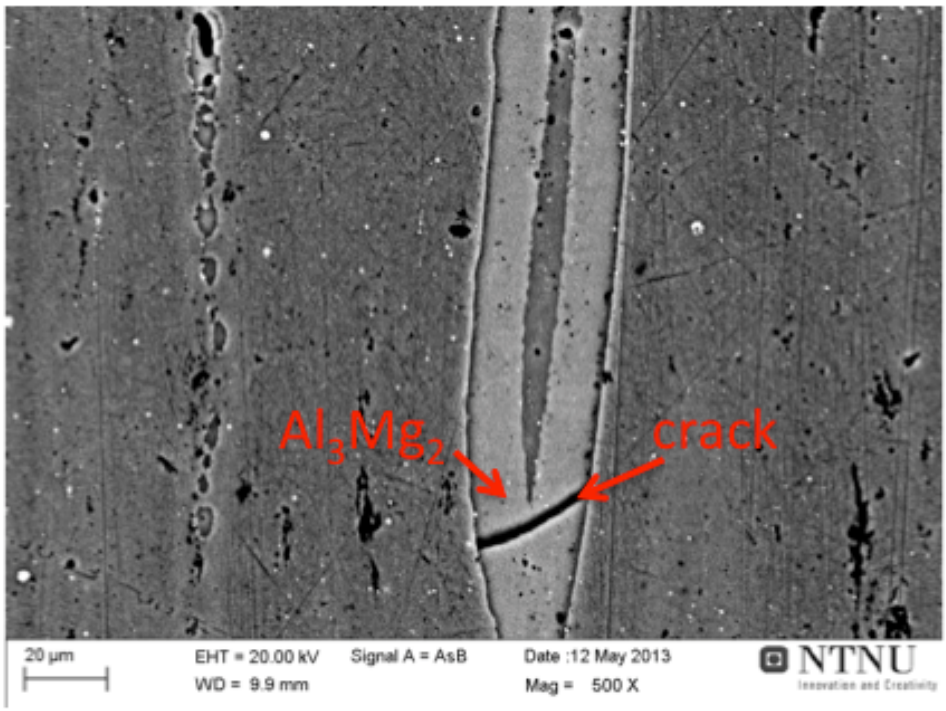

Figure 37: Optical micrograph acquired at 500X magnification and at 9.9 mm WD, showing an intermetallic phase containing a large crack, observed in the longitudinal direction of the Al-10wt% AZ31-2 sample.

4.4 Mechanical Properties

The mechanical properties of the four extrusion profiles were examined by micro- and macro hardness measurements, and by room temperature tensile tests.

4.4.1 Hardness Test results

4.4.1.1 Macro Hardness Test Results

The results from the macro Vickers hardness measurements are presented in Figure 38. The average macro hardness values for the 5-, 7.5-, 10-2, and 10-2wt% AZ31 samples are: 66.4± 6, 73.3± 5.1, 97.0± 7.3, and 62.9± 16.4 HV1, respectively. For all the four extrusion profiles, there are variations in hardness value across the longitudinal cross section. The variations are most likely related to the inhomogeneous, layered microstructure of the profiles, observed both in the OM and the SEM. For the 10-2 sample it was difficult to find an area free of large voids, hence hardness measurements were problematic. It is recognized that voids in immediate distance to a hardness indentation results in errors in the hardness value, usually by lowering the value. This may be a probable explanation for the significant variation in hardness for this sample, and more specifically, the low hardness value at some positions. Still, it has been observed that adjacent to the voids, there are areas of fairly large grains, compared to the fine-grained microstructure of the bulk. The large grain size will also result in lower hardness values, but most likely not in the extreme low range (< 30HV1) as obtained at some positions in the 10-2 sample. It is now known that the 5-, 7.5, and 10-2wt% AZ31 profiles contain a fairly large amount of intermetallic phases. These phases are harder than the Al-matrix, and can influence the hardness measurements, but in contrast to the voids, the effect would be an increase in hardness value. However, the precise hardness of these phases must be examined by micro hardness testing.

The Al-10wt% AZ31-2 sample aside, it can be observed that the trend is that the hardness increases with increasing additions of AZ31. This is not unlikely as there will be an increasing amount of Mg in solid solution, since extensive local melting seems to have occurred during the present extrusion trial. The magnesium atoms in solid solution will improve the hardness of the matrix. The Al-10wt% AZ31-2 sample furthermore contains a high amount of MgO precipitates, which may also influence the hardness. Additional elements, which may influence the hardness of the samples, are dislocation density variations arising from different degree of deformation of the material, and various grade of grain size refinement.

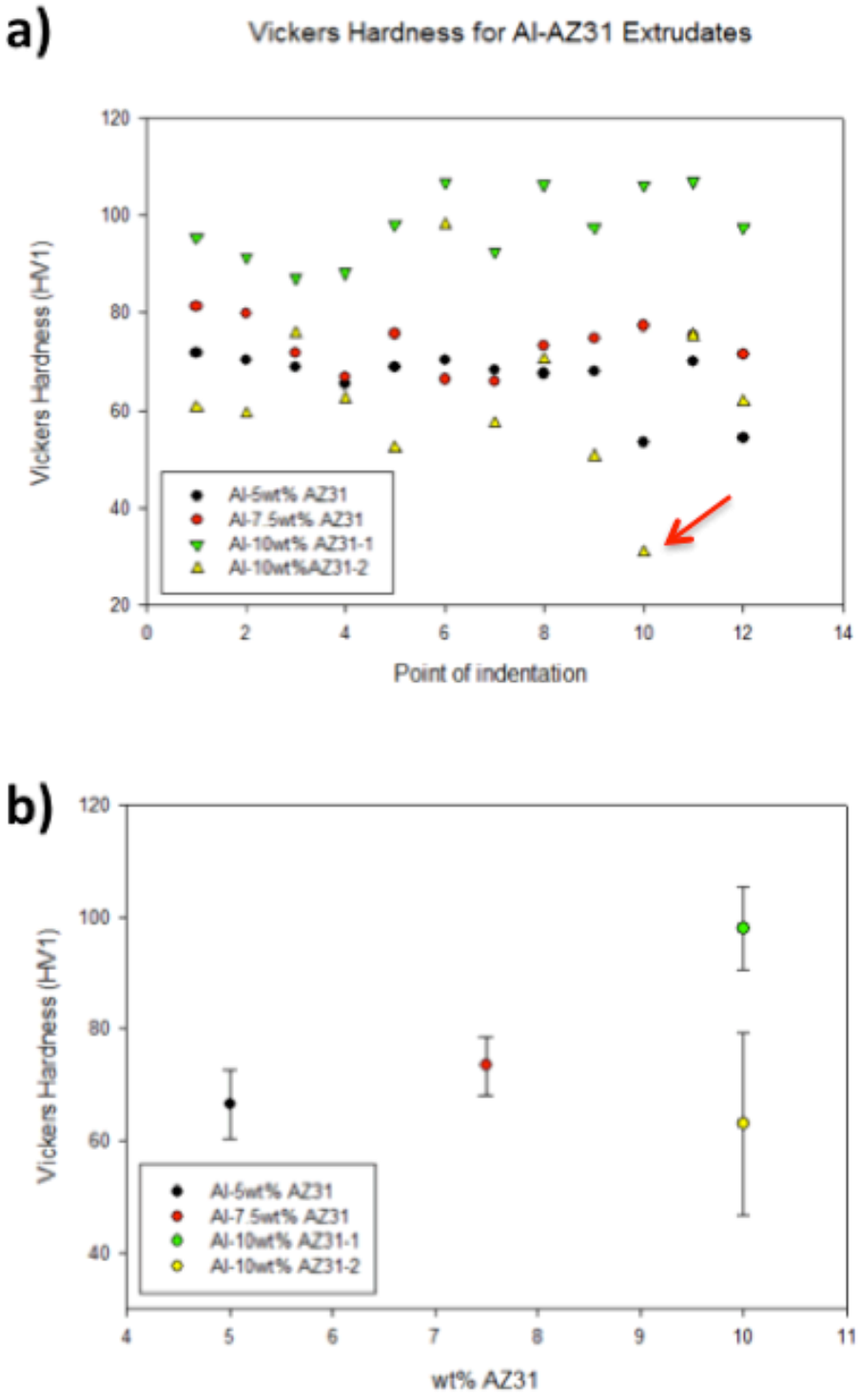

Figure 38: Vickers hardness measurements for the four different Al-AZ31 extrusion profiles. a) Vickers hardness value vs. position of the indentation, ref. Figure 14. b) Vickers hardness value with increasing additions of AZ31. In the first graph, please notice the extreme low value (<30 HV1) obtained for the 10-2 sample, indicated with a red arrow. It is likely that this indentation was performed near a void in the sample, and the low value is thus a result of an edge effect.

4.4.1.2 Micro Hardness Test Results

Micro hardness measurements were performed to investigate the hardness of the individual phases in the microstructure. Examinations in the OM and the SEM have revealed that the Al-10wt% AZ31-2 samples contain the largest individual phases. Micro hardness measurements were thus performed on a longitudinal sample collected from this profile. The micro hardness was examined in three distinct areas of the microstructure: in the bulk, near the voids, and in the intermetallic phases. A total of twelve hardness indentations were performed in each phase. Due to the small size of the phases, especially the intermetallic ones, measurements were conducted in several similar areas.

The following average hardness values were obtained for the bulk, near the void, and in the intermetallic phases: 97.0±13.5, 48.9±10.2, and 257.8±32.2 HV5gf, respectively. It is evident that the intermetallic phases are significantly harder than the matrix. Still, these areas are very small, so the effect they may have had on the macro hardness measurements is uncertain. The average hardness value of the bulk is remarkable equal to the values obtained in the macro hardness measurements of the Al-10wt% AZ31-2 sample. The areas adjacent to the voids have the lowest hardness, as also observed in the macro hardness measurements. A possible explanation may be error in measurement due to edge effects, but most likely the low hardness is due to the microstructure in this area consists of larger grains.

It can be observed that for all phases, there are high deviations in hardness values. For the bulk and void-areas, a probable cause may be variation in grain size, dislocation density, and concentration of magnesium. As already mentioned, the intermetallic phases are small. A possible explanation for the high deviation in the hardness value obtained for these phases may thus be incorrect position of the indentation. Also, it was not possible to distinguished between β and γ phase during the measurements; bearing in mind that these two intermetallic phases have slightly different crystal structures, it is not unthinkable that they also have differences in hardness.

4.4.2 Tensile test results

In this section the tensile test results are presented. Tensile testing of 16 tensile test specimens machined from the extrusion profiles was performed and the full results from the tensile testing are given in Figure 40. The engineering stress-strain curves in Figure 39a presents the mechanical properties of screw extruded Al-AZ31 composites with increasing AZ31 additions. The trend in yield strength, ultimate tensile strength (UTS) and elongation at failure, with increasing AZ31 addition are displayed in Figure 41a-c, respectively.

It is evident that the strength of the Al-AZ31 composites increases with increasing additions of AZ31, and that the elongation at failure decreases accordingly. Highest UTS is recorded for sample 10.2-1 and is 368 MPa, Surprisingly, this sample shows also the maximum elongation at failure - 33%. However, this is an exception to the rest of the Al-10wt% AZ31-2 samples as the rest display ductility lower than the 5- and 7.5wt% AZ31 samples. Highest stress at offset yield was also recorded for Al-10wt% AZ31-2 sample and was 256 MPa.

Even though the ductility decreases with increasing AZ31 content, the ductility is still remarkably high for most of the samples and the difference in ductility between the 5- and 7.5wt% AZ31 samples is minimal. This does not however hold for the samples from the Al-10wt% AZ31-1 extrudates profiles; these specimens had poor ductility with an elongation at failure of only 1.8 – 3%. These samples fracture before necking occurred, indicating brittle behaviour. Still, the specimens showed a tendency of achieving high UTS; a rapid work hardening behaviour can be observed in the stress-strain curves, before the specimens abruptly fractures. The test specimens from the second 10wt% AZ31 trial have better ductility than the first 10wt% AZ31 specimens, but the stress-strain curves for two of the specimens from the second 10wt% trial, 10.2-3 and 10.2-5, resemble the Al-10wt% AZ31-1 samples.

Serrated yield behaviour is observed for all samples, as displayed in Figure 39b. The serrations start to occur at a strain of about 0.01 and are of variable magnitude, with the stress drop and serration intensity increasing with strain. In addition a peak yield point at the onset of plastic region of the curve indicating Lüders band phenomena are present in all samples *except* in the Al-10wt% AZ31-1 test specimens. It is well known that the PLC effect in aluminium stress-strain curves is caused by magnesium in solid solution.(Robinson, 1994, Wen and Morris, 2003, Wen and Morris, 2004, Abbadi et al., 2002, Chen et al., 2009) As all of the profiles contain high amounts of magnesium, it is not unlikely that this is also the cause here. In Figure 39b it can be observed that the serrations of the Al-10wt% AZ31-1 samples are larger than in the other curves. Remembering that the 10-1

samples did not contain any intermetallic phases, but maintained most of the Mg in solid solution, this can be a reasonable explanation for the enlarged serrations.

It is desirable that tensile specimens machined from the same extrusion profile exhibit similar mechanical properties. In Figure 41a-c the trend in yield stress, UTS, and elongation at failure for all samples is graphed with error bars. It can be clearly seen that there is significant scatter in the mechanical properties for the two -10wt% AZ31 parallels. Especially for the UTS a great deviation is displayed. Furthermore, the ductility of the Al-10wt% AZ31-2 varies greatly. As already mentioned this parallel has the highest ductility, while at the same time specimens with ductility below 5% is observed here. The Al-10wt% AZ31-1 samples have on the other hand a poor, but with low variation ductility. The 5- and 7.5wt% AZ31 samples show little variation in mechanical properties and the Al-7.5wt% AZ31 specimen parallel display the most homogenous tensile testing performance.

It is observed distinctive differences in how the specimens underwent fracture. Sample 5-1 fractured in a discontinuous manner and this characteristic fracture behaviour is also observed in the Al-10wt% AZ31-2 samples: 10.2-2, -3, and -4. In stead of fully break off, the samples fractures in a way characteristically for delaminating fracture.

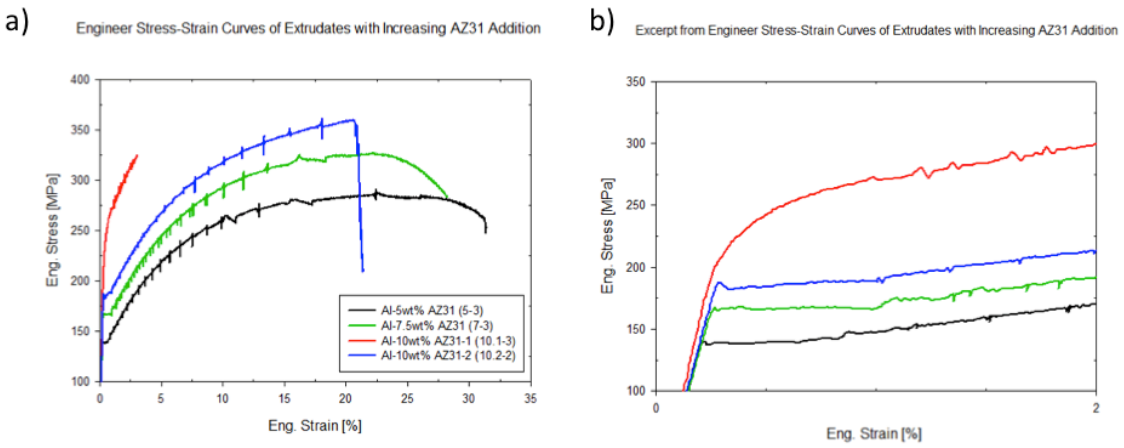

Figure 39: a) Engineering stress-strain curves for extrusion profiles with increasing AZ31 additions. Tensile testing performed at room temperature, b) Close up from stress-strain curve in a) showing serrated flow behavior in all four curves. Please notice that a peak yield point indicating Lüders band phenomena is present in specimen 5-3, 7-3, and 10.2-2 but not in 10.1-3.

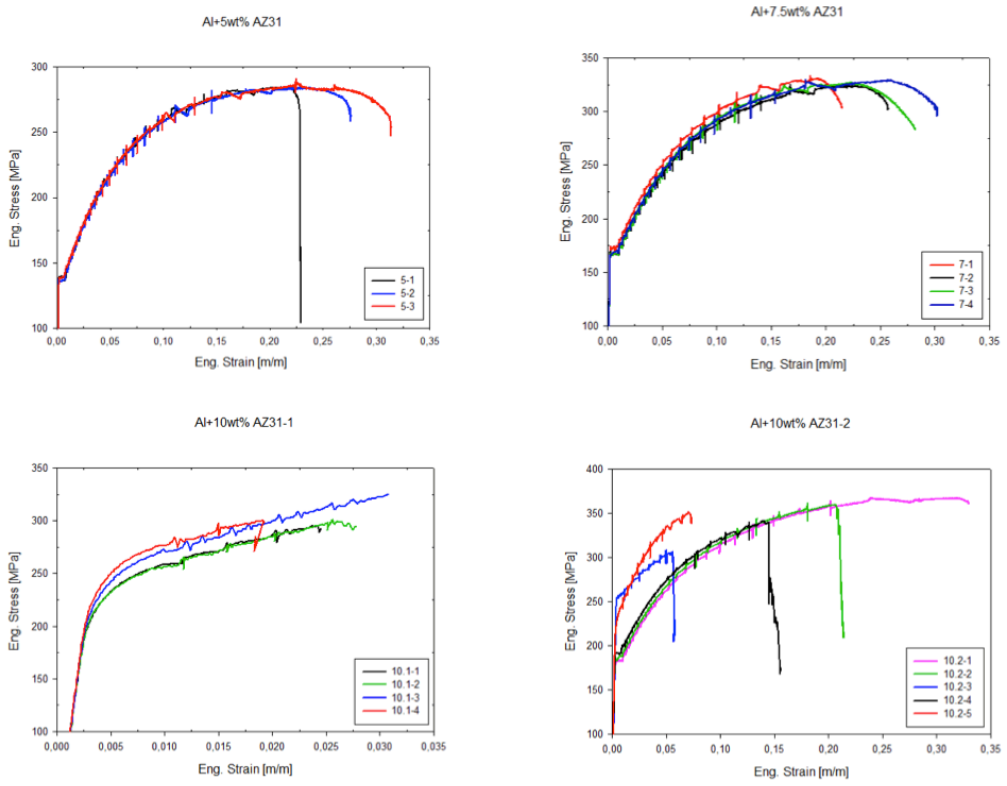

Figure 40: Engineering stress-strain curves for the four extrusion profiles. a) the 5wt% AZ31, b) the 7.5wt% AZ31, c) the 10-1wt% AZ31, and d) the 10-2 wt% AZ31. Please notice that the 10-1 parallel is plotted with a much lower scale on the x-axis. In the latter graph, please observe the characteristic fracture behavior of sample 10.2-2, -3, and -4.

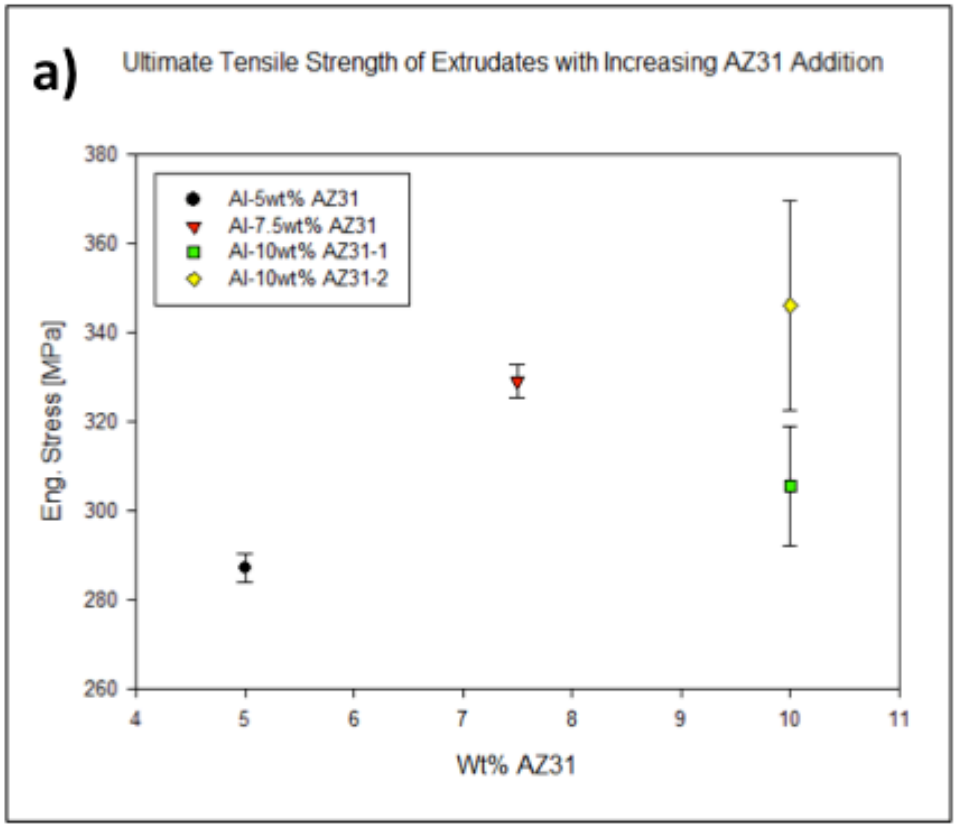
a)
Ultimate Tensile Strength of Extrudates with Increasing AZ31 Addition
Al-5wt% AZ31
Al-7.5wt% AZ31
Al-10wt% AZ31-1
Al-10wt% AZ31-2
Eng. Stress [MPa]
Wt% AZ31
380
360
340
320
300
280
260
4
5
6
7
8
9
10
11

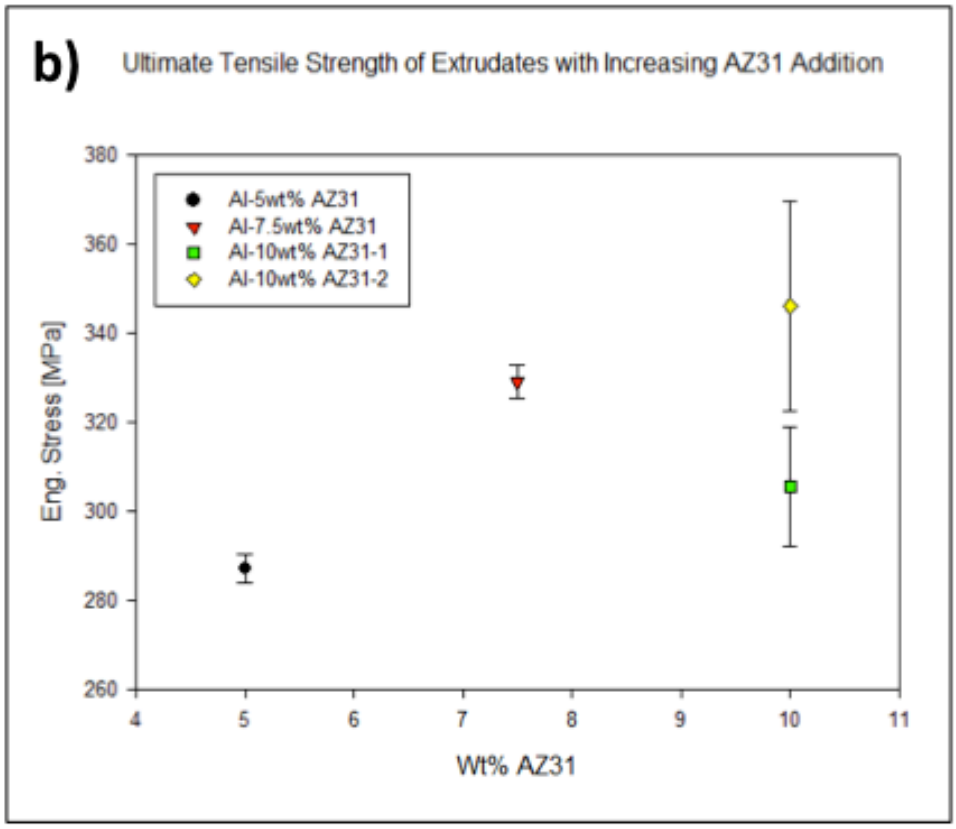
b)
Ultimate Tensile Strength of Extrudates with Increasing AZ31 Addition
Al-5wt% AZ31
Al-7.5wt% AZ31
Al-10wt% AZ31-1
Al-10wt% AZ31-2
Eng. Stress [MPa]
Wt% AZ31
380
360
340
320
300
280
260
4
5
6
7
8
9
10
11

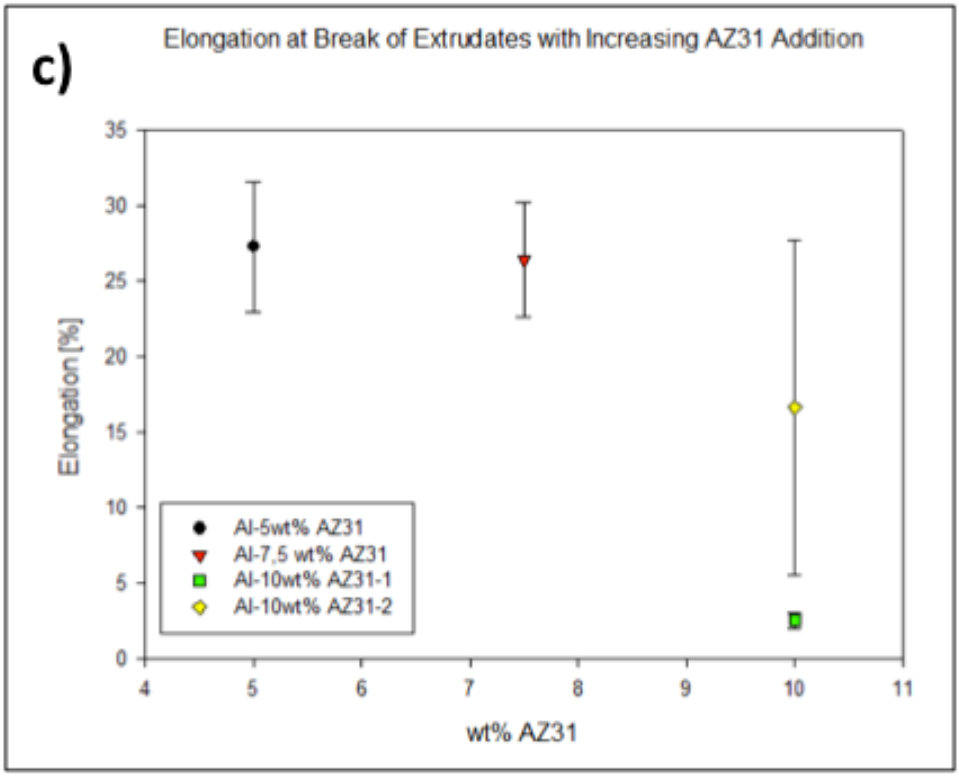

Figure 41: Trend in a) yield strength, b) UTS, and c) elongation at break with increasing additions of AZ31.

4.4.3 Tensile Test Specimen Fractography

The tensile testing performed in this study was executed until full fracture of specimen had occurred. In this section a selection of the fracture surfaces from the four extrusion parallels are presented and discussed. The author has limited experience with fractography, and the following interpretation of the fracture surfaces will therefore also be limited. The fractographic examination was performed in SEM with a secondary electron detector at 15 kV. Fractographs for all tensile test specimens are included in Appendix B: Fractographs .

From examination in the OM and the SEM it is now known that the extrusion profiles produced in this study have a highly inconsistent microstructure. This is further observed during the examination of the fracture surfaces of the tensile specimens, e.g. no fracture surfaces are alike. Significant variations between the testing parallels were observed, but also within each parallel it was found large differences in the fracture surface features. In fact, across the fracture surface of each specimen, different fracture features could be observed. Nonetheless, in Figure 42, it is attempted to display the typical fracture surfaces of the four tensile test parallels. In this figure, the fracture surfaces of the test specimens: 5-1, 7-4, 10.1-4, and 10.2-3 are shown, where each specimen is chosen to represent the characteristic fracture feature within its parallel.

Figure 42a-b, reveals the fracture surface of sample 5-1. This specimen has a typical cup-and-cone fracture surface, which indicates that this specimen fractured in a ductile manner. This is further verified by the characteristic dimple structure observed over the whole fracture surface, displayed in Figure 42b. In all of the Al-5wt% AZ31 samples, fracture surfaces consisting of large and small dimples were observed. This is consistent with the stress-strain curves obtained for this parallel: The Al-5wt% AZ31 test specimens displayed high ductility with an elongation at fracture between 20 and 30%. The most distinctive difference between the three samples is the way sample 5-1 underwent fracture. This specimen fractured in a discontinuous manner, and examination of the fracture surface reveals an area with a delaminated surface, indicated with an arrow in the overview fractograph. The delamination effect is further discussed under the section concerning the Al-10wt% AZ31-2 specimens.

Figure 42c-d pictures the fracture surface of sample 7-4. This specimen has a typical ductile shear surface, which is a characteristic for binary Al-Mg specimens subjected to tensile testing. At high magnification the fracture surface is observed to comprise of similar dimple structure as observed in the 5wt% AZ31 samples. This is not a surprise, as these two parallels showed similar behaviour during tensile testing. In the bottom of the dimples there is often observed small particles, which is typical for ductile rupture.

Figure 42e-f depicts the fracture surface of sample 10.1-4. This sample fractured in a brittle matter; the fracture surface is fairly flat, no necking occurred prior to fracture, and a very low elongation at fracture was obtained, only 2%. Figure 42 shows the fracture surfaces of the centre of the specimen at high magnification, and a quasi-ductile surface can be observed. Because of this, some ductility should be expected in the specimen. However, the 10-1 specimens contain a high number of *large* particles, as observed in the OM and the SEM. In Figure 43, typical features observed in the 10-1 fracture surfaces are presented. In Figure 43a-b, it is indicated with arrows a high number of cracked particles. Each of these particles has the possibility of functioning as a crack initiation point, and may thus adversely decrease the fracture resistance. In Figure 43c-d, a large secondary phase is seen, with an approximate dimensions 150×250 μm. Figure 43d display the secondary phase at higher magnification, and it seems to comprise of a mixture of brittle and ductile structure. In Figure 43e-f, a massive particle is displayed. The size of this particle resembles the MgO particles observed in the SEM. In Figure 43f, a fractured particle of similar size as the one in Figure 43e is shown. This particle has a typical cleavage appearance, and a possible crack initiation point is indicated. This is a typical feature for brittle fractures. Taking into consideration all of the above, a possible explanation for the low fracture resistance of the 10-1 specimens is the presence of large, brittle oxide particles in the matrix.

The greatest variation in fracture surface appearance is found within the specimens for the Al-10wt% AZ31-2 profile. This is in agreement with the stress-strain curves obtained for this testing parallel: some of the samples showed high ductility, while others fractured at very short elongations, with little or no necking prior to the fracture. In Figure 42g-h, the fracture surface of sample 10.2-3 is displayed. This sample fractured in a discontinuous way, which can be observed in the stress-strain curve. Examination of the fracture surface reveals that the sample has become delaminated during the testing. Large cracks have formed and it is clear that these cracks are located in the same spiral pattern as observed in the OM and the SEM. Figure 44 displays two cracks observed in the 10-4 sample. In Figure 44a-b, a crack located towards the outer edge of the sample is observed. It was possible to perform an EDS point analysis of the fractured phase in the middle of the crack, and this was identified as the intermetallic Al_3Mg_2. The smooth surface towards was identified as Al, and the composition of the crack thus resembles the type 1 phase discussed in the section concerning the SEM micrographs. It was not possible to obtain a quantitative measurement of the chemical concentration in the surrounding area with the dimple structure, but it was indicated that it mostly contained Al with small amounts of Mg. In Figure 44c-d, a crack in the centre of the sample is displayed. Also here, the intermetallic phase is present in the crack. In all of the samples examined, it is observed that neighbouring the cracks are areas with what resembles slip lines, or a structure indicating that a much faster fracture

mode has occurred, as illustrated in Figure 44d. The fact that the delamination feature is found in both the 5-, and 10-2wt% AZ31 samples implies that the effect is related to the bands of intermetallics observed in these profiles, please refer to the OM and the SEM observations.

In Figure 46a, an area in sample 7-3, containing several of these “slip-line” features is highlighted, and magnified in Figure 46b. These features are observed, in varying amount, in all of the samples. Furthermore, they are often located in an arrangement similar to the screw extrusion spiral pattern, and adjacent to regions with a “fast mode” fracture appearance. A hypothesis may thus be that these features are connected to unsuccessful bonding between the layers of the extrusion profile, and in some way have led to a faster fracture mode.

In Figure 45, the fracture surfaces of the specimens with the highest and lowest ductility in the 10-2 parallel, specimen 10.2-1, and 10.2-5, are compared. 10.2-1 is the specimen that displayed the highest ductility among all the samples tested, independent of parallels. It can be observed that delamination of the fracture surface has occurred, but not to same extent as in the 10.2-3 specimen. Sample 10.2-5 resembles the fracture surfaces observed for the Al-10wt% AZ31-1 samples. The fracture surface is flat, no delamination effect, and with a high number of cracked particles present. The extreme difference in fracture surface appearance of the 10.2-5 may suggest this specimen must either be: 1) machined from a very different section of the Al-10wt% AZ31-2 profile, or 2) that a mix-up has occurred during the machining- or testing process and that this specimen actually belongs to the Al-10wt% AZ31-1 profile. Furthermore, the difference in the fracture surface and mechanical properties between these two samples, suggest that large oxide particles are more harmful for the ductility, than the delamination effect, most likely caused by the presence of intermetallic phases.

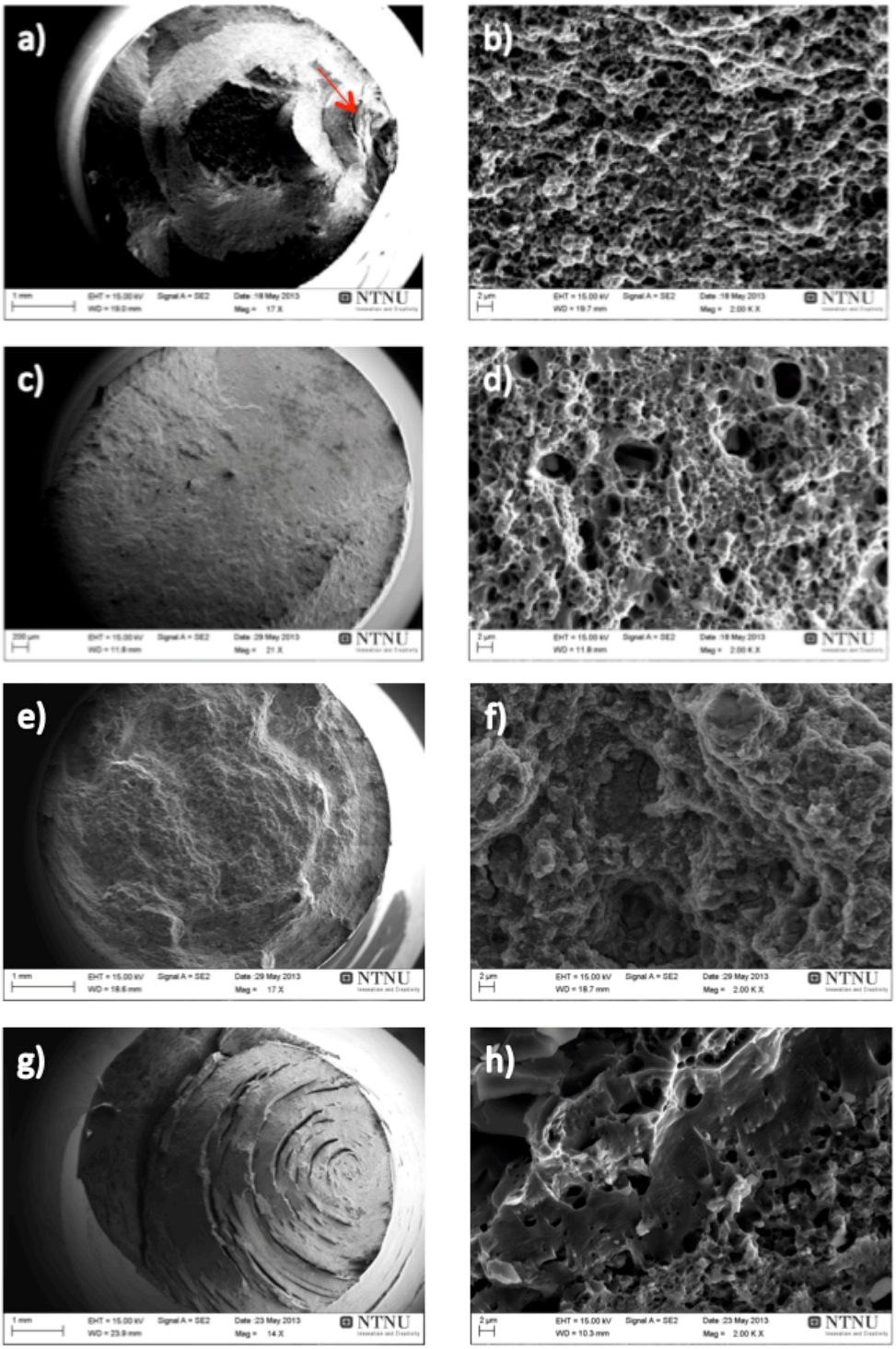

Figure 42: Fracture surfaces for tensile test specimen: a-b) 5-1, c-d) 7-4, e-f) 10.1-4, and g-h) 10.2-3.

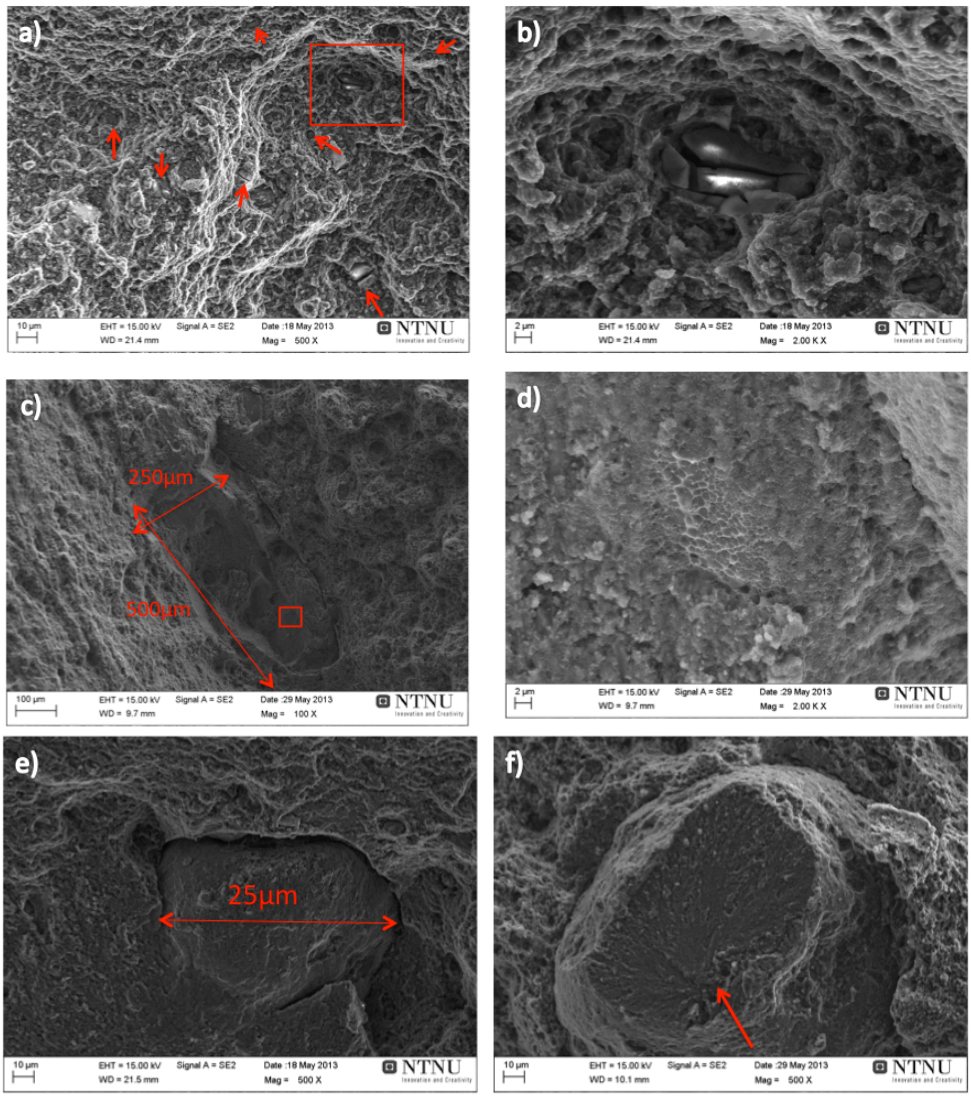

Figure 43: Fractographs showing characteristics features of the Al-10wt% AZ31-1 specimens. a-b) Fractured oxide particles, c-d) large secondary phases with brittle fracture structure, and e-f) large MgO particles, showing a typical cleavage fracture appearance.

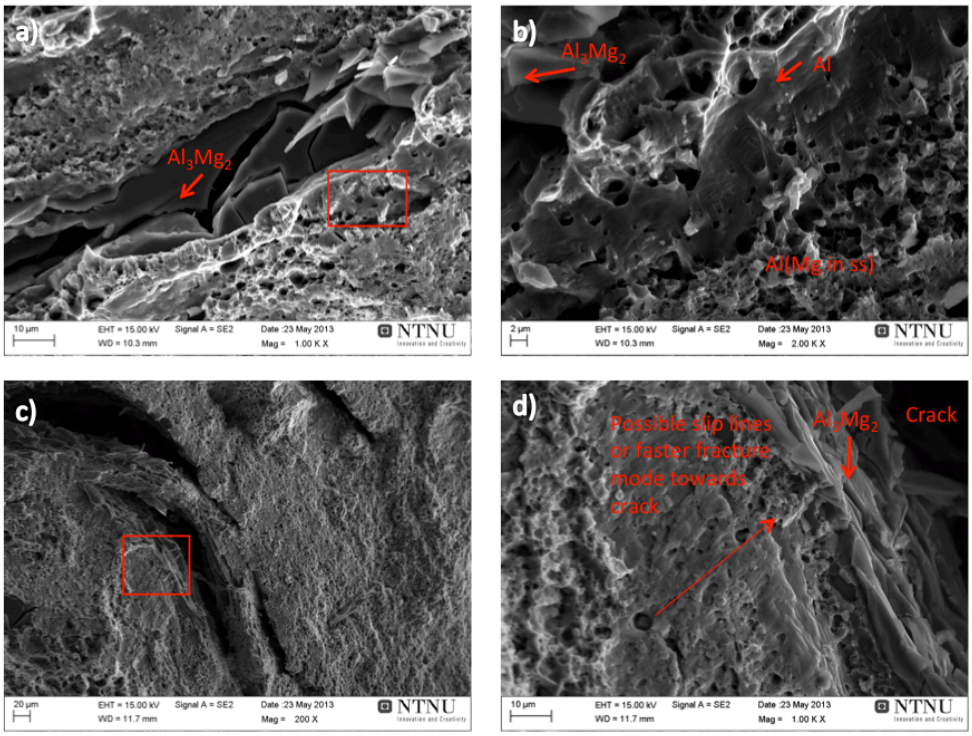

Figure 44: Fractographs showing typical features in the Al-10wt% AZ31-2 specimens: a-b) A large crack located near the edge of the surface, comprising of an intermetallic phase, c-d) similar crack located in the centre of the surface.

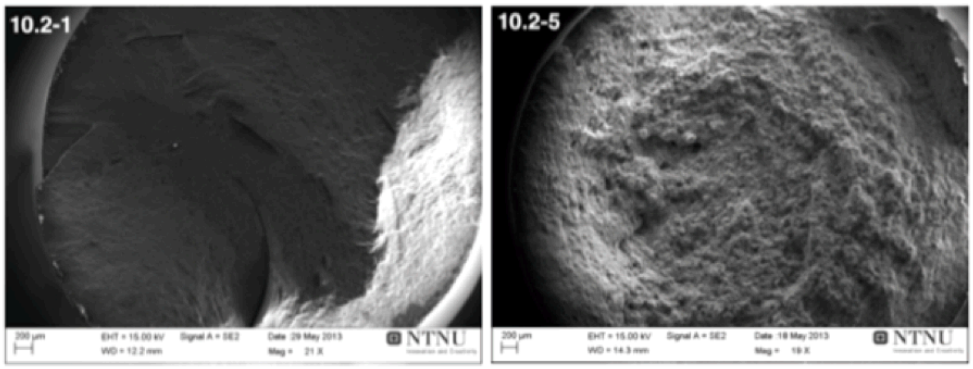

Figure 45: Comparison of the fracture surfaces of the specimens with the highest and lowest elongation at failure, respectively, within the Al-10wt% AZ31-2 parallel: a) 10.2-1, and b) 10.2-5. Please notice how the surface of specimen 10.2-5 resembles the surface of specimen 10.1-4 in Figure 42.

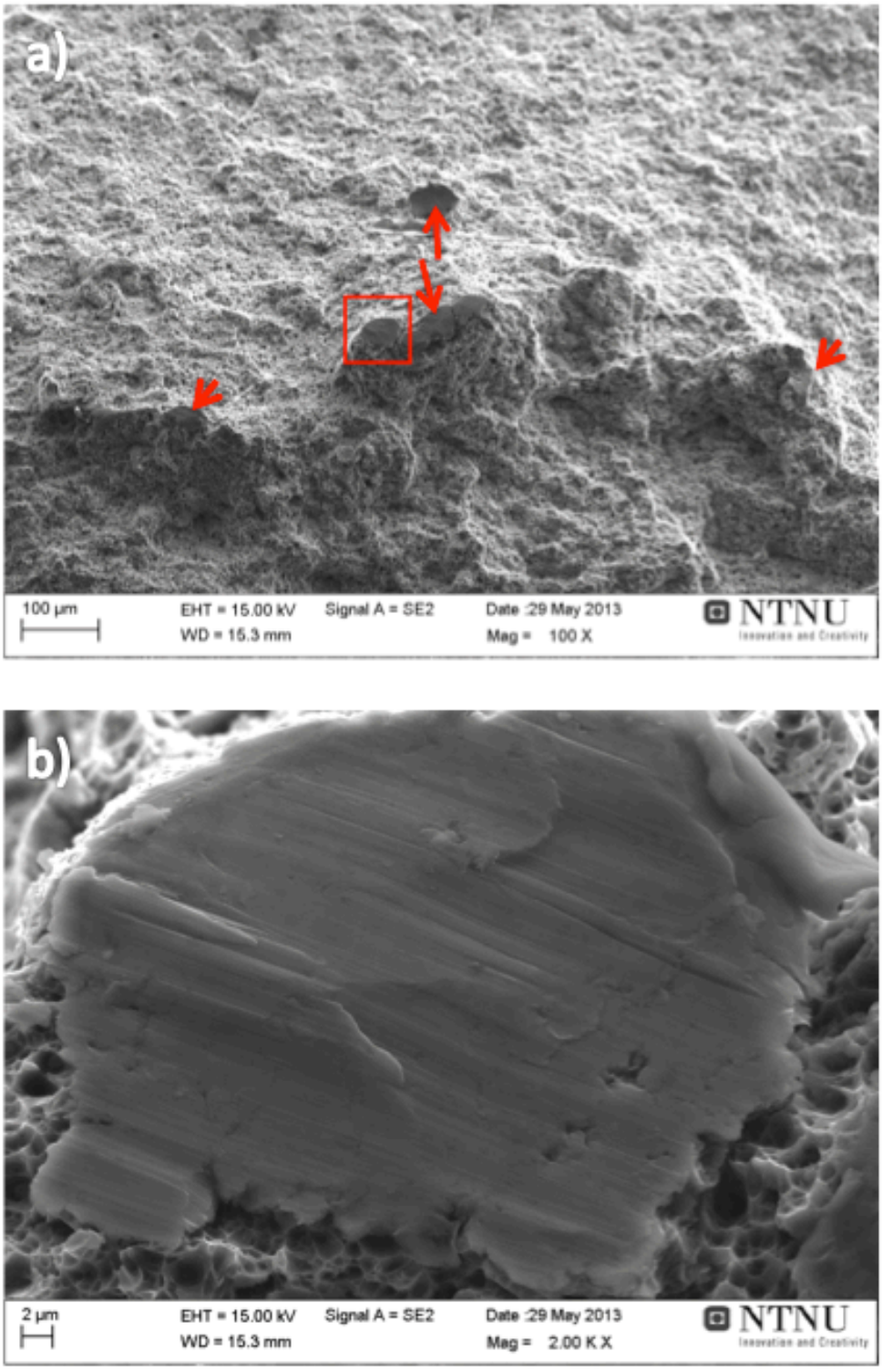

Figure 46: a) Areas with a characteristic feature resembling sip lines are indicated with arrows, and magnified in b).

5 Shortcomings

The present study has its limitations and weaknesses. The most obvious weakness is related to the execution of the screw extrusion trials. It is unmistakable that the extrusion temperature and the rotation speed have a great impact on the microstructure, and corresponding mechanical properties of the extrudates. This thesis concerns the manufacture of Al-AZ31 metallic composites. Hence, the effect of increased additions of AZ31 to the composite system on the mechanical properties of the extrudates is a key aspect of this study. It is therefore particularly vital to know if different strength levels, or ductility, between the profiles, are a product of higher additions of AZ31, or just a result of more suitable process parameters during the extrusion. As a consequence, it is a clear disadvantage that the extrusion trials were performed without a control system for the process parameters, as this makes the subsequent examination of extrusion profile microstructure ambiguous.

6 Concluding Remarks and Further Work

This thesis explored screw extrusion as a possible solution for mass production of an aluminum-AZ31 magnesium alloy bimetallic composite systems. In the approach, extrusion profiles with the following compositions: Al-5wt% AZ31, Al-7.5wt% AZ31, and Al-10wt% AZ31, were produced. The profiles were characterized by microstructural examination in optical- and scanning electron microscopes, and by tensile testing and hardness measurements.

From the results obtained from the different extrusion profiles, the following can be concluded: In contrast to what was expected, it was not achieved to produce pure Al-AZ31 bimetallic composites by the screw extrusion process. It was anticipated that the profiles would comprise of an aluminium matrix with the AZ31 magnesium alloy present as an integrated reinforcing constituent. In stead, a material with similar composition as a binary Al-Mg alloy was obtained, e.g. almost the entire AZ31 additions had become dissolved in the Al. This was unexpected, and also disappointing, as the objective was to produce a *composite* system. The relative small size of the AZ31 feed stock material plays most likely a key role for the absence of reinforcing AZ31 constituents in the extrudates. Possible theories for the complete dissolution of the AZ31 turnings are: (1) high temperatures during the extrusion have led to local melting at the Al-AZ31 interfaces, or (2) high extrusion temperatures, together with the high strains involved in the process, have given rise to extensive diffusion of Mg and Zn into the Al. Therefore, in further manufacturing trials of bimetallic systems by the screw extrusion process, it is recommended that the feed stock reinforcing constituents should be of a more substantial size. Furthermore, to avoid local melting, it is suggested that a metal with a melting point higher than Al should be chosen as the reinforcing phase.

The profiles obtained in this study have a profound inhomogeneity in their microstructure. This is a disadvantage as it gives rise to corresponding inconsistencies in the mechanical properties. Large variations in both grain size and chemical compositions are present throughout the profiles. Whereas the inconsistent grain structure is a product of the material flow in the screw extrusion process, the composition variations are most likely linked to the mechanical mixing and compaction process of the feed stock material. Great variations in composition may lead to formation of brittle intermetallic phases at the sites that are high in Mg concentration. Therefore, to obtain a more uniform chemical composition in the extrusion profile, it is important that the reinforcing feed stock material consists of coarser units and that the mixing process becomes more optimized. Furthermore, the specific condition of the feed stock material is vital for the mechanical properties. It can be argued that the oxide layers of the pure Al-

and AZ31 turnings are just as important for the properties of the final product, as the amount of AZ31 added. This is evident in the mechanical results obtained for the two 10wt% AZ31 profiles, as compared to the lower grade mixtures.

The extrudates display mechanical properties that are not inferior to other commercial Al-Mg alloys. Especially, tensile testing of the Al-10wt% AZ31-2 profile revealed a relatively high strength, combined with elongations at failure above 30%. Hence, the ductility of the extrudates is superior to other Al alloys with similar Mg content. So, even though the attempt in producing a bimetal was unsuccessful, the screw extrusion process shows promising results for e.g. recycling of aluminum and magnesium alloys, especially since this method is continuous and offers a wide span of opportunities for mixing and consolidating various constituents.

7 References

ABBADI, M., HÄHNER, P. & ZEGHLOUL, A. 2002. On the characteristics of Portevin–Le Chatelier bands in aluminum alloy 5182 under stress-controlled and strain-controlled tensile testing. *Materials Science and Engineering: A,* 337**,** 194-201.

ASKELAND, D. R. & PHULÉ, P. P. 2006. *The Science and Engineering Of Materials*, Nelson.

AZUSHIMA, A., KOPP, R., KORHONEN, A., YANG, D., MICARI, F., LAHOTI, G., GROCHE, P., YANAGIMOTO, J., TSUJI, N. & ROSOCHOWSKI, A. 2008. Severe plastic deformation (SPD) processes for metals. *CIRP Annals-Manufacturing Technology,* 57**,** 716-735.

BILSBAK, A. 2012. *Microstructure and mechanical properties of screw extruded aluminium* Master Thesis, Dep. of Material Science and Engineering, Norwegian University of Science and Technology.

BRENNAN, S., BERMUDEZ, K., KULKARNI, N. S. & SOHN, Y. 2012. Interdiffusion in the Mg-Al System and Intrinsic Diffusion in β-Mg2Al3. *Metallurgical and Materials Transactions A,* 43**,** 4043-4052.

CHANDRASEKARAN, M. & JOHN, Y. M. S. 2004. Effect of materials and temperature on the forward extrusion of magnesium alloys. *Materials Science and Engineering: A,* 381**,** 308-319.

CHANG, H., ZHENG, M., XU, C., FAN, G., BROKMEIER, H. & WU, K. 2012. Microstructure and mechanical properties of the Mg/Al multilayer fabricated by accumulative roll bonding (ARB) at ambient temperature. *Materials Science and Engineering: A,* 554**,** 249-256.

CHEN, J.-Z., ZHEN, L., FAN, L.-W., YANG, S.-J., DAI, S.-L. & SHAO, W.-Z. 2009. Portevin-Le Chatelier effect in Al-Zn-Mg-Cu-Zr aluminum alloy. *Transactions of Nonferrous Metals Society of China,* 19**,** 1071-1075.

CHEN, M.-C., KUO, C.-W., CHANG, C.-M., HSIEH, C.-C., CHANG, Y.-Y. & WU, W. 2007. Diffusion and formation of intermetallic compounds during accumulative roll-bonding of Al/Mg alloys. *Materials transactions,* 48**,** 2595-2598.

CUI, J. 2011. *Solid state recycling of aluminium scrap and dross characterization.* PhD Thesis, Norwegian University of Science and Technology.

CZERWINSKI, F. 2003. The Oxidation of Magnesium Alloys in Solid and Semisolid States. *Magnesium Technology 2003***,** 39-42.

DEHSORKHI, R. N., QODS, F. & TAJALLY, M. 2011. Investigation on microstructure and mechanical properties of Al-Zn composite during accumulative roll bonding (ARB) process. *Materials Science and Engineering: A,* 530**,** 63-72.

DIETER, G. E. & BACON, D. J. 1988. *Mechanical Metallurgy*, McGraw-Hill.

DOHERTY, R., HUGHES, D., HUMPHREYS, F., JONAS, J., JENSEN, D. J., KASSNER, M., KING, W., MCNELLEY, T., MCQUEEN, H. & ROLLETT, A. 1997. Current issues in recrystallization: a review. *Materials Science and Engineering: A,* 238**,** 219-274.

EIZADJOU, M., KAZEMI TALACHI, A., DANESH MANESH, H., SHAKUR SHAHABI, H. & JANGHORBAN, K. 2008. Investigation of structure and mechanical properties of multi-layered Al/Cu composite produced by accumulative roll bonding (ARB) process. *Composites Science and Technology,* 68**,** 2003-2009.

7 REFERENCES

FUJITA, T., HORITA, Z. & LANGDON, T. G. 2002. Characteristics of diffusion in Al-Mg alloys with ultrafine grain sizes. *Philosophical Magazine A,* 82**,** 2249-2262.

GRONOSTAJSKI, J. & MATUSZAK, A. 1999. The recycling of metals by plastic deformation: an example of recycling of aluminium and its alloys chips. *Journal of Materials Processing Technology,* 92**,** 35-41.

GUO-ZHENG, Q. 2013. Characterization for Dynamic Recrystallization Kinetics Based on Stress-Strain Curves. *In:* WILSON, P. (ed.) *Recent Developments in the Study of Recrystallization.* Online: InTech.

HJELEN, J. 1989. *Scanning elektron-mikroskopi,* Trondheim, Metallurgisk institutt, NTH.

HU, M., JI, Z., CHEN, X. & ZHANG, Z. 2008. Effect of chip size on mechanical property and microstructure of AZ91D magnesium alloy prepared by solid state recycling. *Materials Characterization,* 59**,** 385-389.

HUMPHREYS, F. 1997. A unified theory of recovery, recrystallization and grain growth, based on the stability and growth of cellular microstructures—I. The basic model. *Acta Materialia,* 45**,** 4231-4240.

HUMPHREYS, F. J. & HATHERLY, M. 2004. *Recrystallization and related annealing phenomena*, Elsevier Oxford.

KAZANOWSKI, P., EPLER, M. E. & MISIOLEK, W. Z. 2004. Bi-metal rod extrusion—process and product optimization. *Materials Science and Engineering: A,* 369**,** 170-180.

KIM, D., YOON, E. & KIM, J. 1996. Oxidation of an aluminum-0.4 wt% magnesium alloy. *Journal of materials science letters,* 15**,** 1429-1431.

LI, Y., LIU, P., WANG, J. & MA, H. 2007. XRD and SEM analysis near the diffusion bonding interface of Mg/Al dissimilar materials. *Vacuum,* 82**,** 15-19.

LIU, H., ZHANG, B. & ZHANG, G. 2011. Microstructures and mechanical properties of Al/Mg alloy multilayered composites produced by accumulative roll bonding. *Journal of Materials Science & Technology,* 27**,** 15-21.

LIU, X., CHEN, R. & HAN, E. 2009. Preliminary investigations on the Mg–Al–Zn/Al laminated composite fabricated by equal channel angular extrusion. *Journal of Materials Processing Technology,* 209**,** 4675-4681.

LLOYD, G. E. 1987. Atomic number and crystallographic contrast images with the SEM: a review of backscattered electron techniques. *Mineralogical Magazine,* 51**,** 3-19.

MARKUSHEV, M. & MURASHKIN, M. Y. 2004. Structure and mechanical properties of commercial Al–Mg 1560 alloy after equal-channel angular extrusion and annealing. *Materials Science and Engineering: A,* 367**,** 234-242.

MC CHEN, B. & WU, W. T. 2007. Microstructure changed during Accumulative roll bonding of Al/Mg composite. *Solid State Phenomena,* 124**,** 1445-1448.

MURRAY, J. L. 1982. The Al– Mg (Aluminum– Magnesium) system. *Bulletin of Alloy Phase Diagrams,* 3**,** 60-74.

PARAMSOTHY, M., SRIKANTH, N. & GUPTA, M. 2008. Solidification processed Mg/Al bimetal macrocomposite: Microstructure and mechanical properties. *Journal of Alloys and Compounds,* 461**,** 200-208.

PENG, L., YAJIANG, L., HAORAN, G. & JUAN, W. 2006. Investigation of interfacial structure of Mg/Al vacuum diffusion-bonded joint. *Vacuum,* 80**,** 395-399.

RINGSTAD, R. 2009. *Karakterisering av mikrostruktur og mekaniske egenskaper til skruekstrudert aluminium.* Specialization Project, Master Thesis, Dep. of

Material Science and Engineering, Norwegian University of Science and Technology.

ROBINSON, J. 1994. Serrated flow in aluminium base alloys. *International Materials Reviews,* 39**,** 217-227.

SHABANI, A., REZA TOROGHINEJAD, M. & SHAFYEI, A. 2012. Fabrication of Al/Ni/Cu composite by accumulative roll bonding and electroplating processes and investigation of its microstructure and mechanical properties. *Materials Science and Engineering: A,* 558**,** 386-393.

SHENG, L., YANG, F., XI, T., LAI, C. & YE, H. 2011. Influence of heat treatment on interface of Cu/Al bimetal composite fabricated by cold rolling. *Composites Part B: Engineering,* 42**,** 1468-1473.

SKORPEN, K. G. 2011. *Characterization of Extruded Aluminium.* Master Thesis, Dep. of Material Science and Engineering, Norwegian University of Science and Technology.

SOLBERG, J. K. 2010. *Teknologiske metaller og legeringer,* Trondheim, Norway, Institute for Material Science, Norwegian University of Science and Technology

WANG, J., LI, Y., LIU, P. & GENG, H. 2008. Microstructure and XRD analysis in the interface zone of Mg/Al diffusion bonding. *Journal of Materials Processing Technology,* 205**,** 146-150.

WEN, W. & MORRIS, J. 2003. An investigation of serrated yielding in 5000 series aluminum alloys. *Materials Science and Engineering: A,* 354**,** 279-285.

WEN, W. & MORRIS, J. 2004. The effect of cold rolling and annealing on the serrated yielding phenomenon of AA5182 aluminum alloy. *Materials Science and Engineering: A,* 373**,** 204-216.

WERENSKIOLD, J. C., AURAN, L., ROVEN, H. J., RYUM, N. & REISO, O. 2007. Screw extruder for continuous extrusion of materials with high viscosity. WO Patent 2,008,063,076.

WIDERØE, F. & WELO, T. 2012. Using contrast material techniques to determine metal flow in screw extrusion of aluminium. *Journal of Materials Processing Technology,* 213**,** 1007-1018.

WU, K., CHANG, H., MAAWAD, E., GAN, W., BROKMEIER, H. & ZHENG, M. 2010. Microstructure and mechanical properties of the Mg/Al laminated composite fabricated by accumulative roll bonding (ARB). *Materials Science and Engineering: A,* 527**,** 3073-3078.

YANG, D., CIZEK, P., HODGSON, P. & WEN, C. E. 2010. Ultrafine equiaxed-grain Ti/Al composite produced by accumulative roll bonding. *Scripta materialia,* 62**,** 321-324.

Appendix A: Screw Extrusion Process Parameters

In this section, the process parameters during the screw extrusion of the different profiles are presented. In Figure A 1, the variation in rotation speed is displayed. In Figure A 2, the various temperatures in the screw extruder, e.g. in the die, compacting chamber, liner rear, and screw attachment, are plotted.

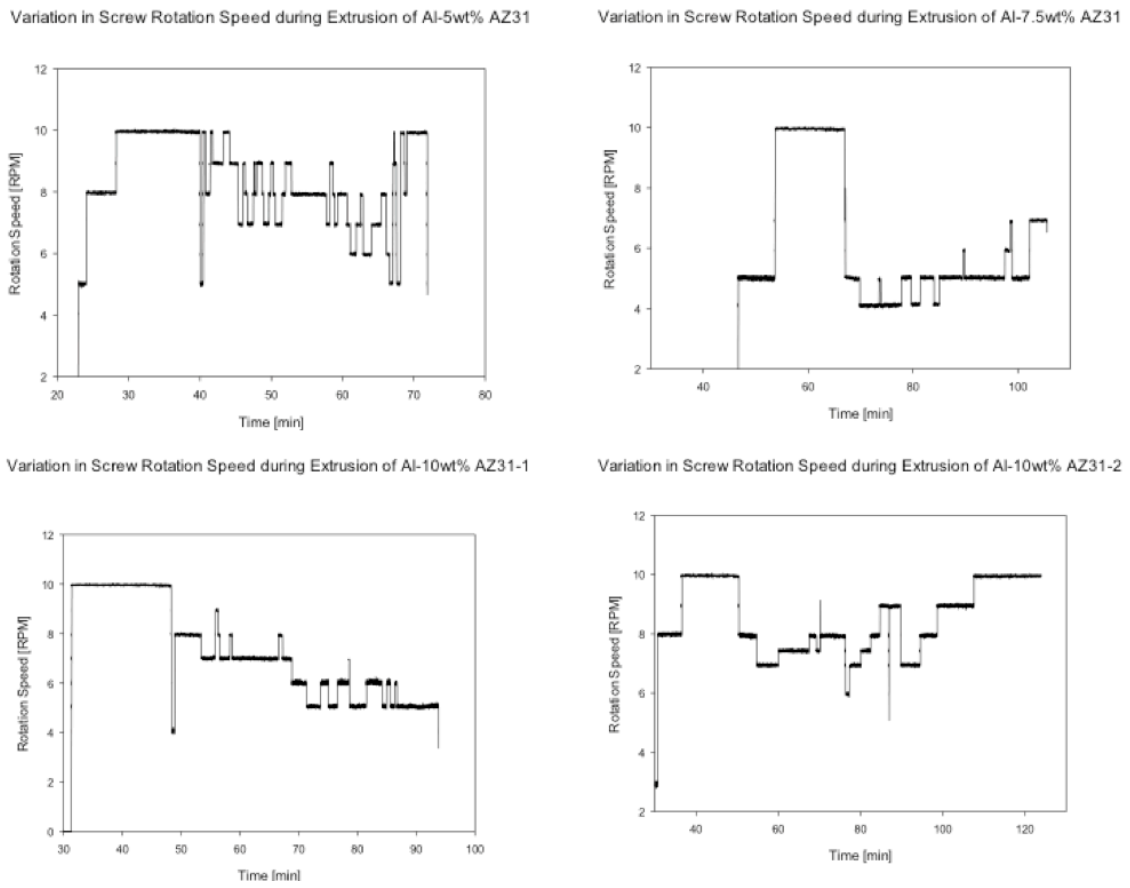

Figure A 1: Variation in rotation speed during the extrusion of the four different extrusion profiles: Al-5wt% AZ31, Al-7.5wt% AZ31, Al-10wt% AZ31, and Al-10wt% AZ31-2.

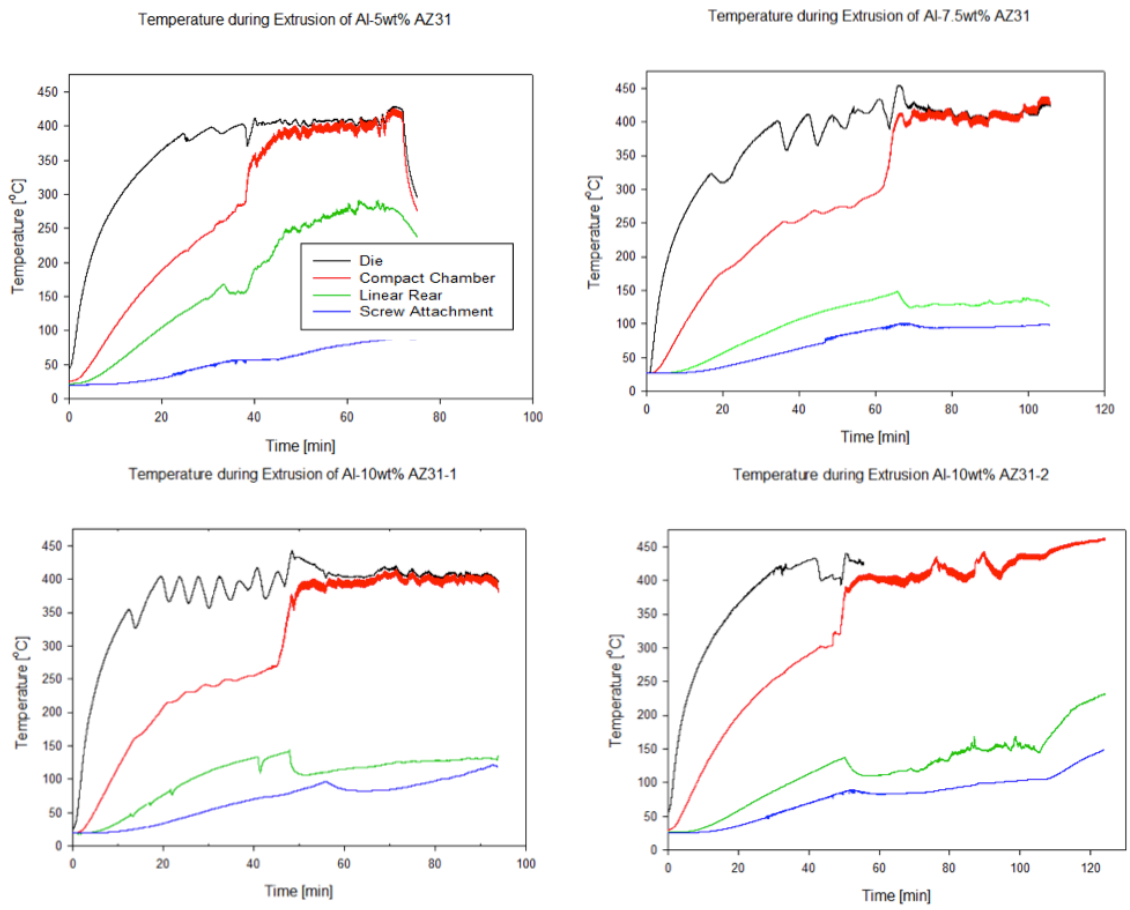

Figure A 2: Temperature variations in the die, compacting chamber, liner rear, and screw attachment, during the extrusion of the different profiles: Al-5wt% AzZ31, Al-7.5wt% AZ31, Al-10wt% AZ31-1, and Al-10wt% AZ31-2.

Appendix B: Fractographs

In this section, the fractographs of all tensile test specimens are presented. The fractographs are displayed in Figure B 1-4, and are arranged by testing parallel, and presented in the following order: Al-5wt% AZ31, A-7.5wt% AZ31, Al-10wt% AZ31-1, and Al-10wt% AZ31-2. Please notice that some of the fractographs have a different measuring bar.

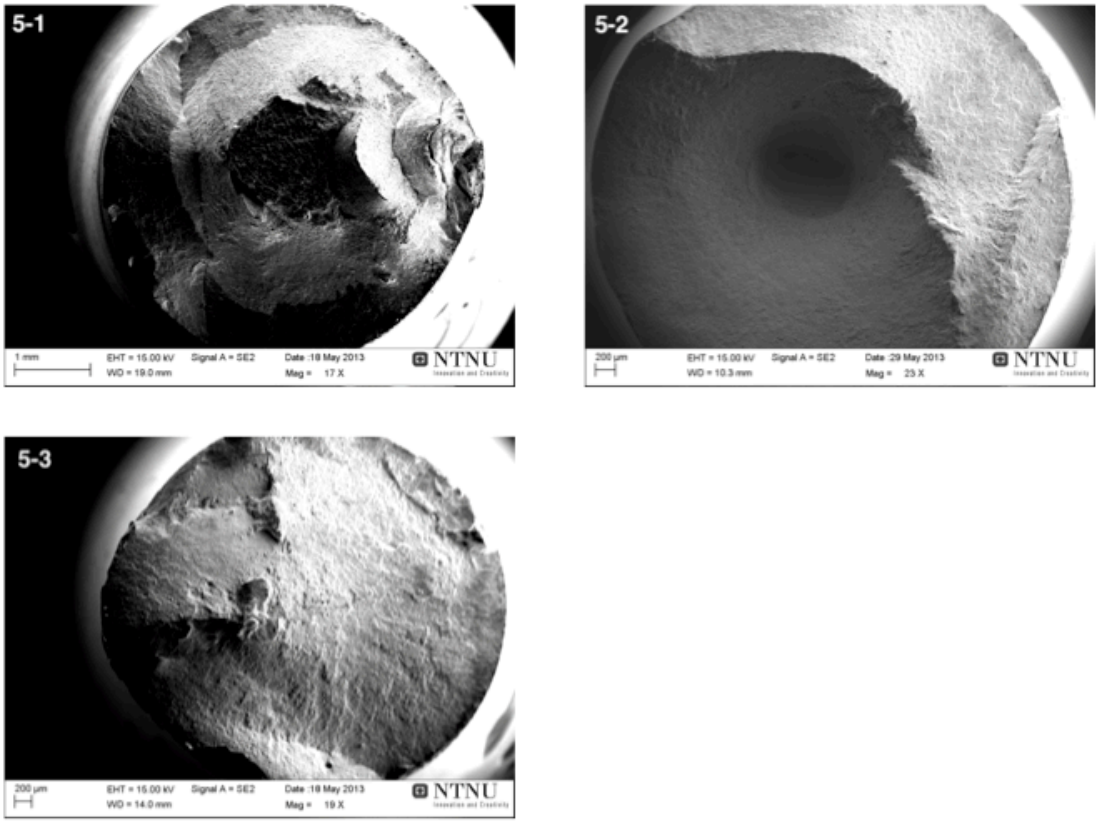

Figure B 1: Fractographs of the fracture surfaces of the Al-5wt% AZ31 tensile test parallel.

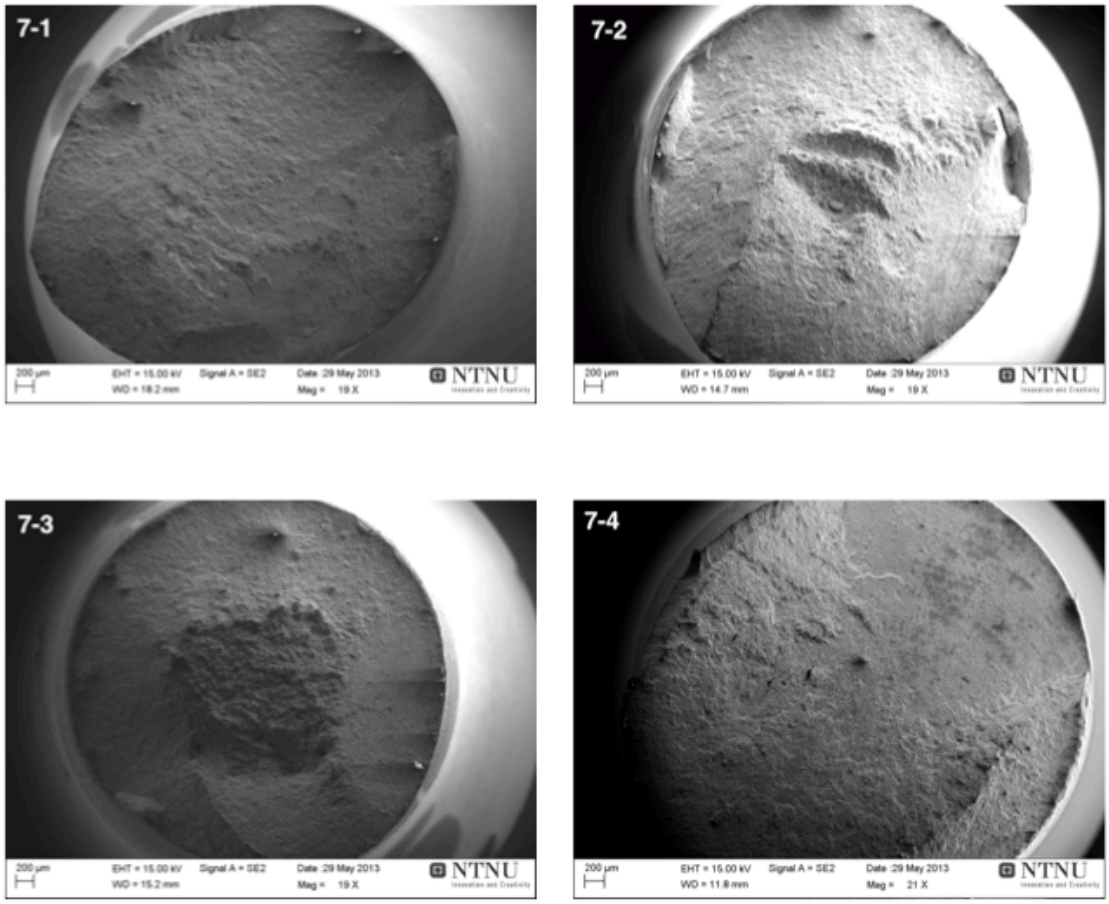

Figure B 2: Fractographs of the fracture surfaces of the Al-7.5wt% AZ31 tensile test parallel.

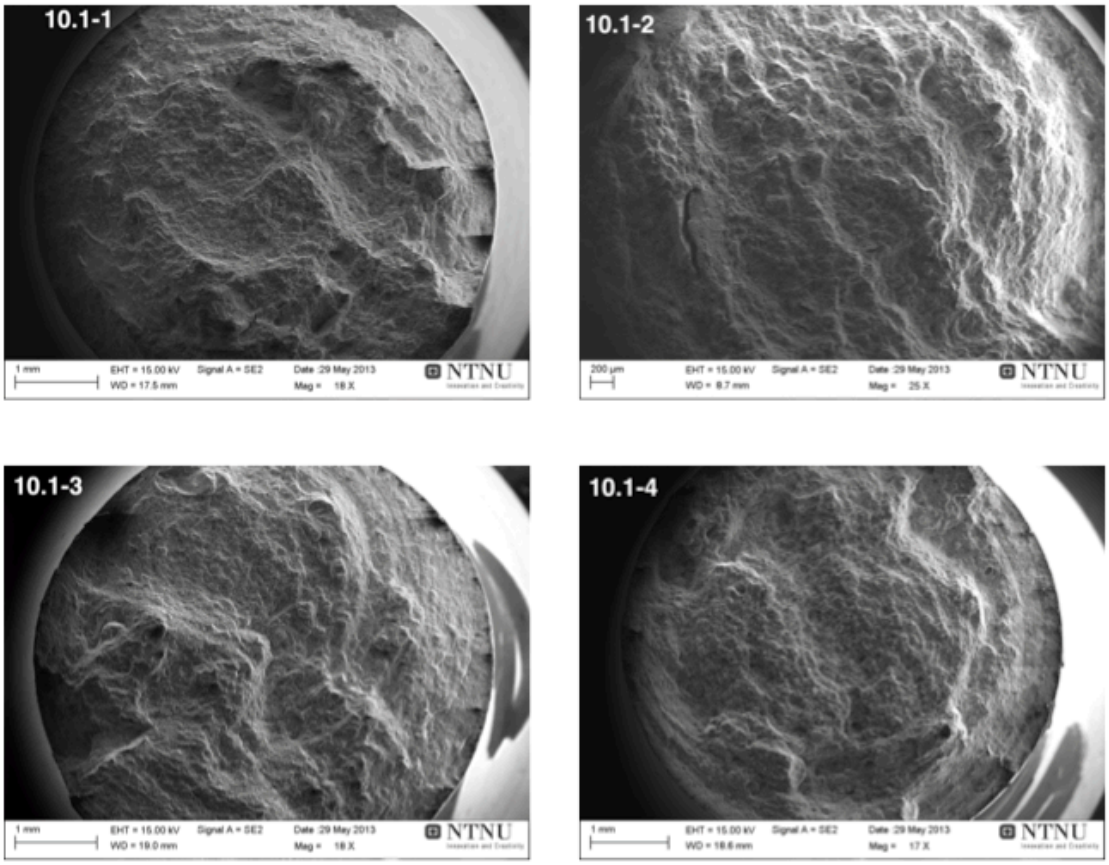

Figure B 3: Fractographs of the Al-10wt% AZ31-1 tensile test parallel.

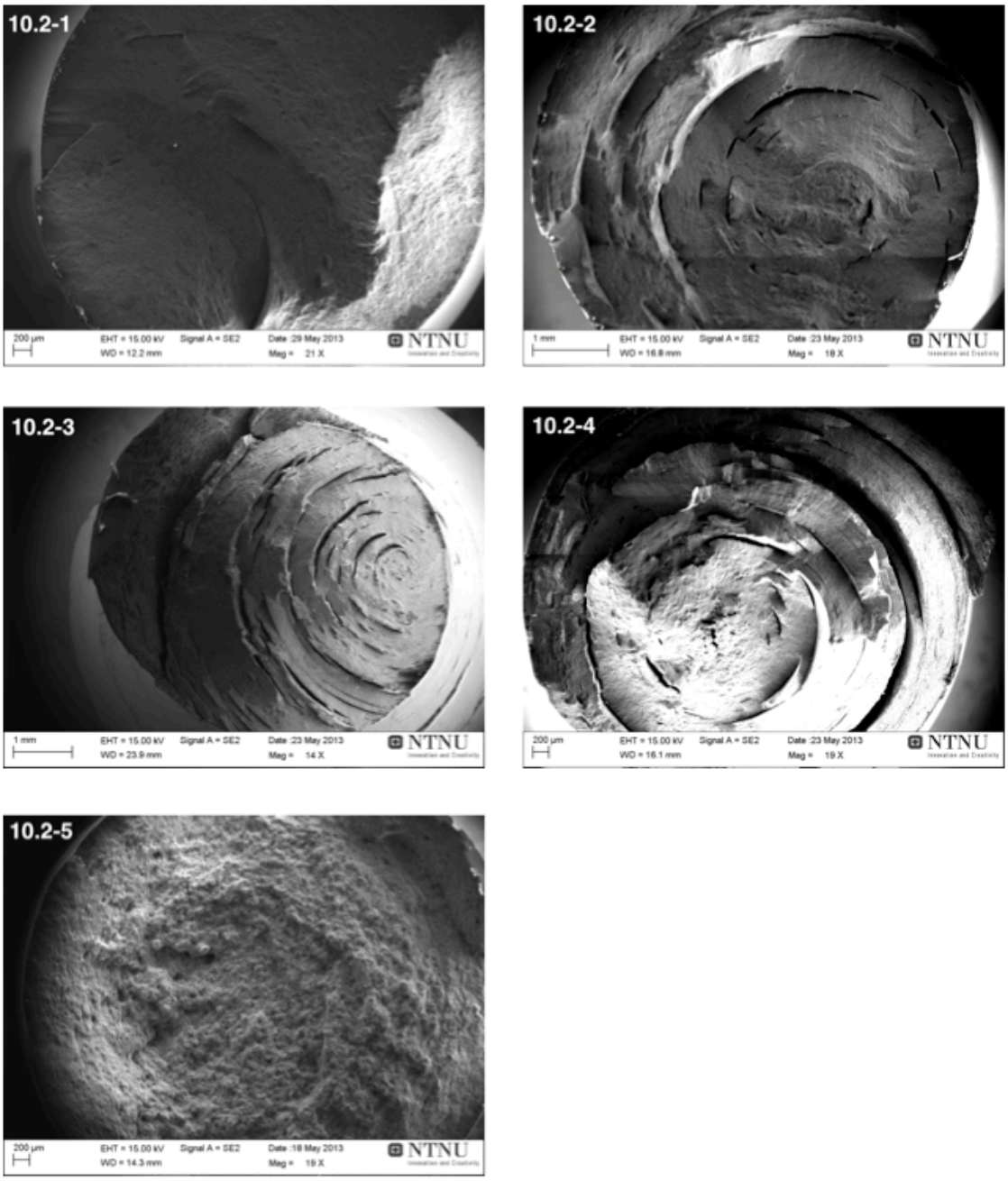

Figure B 4: Fractographs of the Al-10wt% AZ31-2 tensile test parallel.

Appendix C: XRD results

In this section the results from the XRD examination of the oxide powder collected from the Al-10wt% AZ31-1 feed stock material, is presented Figure C 1.

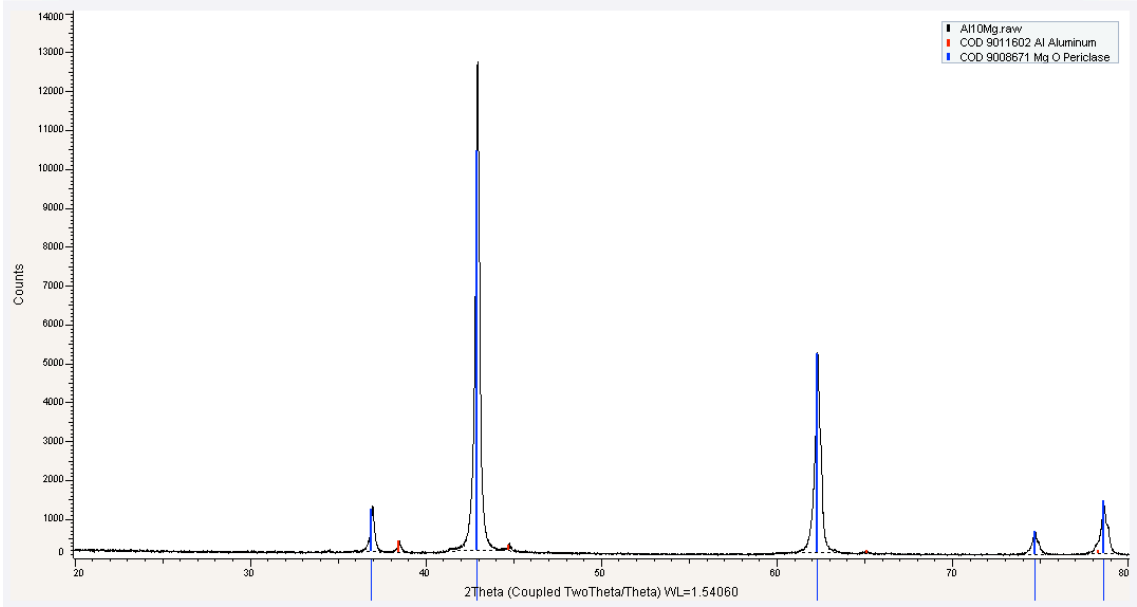

Figure C 1: XRD specter obtained for the oxide powder collected from the Al-10wt% AZ3-1 batch feed stock material. Please notice that the possible constituents are indicated in the legend in upper right corner. For this sample, the most probable constituent is MgO.